PREPARATION AND CHARACTERIZATION OF NANOCOMPOSITES WITH A THERMOPLASTIC MATRIX AND SPHERICAL REINFORCEMENT

**A THESIS SUBMITTED TO
THE GRADUATE SCHOOL OF NATURAL AND APPLIED SCIENCES
OF
MIDDLE EAST TECHNICAL UNIVERSITY**

BY

DILEK ERSU

**IN PARTIAL FULFILLMENT OF THE REQUIREMENTS
FOR
THE DEGREE OF MASTER OF SCIENCE
IN
CHEMICAL ENGINEERING**

JULY 2006

Approval of the Graduate School of Natural and Applied Sciences

Prof. Dr. Canan Özgen
Director

I certify that this thesis satisfies all the requirements as a thesis for the degree of Master of Science.

Prof. Dr. Nurcan Baç
Head of Department

This is to certify that we have read this thesis and that in our opinion it is fully adequate, in scope and quality, as a thesis and for the degree of Master of Science.

Prof. Dr. Hayrettin Yücel
Co-supervisor

Prof. Dr. Ülkü Yılmazer
Supervisor

Examining Committee Members

Prof. Dr. Teoman Tinçer	(METU,CHEM)	
Prof. Dr. Ülkü Yılmazer	(METU,CHE)	
Prof. Dr.Hayrettin Yücel	(METU,CHE)	
Assoc. Prof. Dr. Göknur Bayram	(METU,CHE)	
Dr. Cevdet Öztin	(METU,CHE)	

I hereby declare that all information in this document has been obtained and presented in accordance with academic rules and ethical conduct. I also declare that, as required by these rules and conduct, I have fully cited and referenced all material and results that are not original to this work.

Name, Last name : Dilek Ersu

Signature

ABSTRACT

PREPARATION AND CHARACTERIZATION OF NANOCOMPOSITES WITH A THERMOPLASTIC MATRIX AND SPHERICAL REINFORCEMENT

Ersu, Dilek

M.S., Department of Chemical Engineering

Supervisor   : Prof. Dr. Ülkü Yılmazer

Co-Supervisor : Prof. Dr. Hayrettin Yücel

July 2006, 122 pages

The aim of this study is to investigate the effects of compatibilizers, fumed silica and mixing order of components on morphological, thermal, mechanical and flow properties of LDPE/Fumed silica nanocomposites. As compatibilizer(Co); ethylene/n-butyl acrylate/maleic anhydride (E-nBA-MAH), ethylene/glycidyl methacrylate (E-GMA) and ethylene/methyl acrylate/glycidyl methacrylate (E-MA-GMA) Lotader® resins; as silica Cab-o-sil® M5 fumed silica were used. All samples were prepared by means of a lab scale co-rotating twin screw extruder and injection molded into standard samples.

In the first step, individual effects of filler and compatibilizers were studied in binary systems with LDPE. Then, keeping the amount of compatibilizer constant at 5%, ternary nanocomposites were prepared by adding 2 or 5% of fumed silica using different component mixing orders.

Among investigated mixing orders, mechanical test results showed that the best sequences of component addition are FO1 [(LDPE+Co)+M5] and FO2 [(LDPE+M5)+Co] mixing orders. Considering the compatibilizers, E-nBA-MAH

terpolymer showed the highest performance in improving the mechanical properties, E-GMA copolymer also gave satisfactory results.

According to the DSC analysis, since addition of fumed silica and compatibilizer does not influence the crystallization behavior of the compositions, it is concluded that, neither fumed silica nor any of the compatibilizers have nucleation activity on LDPE.

MFI test results showed that, addition of fumed silica increases the melt viscosity, decreasing MFI values of samples. This change seems to be directly proportional to fumed silica amount.

Keywords: low density polyethylene, nanocomposite, compatibilizer, fumed silica, extrusion.

ÖZ

TERMOPLASTİK MATRİS VE KÜRESEL DOLGU MADDESİ İÇEREN NANOKOMPOZİTLERİN HAZIRLANMASI VE ÖZELLİKLERİNİN BELİRLENMESİ

Ersu, Dilek

Yüksek Lisans, Kimya Mühendisliği

Tez Yöneticisi   :Prof. Dr. Ülkü Yılmazer

Ortak Tez Yöneticisi : Prof. Dr. Hayrettin Yücel

Temmuz 2006, 122 sayfa

Bu çalışmanın amacı, uyum sağlayıcı çeşidi, dumanlı silika ve bileşenlerin ekleme sırasının alçak yoğunluklu polietilen (AYPE) bazlı nanokompozit sistemlerinin morfolojik, ısıl, mekanik ve akış özelliklerine etkisini incelemektir. Uyum sağlayıcı (US) olarak etilen/bütil akrilat/maleik anhidrit (E-nBA-MAH), etilen/glisidil metakrilat (E-GMA) ve etilen/metil akrilat/glisidil metakrilat (E-MA-GMA) Lotader® elastomerleri; silika olarak Cab-o-sil® M5 dumanlı silika kullanılmıştır. Tüm numuneler laboratuar ölçekli, aynı yönde dönen çift vidalı ekstrüder ile hazırlanmış ve enjeksiyonlu kalıplama yöntemi ile standart numuneler haline getirilmiştir.

İlk adımda, dolgu maddesi ve uyum sağlayıcının bağımsız etkileri alçak yoğunluklu polietilenle ikili sistemlerinde incelenmiştir. Daha sonra, uyum sağlayıcı miktarı %5' de sabit tutulup, %2 ve 5 dumanlı silika eklenerek değişik bileşen ekleme sıralarıyla üçlü nanokompozitler hazırlanmıştır.

İncelenen bileşen ekleme sıraları arasında, mekanik test sonuçları en iyi sıralamaların FO1 [(AYPE+US)+M5] ve FO2 [(AYPE+M5)+US] karıştırma

düzenleri olduğunu göstermiştir. Uyum sağlayıcı tiplerine bakıldığında (E-nBA-MAH) terpolimeri mekanik özellikleri arttırmada en iyi performansı göstermiş ve E-GMA kopolimeri tatmin edici sonuçlar vermiştir.

DSC analiz sonuçlarına göre, dumanlı silika ve uyum sağlayıcı eklenmesi, bileşiklerin kristalleşme özelliklerini etkilemediğinden ne dumanlı silikanın ne de herhangi bir çeşit uyum sağlayıcının AYPE içinde kristalleşme başlatıcı özelliğe sahip olmadığı sonucuna varılmıştır.

Eriyik akış indeksi test sonuçları, dumanlı silika eklenmesinin akış viskozitesini arttırdığını ve akış indeks değerlerini düşürdüğünü göstermiştir. Bu değişim dumanlı silika miktarıyla doğru orantılı olarak gözükmektedir.

Anahtar kelimeler: Alçak yoğunluklu polietilen, nanokompozit, uyum sağlayıcı, dumanlı silika, ekstrüzyon.

To My Dear Family...

ACKNOWLEDGEMENTS

TABLE OF CONTENTS

LIST OF TABLES

TABLES

LIST OF FIGURES

FIGURES

xix

NOMENCLATURE

A_0 Original, undeformed cross-sectional area, mm^2

b   Width, mm

d   Thickness, mm

D   Deflection, mm

E   Tensile Modulus, MPa

E_B Modulus of Elasticity, MPa

F   Force, N

L   Support span, mm

L_0 Initial gauge length, mm

ΔL Change in sample length, mm

m   Slope of the tangent to the initial straight-line portion of the load deflection curve, N/mm

r   Maximum strain in the outer fibers, mm/mm

S   Stress in the outer fibers at midspan, MPa

T_c Crystallization temperature, °C

T_g Glass transition temperature, °C

T_m Melting temperature, °C

Greek Letters

Є   Tensile strain, mm/mm

λ   Wavelength, nm

σ   Tensile stress, MPa

Abbreviations

ASTM	American Society for Testing and Materials
DSC	Differential Scanning Calorimetry
E-GMA	Ethylene-Glycidyl Methacrylate
E-MA-GMA	Ethylene-Methyl Acrylate-Glycidyl Methacrylate
E-nBA-MAH	Ethylene-Butyl Acrylate-Maleic Anhydride
FO	Feeding Order
GMA	Glycidyl Methacrylate
HDPE	High Density Polyethylene
IPP	Isotactic Propylene
LDPE	Low Density Polyethylene
MAH	Maleic Anhydride
MFI	Melt Flow Index
PE	Polyethylene
PP	Polypropylene
SEM	Scanning Electron Microscopy
SF	Simultaneous Feeding
TS	Turkish Standard

CHAPTER 1

INTRODUCTION

Plastics have become one of the most important materials in our daily life over the past four decades. Increasing demand for using them forced the material scientists to improve their properties. Therefore, in recent years, inorganic nanoparticle filled polymer composites have received increasing research interest, mainly due to their ability to improve material properties of plastics.

Nanocomposites are homogeneous materials, made by combination of two or more unlike materials, at least one of which is in nanoscale. The filler/matrix interface in these nanocomposites constitute a large area and hence influence the properties of composites to a much greater extent at rather low filler concentration as compared to conventional micro-particulate composites. Polymer matrix nanocomposites are the most popular nanocomposites group, in which a nano sized filler is used to modify a polymer matrix. The characteristics of nanocomposites are determined according to the properties of constituents.

Homogeneous dispersion of nano-sized fillers in the matrix provides a large interfacial area; otherwise the loosely agglomerated nanoparticles would easily result in failure of the composites when they are subjected to force. A homogeneous product, incorporation of any additives requires a serious mixing in molten state, which is primarily provided by melt blending process by means of extrusion. In this study, nanocomposites were produced by means of a co-rotating twin screw extruder in two extrusion steps.

Low density polyethylene is one of the major types of polyethylene and is the most popular plastic in the world. The ease of processing, good chemical and physical properties and stability of LDPE make it very useful.

Nano-silica, being one of the first nanoparticles produced is one of the most commonly used inorganic nanoparticles. Fumed nano silica is produced by vapor phase hydrolysis of silicon tetrachloride in a hydrogen oxygen flame and used as a filler for mainly rubber applications. It is very effective for polymer systems, since it provides very large surface area improving the mechanical properties. Owing to the hydrophilic nature of fumed silica, it is not compatible with hydrophobic polyethylene and needs an appropriate compatibilizer.

Compatibilizer is usually a polymeric additive that bonds the two phases to each other more tightly and provides a strong filler-matrix adhesion. It is used to increase the toughness of engineering plastics and compatibility of the fillers. The physical and mechanical properties of incompatible polymer-filler systems may be enhanced by compatibilizers through the introduction of physical and/or chemical interactions between the components.

This study is focused on the effects of compatibilizers, fumed silica and mixing order of components on final properties of ternary nanocomposites with LDPE matrix. As compatibilizer; ethylene/n-butyl acrylate/maleic anhydride (E-nBA-MAH), ethylene/glycidyl methacrylate (E-GMA) and ethylene/methyl acrylate/glycidyl methacrylate (E-MA-GMA) Lotader® resins; as silica Cab-o-sil® M5 fumed silica are used.

Binary LDPE/Fumed silica and ternary LDPE/Compatibilizer/Fumed silica nanocomposites and LDPE/compatibilizer blends are prepared by two step extrusion process. The standard test specimens for all the samples are prepared by injection molding to be used in the characterization of nanocomposites.

The extent of dispersion of fumed silica is examined by scanning electron microscopy (SEM) and the thermal characterization of the nanocomposites is performed by differential scanning calorimetry (DSC). The change in flow properties of the nanocomposites are determined with melt flow index measurements. Mechanical characterization of the nanocomposites is studied by means of tensile and flexural properties of all samples.

CHAPTER 2

BACKGROUND

2.1 Composites

Composite materials have been utilized to solve technological problems for a long time but only in the 1960s did these materials start capturing the attention of industries with the introduction of polymer-based composites. Since then, composite materials have become common engineering materials and are designed and manufactured for various applications including automotive components, sporting goods, aerospace parts, consumer goods and in the marine industry [1].

Composite, is a homogeneous material, made by combination of two or more different materials that are insoluble in each other. The properties of composites, which usually consist of a reinforcing material dispersed in a matrix, are a function of the properties of the constituent phases, their relative amounts, as well as of the geometry of the dispersed phase (i.e., shape and size of the reinforcing component, their distribution and orientation) [2].

Reinforcing agents are used in polymers for a variety of reasons: cost reduction, process improvement, density control, optical effects, control of thermal, electrical, magnetic properties, flame retardancy and improved mechanical properties, such as hardness and tear resistance [3]. These filler materials can be minerals, metallic powders, organic by-products or synthetic inorganic compounds [4]. There are also different types of these groups varying according to their geometry as; fibers, particles or flakes which have different properties. These structural constituents determine the internal structure of the composite [5].

The matrix phase of the composite is the body constituent serving to surround the composite and give it its bulk form [5]. It binds together and protects the components and determines the thermo-mechanical stability of the composite [2]. According to the matrix, composites are commonly classified as metal, carbon, ceramic or polymer matrix composites.

2.2 Polymer Matrix Composites

Polymer matrix composites are the most developed composite materials group and they have found widespread applications since they have the advantage of being easily fabricated into any large complex shape [2]. Owing to the relatively low processing temperatures required, it's much easier to fabricate them than metal, carbon and ceramic matrix composites, whether the polymer is a thermoset or thermoplastic [6].

Composites can have thermoplastic or thermosetting matrices. Thermosetting and thermoplastic matrix composites are in many ways superior materials compared to common metals and ceramic materials. Their reliability is confirmed by their large use in the aerospace industry. Matrix selection is performed based on chemical, thermal, electrical, flammability, environmental, cost, performance and manufacturing requirements [1].

Thermosetting materials, as they form three-dimensional molecular chains, called crosslinking, cannot be remelted and reshaped once they are cured. The higher the number of cross-links, the more rigid and thermally stable the material will be. Thermosets are brittle and are generally used with some filler and reinforcements [1]. The most common thermoset polymer matrix materials are polyesters, epoxies and polyamides [2].

Thermoplastic materials generally have more toughness values and proper damage tolerances than thermosetting materials and are used for a wide variety of nonstructural applications without fillers and reinforcements [1,2]. Since thermoplastic molecules do not cross-link, they can be reshaped with heat and pressure and this provides them the property of being easily fabricated by

4

conventional plastics processing techniques such as extrusion, injection molding and blow molding. Thermoplastic materials also provide low cost-high volume processing of composite structures [2]. The most common thermoplastic matrices are polyolefinics (polyethylene, polypropylene), vinylic polymers (polyvinyl chloride, polyamides) [2].

2.3 Nanocomposites

The benefits of using nanomaterials, which always existed in nature, have been widely studied since the early 1990's with the Toyota's first use of clay/nylon-6 nanocomposite in production of timing belt covers [7]. The nanoscale should be defined by the "nano" term that refers to a size scale measured in nanometers (nm), which is 10^{-9} m. Nanocomposites are a subset of nanotechnology with filler loading often less than 5% by weight as compared to 20-40% loading of conventional materials [8]. To be defined as a nanocomposite, the loaded fillers must have at least one dimension at the range of 1-100 nm. Nanotechnology has wide effects in many industrial sectors, including; packaging, wire and cable, automotive, pipes and tubing and construction [3].

In recent years, inorganic nanoparticle filled polymer composites have received increasing research interest, since they exhibit larger filler/matrix interface and small interparticle distance which affect the composites' properties to a much greater extent at rather low filler concentration as compared to conventional micro-particulate composites [8,9]. For example, tensile strengths of the nanocomposites of PP are higher than that of neat polymer. This is different from what is observed in conventional micrometer particles/polymer composites, i.e., tensile strength of the composites remarkably decreases with the addition of the particulate fillers due to the poor bonding at the interface [10,11].

2.4 Particulate Polymer Composites

Particulate composites include a wide range of materials [12]. The two basic reasons for adding particulate reinforcement to a polymer are to fill the system

by replacing some part of the more expensive polymer with less expensive filler and to modify thermal and mechanical properties, electrical conductivity of the matrix material, improve its processability, fire retardancy and appearance, reduce friction and provide color [13].

2.4.1 Fumed Silica

Fumed silica is a white powder composed of silicon dioxide. It is manufactured from silicon tetrachloride into very pure (>99.8%) silicon dioxide. This fumed silicon dioxide is amorphous and distinct from naturally occurring and precipitated silicas [13]. Light and fluffy fumed silica, with low bulk density, is used in a variety of markets as an industrial inorganic chemical and a performance additive [14]. Fumed silica's extremely small particle size, its enormous surface area, its high purity and its chain-forming tendencies set it apart in a class of its own [15].

Fumed silica is produced by vapor phase hydrolysis of silicon tetrachloride in a hydrogen oxygen flame. The reactions are:

$$2H_2 + O_2 \longrightarrow 2H_2O$$
$$SiCl_4 + 2H_2O \longrightarrow SiO_2 \downarrow + 4HCl \uparrow$$

(Overall reaction) :

$$SiCl_4 + 2H_2 + 2O_2 \xrightarrow{1800^oC} SiO_2 \downarrow + 4HCl \uparrow$$
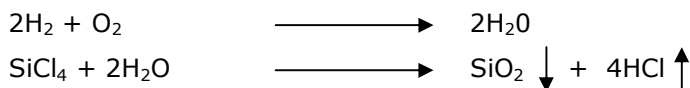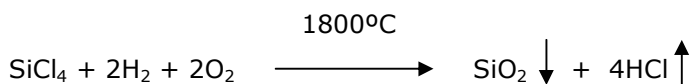
This process is known for at least fifty years [16]. In the burner, hydrogen is burned in the presence of oxygen from air, to create a high-temperature flame at 1800ºC. Silicon tetrachloride is sent into this flame and silicon dioxide molecules form as a result of the combustion process. Then, they condense and form particles. These particles collide, attach and sinter together forming three-dimensional branched chain aggregates. Once the aggregates cool below the fusion point of silica (1710°C), further collisions result in mechanical

6

entanglement of the chains, termed agglomeration [17]. This process is schematically showed in Figure 2.1.
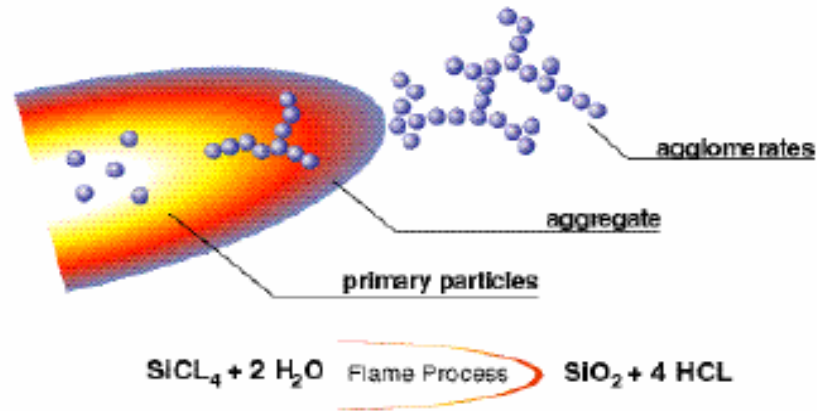
Figure 2.1 Schematic diagram of the flame process manufacture of CAB-O-SIL® fumed silica [17]

The market available nanoparticles generally take the form of agglomerates, which are hard to be broken apart during compounding due to the strong interaction among the nanoparticles, the limited shear force provided by the mixing device and the high melt viscosity of polymer melts [9].

Fumed silica is a reinforcing filler for elastomers or rubber applications, used for improving the modulus, elongation and tensile strength. It is very effective for polymer systems since it provides very large surface area available for polymer/filler interaction due to the small particle size and open branched chain nature of the silica aggregates [15].

The second factor is the reactivity of the surface. During formation of fumed silica, hydroxyl groups become attached to some of the silicon atoms on the particle surface. This makes its surface hydrophilic and capable of hydrogen bonding with suitable molecules of materials in vapor, liquid or solid form [17]. The chemical groups occurring on the surface of fumed silica are the siloxane,

the isolated hydroxyl and the hydrogen-bonded hydroxyl groups. These groups are schematically shown in blue, purple and green in Figure 2.2 from left to right respectively.
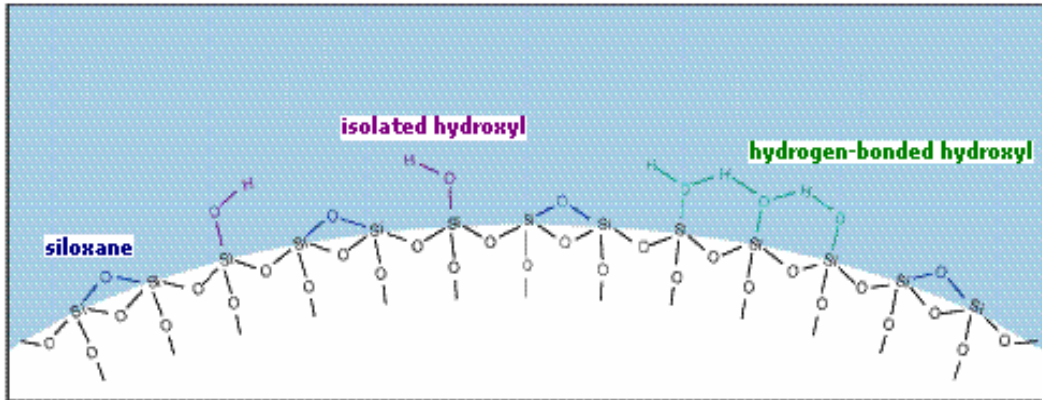
Figure 2.2 Typical groups which can occur on the fumed silica [17]

The presence of hydroxyl groups on the surface of the fumed silica is the key to the mechanism that makes it able to perform many of its functions [17].

2.5 Polyethylene (PE)

Polyethylene, being the major group of polyolefins, is the most popular plastic in the world. As well as being so versatile, it has the simplest structure among all commercial plastics. Schematic drawing of polymerization of polyethylene from ethylene monomer is given in Figure 2.3.

```
Initiator (R)₂  ............................................................... 2R'

R' + CH₂CH₂  ............................................................. RCH₂CH₂'


Propagation :  RCH₂CH₂' + CH₂CH₂ ...................................................... RCH₂CH₂CH₂CH₂'


Termination step occurs either by combination (1) or disproportion (2)

                    1        RCH₂CH₂' + 'CH₂CH₂R ............................................... RCH₂CH₂CH₂CH₂R
Termination :
                    2        RCH₂CH₂' + 'CH₂CH₂R ................................................ RCH₂CH₃  +  RCHCH₂
```
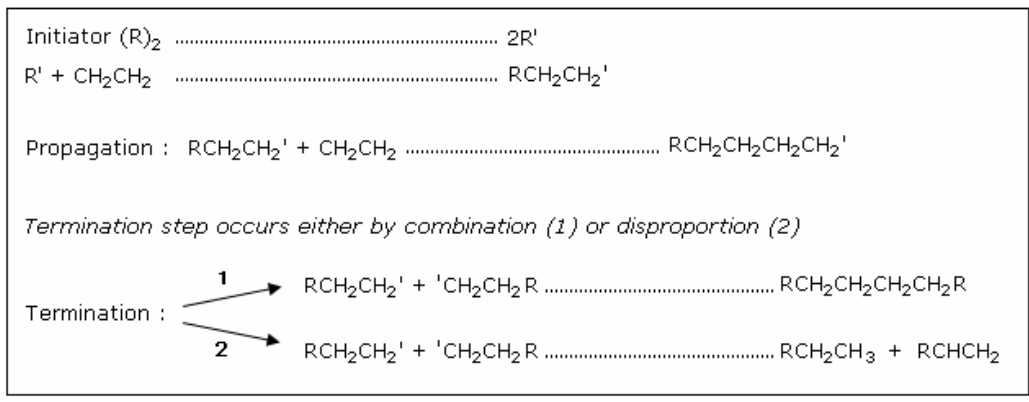
Figure 2.3 Schematic drawing of polymerization of polyethylene [18]

Polyethylene is popular since it is inexpensive, light, flexible and resistant to most solvents and has good toughness at low temperatures. Since the processing temperatures for many additives are limited to temperatures below 200°C, the use of polyethylene is preferable over many other thermoplastics due to its lower melting point. It is mostly used in films, molding, insulation, cable and pipe.

Polyethylene is classified into several different categories based mostly on its density and branching. Its simple basic structure, of ethylene monomers, can be linear as in high-density (HDPE) and ultrahigh-molecular-weight polyethylene (UHMWPE); or branched to a greater or lesser degree as in low-density (LDPE), linear low-density polyethylene (LLDPE) and medium density polyethylene (MDPE).

The branched polyethylenes have similar structural characteristics, properties and uses such as low crystalline content, high flexibility and use in packaging film, plastic bags, insulation, squeeze bottles, toys, and house wares. HDPE has a dense, highly crystalline structure of high strength and moderate stiffness; uses include bottles, boxes, barrels, and luggage. UHMWPE is made in molecular weights above 2×10^6 [19].

The most common types of polyethylene, their densities and branching properties are listed in Table 2.1. These different types are produced at high pressures and temperatures in the presence of any of several catalysts, depending on the desired properties for the finished product. The mechanical properties of polyethylene significantly depend on variables such as the extent and type of branching, the crystal structure, and the molecular weight.

Table 2.1 Types of polyethylene [20,21].

Name	Density Range (g/cm^3)	Degree of Branching
Low density PE (LDPE)	0.910 - 0.940	high degree of short and long chain branching
Linear low density PE (LLDPE)	0.915 - 0.925	significant numbers of short branches
Medium density PE (MDPE)	0.926 - 0.940	relatively low branching
High density PE (HDPE)	≥0.941	no branching

Density is a measure of crystallinity of the polymer which is an important parameter that affects product's stiffness, rigidity, environmental stress-crack resistance (ESCR) and barrier properties. The lower the crystallinity, and hence the density, the softer and more flexible the material is [22].

2.5.1 Low Density Polyethylene (LDPE)

Low Density Polyethylene (LDPE), the first thermoplastic polyolefin used commercially, was originally prepared in 1933 by the high pressure polymerization of ethylene [22]. After its discovery, LDPE quickly found war-time utility in high frequency cables for radar equipment. The balance of chemical inertness, thermal and environmental stability, ease of processing, physical properties, stiffness and optical properties made this polyolefin polymer useful in

a variety of applications after the war. LDPE is still one of the most useful plastics and predominantly used in film applications due to its toughness, flexibility and relative transparency. Its inert, nontoxic, safe characteristics make LDPE be extensively used in a variety of food contact and medical applications.

LDPE is also known as "high pressure, low density" or HPLD, because it is exclusively made by the high pressure process. LDPE is produced under high pressures between 81-276 MPa and high temperatures among 130-330°C with a free radical initiator, such as peroxide or oxygen. The polymerization mechanism is a free-radical reaction that leads to the formation of long-chain branches, which can be as long as the main polymer backbone. The free-radical mechanism also leads to the formation of short-chain branches, typically one to five carbon atoms long [22]. In LDPE, branching occurs on about 2% of the carbon atoms [20].

Typically, the crystallinity of LDPE is between 50-60% and that makes it useful for manufacture of flexible films such as those used for plastic bags, some flexible lids and bottles. LDPE is also widely used in wire and cable applications for its stable electrical properties and processing characteristics.

2.6 Compatibilizer

Compatibilizer is a polymeric additive that bonds the two phases to each other more tightly and modifies their interphases. It is used to increase the toughness of engineering plastics and compatibility of the fillers. A strong filler-matrix adhesion leads to enhanced strength of particulate composites and this can be provided by a suitable compatibilizer.

Since polyolefins are widely used economical thermoplastic polymers, it is beneficial to upgrade the properties of polyolefins by using some additives. However, because of their hydrophobic nonpolar structures, polyolefins are not able to make strong connections with polar hydrophilic fillers. In such cases, surface modification of the filler increases the miscibility, but the modification process requires the usage of some solvents which are not so advantageous economically and for the environment. Using compatibilizer shows the same effect as surface modification, without the disadvantages of using solvents [1].

A compatibilizer for the PE-silica system must be highly reactive to hydroxyl groups while at the same time having a non-polar chain preferably of the same type as the matrix [23]. These compatibilizers are suitable copolymers which act as emulsifying agents at the interfaces. Ethylene based compatibilizers, made by high pressure radical polymerization, are copolymers of ethylene and fully miscible with LDPE. Their chemical structure and long chain branching provide a good rheology during extrusion. The most widely used reactive functional groups to compatibilize these blends are acrylic ester and maleic anhydride which can react with the hydroxyl or carboxyl end groups [24].

In this study, ethylene/methyl acrylate/glycidyl methacrylate (E-MA-GMA) and ethylene/n butyl acrylate/maleic anhydride (E-nBA-MAH) terpolymers and ethylene/glycidyl methacrylate (E-GMA) copolymer are used as compatibilizers.

2.6.1 Acrylic Ester Functionality

Ethylene-acrylic ester polymers are used as compatibilizers due to the functionality of the acrylate monomers in its structure. Acrylate monomers are esters that contain vinyl groups, that is, two carbon atoms double bonded to each other, directly attached to the carbonyl carbon [20]. The structure of the acrylic ester monomers is represented in Figure 2.4.
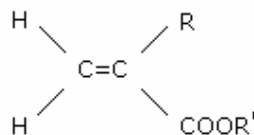
Figure 2.4 Acrylic ester structure

The group R represents H for acrylates and CH_3 for methacrylates. The identity and nature of the R and R′ groups determine the properties of both the monomer and the polymers formed. This R′ side-chain group conveys such a wide range of properties that acrylic ester polymers are used in applications varying from

paints to modifiers [25]. Ethylene acrylic ester polymers can be divided into several product families depending on the acrylic ester type; methyl, ethyl or butyl acrylate. The acrylic esters of the compatibilizers used in this study are methyl and n-butyl acrylate in which, R group is H and R' is CH_3 and C_4H_9 respectively.

The fluid resistance and low temperature properties of ethylene-acrylic elastomers are largely a function of the acrylic ester to ethylene ratio. As the acrylic ester level increases, the polymer has better fluid resistance to aliphatic hydrocarbon oils. Also, the glass transition temperature (T_g) of the polymer increases slightly [22].

These non-corrosive, low odor ethylene acrylates, decrease the crystallinity and increase the polarity of the polymer. They are chosen for improving impact resistance and increasing flexibility in engineering polymers, where a moderate to intermediate level of toughness is wanted at reasonable cost. Also they are preferred to increase the miscibility of fillers and polymers by making bonds with the active groups on filler surfaces.

The compatibilizers used in this study include glycidyl methacrylate (GMA) and maleic anhydride (MAH) active groups which highly increase the reactivity and adhesion. Both of these groups are expected to react with the hydroxyl groups found on the surface of the fumed silica.

2.6.1.1 Glycidyl Methacrylate (GMA) Functionality

Glycidyl methacrylate monomer offers dual functionality, containing both epoxy and acrylic groups. Acrylic and epoxy functionality means that GMA monomer can react with an extremely wide range of monomers and functionalized molecules, providing greater flexibility and freedom in polymer design. The chemical structure of GMA can be seen in Figure 2.5.
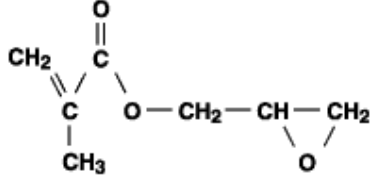
Figure 2.5 The chemical structure of GMA monomer

Acrylic and vinyl functionality allows copolymerization with a variety of other vinyl monomers in aqueous and nonaqueous systems. Resulting polymers feature a unique combination of epoxy functionality with an acrylic backbone.

Epoxy group allows structural modification of the polymer backbone that can result in differentiated properties and higher performance. Also, it enables crosslinking reactions with amines, carboxylic acids, anhydrides and hydroxyl groups [26].

2.6.1.2 Maleic Anhydride (MAH) Functionality

Maleic anhydride easily copolymerizes with acrylates and methacrylates in benzene or dioxane with or without photoinitiation [4]. This non-corrosive, highly polar, active group has a decreasing effect on crystallinity and also has excellent heat stability allowing high processing temperatures. Copolymerization with MAH improves the physicochemical properties of polymers by providing increased polarity, rigidity, T_g and functionality. MAH based functionality promotes hydrophilicity, adhesion, compatibility and provides a reactive group for possible reactions.

MAH increases adhesion to polar substrates and allows the creation of chemical bonds by introducing reactivity with -NH_2, -OH and epoxy groups of the polymer, substrate or filler. The cyclic structure of MAH is given in Figure 2.6.
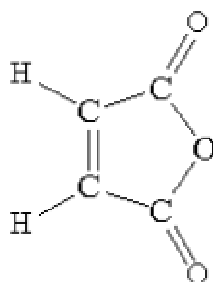
Figure 2.6 The chemical structure of MAH monomer

2.7 Thermoplastic Processing

A variety of thermoplastic polymer processing techniques are available to fabricate the desired thermoplastic product. Extrusion is the most popular and injection molding follows as a preferred processing method being used in all commodity thermoplastics sold worldwide [27,28].

2.7.1 Extrusion

Extrusion is the process of continuously forcing a viscous molten material through a shaping device. The feedstock usually enters the device in the form of solid particles as pellets, flake or powder. It may also be combinations of different kinds of pellets and/or fillers which may be premixed or fed separately from one or more feeders. Since the viscosity of most molten plastic materials is high, extrusion requires the development of pressure in order to force the plastic through a die. As a result of the extrusion, specific profiles can be obtained such as film, sheet, tubing, wire coating or as a molten tube of resin for blow molding or injection molding [4].

2.7.1.1 Extruder

Extruders are the most common machines in the plastics processing industry. They are used not only in extrusion operations, but also in most molding operations, for instance injection molding and blow molding. Essentially every

plastic part has gone through an extruder at one point or another; in many cases, more than once [22].
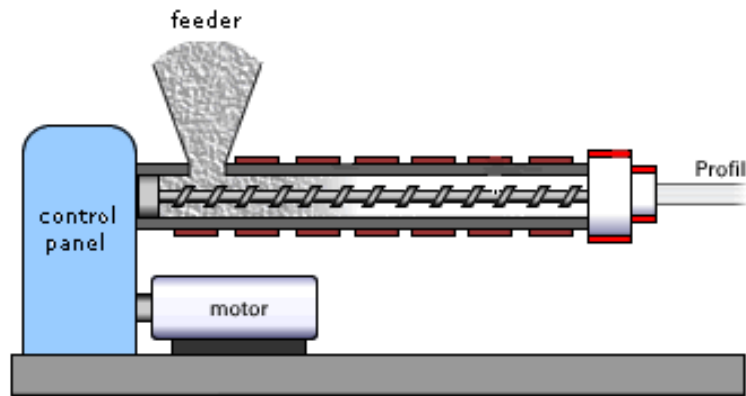
Figure 2.7 Schematic drawing of an extruder

To provide a homogeneous product, incorporation of any additives such as antioxidants, colorants, impact modifiers and fillers requires mixing them into the plastic when it is in molten state, which is done primarily in an extruder. Dry solid particles are fed to the extruder where they melt by the heat transfer through the barrel. In the act of melting, the required amount of mixing is usually achieved through the following sections along the barrel. Venting may also be applied, when removal of undesired volatile components is required. The final part of the extruder is used to develop the pressure for pumping the homogenized melt through the die into a shaping part [27].

2.7.1.2 Extruder Types

In the plastics industry, the most common extruders are the screw extruders, in which a screw rotates in a cylinder, causing a pumping action. These extruders may have one or more screws and are named as single screw extruder and multiscrew extruder respectively. The most common multiscrew extruder is the twin screw extruder with two screws. It provides better dispersion and is more suitable for reactive extrusion, although it is less popular than single screw

extruder in plastic processing industry. Reactive extrusion is the term used to describe the use of an extruder as a continuous reactor for polymerization or polymer modification by chemical reaction. Multiple processes can be achieved in an extruder such as melting, mixing, reacting, side-stream addition and venting [27].

There are several types of twin screw extruders. In most of them, the screws are located side by side. If the screws rotate in opposite directions, the extruder is called as counter rotating, if they both rotate in the same direction, it is called co-rotating twin screw extruder.

Extrusion of thermoplastic polymers has developed into an important plastic fabrication process, providing large growth opportunities for the plastic industry. Growing applications for coextrusion are in automotive, construction, appliance and food packaging markets [22].

2.7.2 Injection Molding

Injection molding is the plastic processing method, which is frequently chosen for production of large quantities of identical pieces. It is an important global manufacturing process for converting simple plastic, ceramic and metal parts into complex products [28].

The injection molding process starts with feeding the hopper with materials. The material can be a resin or combination of base resin and additives, such as fillers, colorants, etc. The material is molten by heat and is injected under high pressure into a relatively cold steel mold. Molten plastic fills the mold cavity and gets its shape when solidifies. When it sufficiently cools, the mold is opened and the shaped plastic is removed. A controller, usually a computer, coordinates and controls the various steps of the process.

There are three important parameters in the molding process, speed, temperature and pressure. An efficient molding requires constant viscosity. The best way to control the speed of the injection plunger accurately is to use computer-controlled machines with feedback systems. It is also easier to arrange

and control the process temperature and pressure with those machines. Since varying amounts of thermal energy are required to melt and increase the flowability of different plastics, melt and mold temperatures are set according to the characteristics of plastic used. The viscosity of the melt must be sufficiently low to allow the injection pressure to force the plastic into the mold. The pressure is applied gradually during the process and the mass of the polymer moves with a rate proportional to the applied stress. The period of the process cycle depends on the time required for melting and cooling of the material.

The injection molding provides low cost fabrication at high production rates. The process permits the manufacture of extremely small parts as well as the large ones.

2.8 Characterization

The design and analysis of composite structures rely heavily on experimental data. The composite materials are characterized according to the results of morphological, mechanical, thermal and flow experiments.

2.8.1 Morphological Analysis with SEM

Scanning electron microscope (SEM) has become commercially available since 1970s [4]. Due to the large depth of focus, greater resolution, and ease of sample preparation SEM has become one of the most heavily used instruments in research areas today [29]. SEM shows very detailed 3-dimensional images at much higher magnifications than is possible with a light microscope. The images created without light waves are reflected black and white.
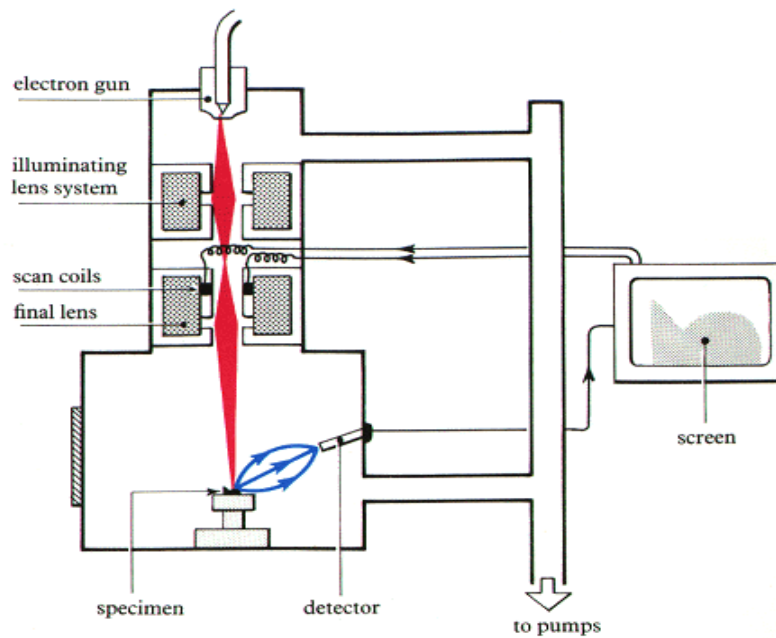
Figure 2.8 Schematic drawing of a SEM with secondary electrons forming the images on the screen [30]

As seen in Figure 2.8, SEM image is formed and presented by a beam of electrons generated under vacuum. That beam is collimated by electromagnetic condensor lenses, focused by an objective lens and scanned across the surface of the sample by electromagnetic deflection coils [31]. The samples have to be prepared carefully to withstand the vacuum and the nonconducting samples have to be made conductive by coating with a suitable material.

The primary imaging method is by collecting secondary electrons that are released by the sample. The secondary electrons are detected by a scintillation material that produces flashes of light from the electrons. The light flashes are then detected and amplified by a photomultiplier tube [31]. SEM yields the best results for observing morphological properties of structures.

2.8.2 Mechanical Tests

Owing to the improvement of polymer nanocomposites, polymers have become highly preferred materials in engineering applications with their improved mechanical properties. The measurement of mechanical properties is concerned with load-deformation or stress-strain relationships. The results of these tests are important to classify the polymeric material.

2.8.2.1 Tensile Test

The tensile test, probably the most fundamental type of mechanical test, is used to test the ductility of a material. In a tensile experiment, the specimen is gripped firmly by mechanical jaws on both sides and extended by a computer controlled tensile testing machine. Pulling is carried out at a constant rate depending on the type and dimensions of plastic being tested. Typical tensile testing machine and dog bone shaped sample used can be seen in Figure 2.9.
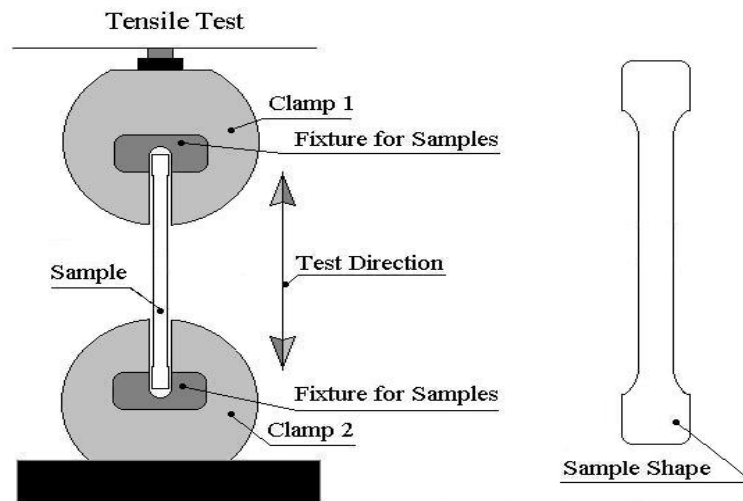
Figure 2.9 Tensile testing machine and test sample [32]

Tensile test is a measure of the withstanding ability of material to the force of pulling and shows the stretching amount of material until breaking. The tensile

profile of the sample is expressed in terms of a curve showing the reaction of the material against applied pulling force. Figure 2.10 shows a typical tensile test curve.
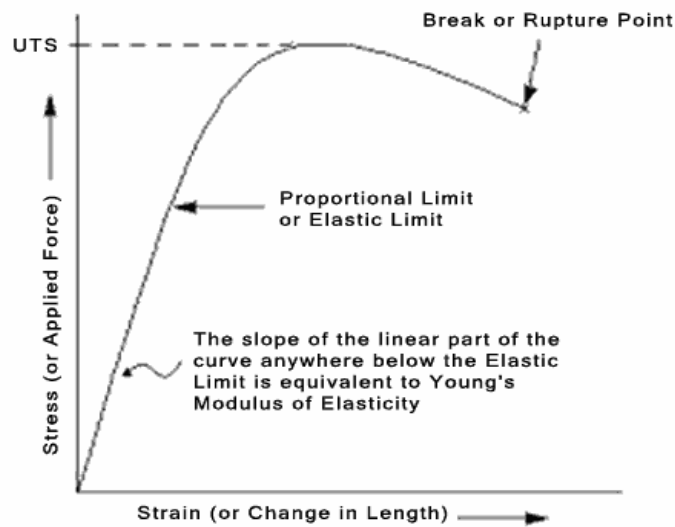
Figure 2.10 Typical tensile test curve [33]

For most tensile testing of materials, in the initial portion of the test, the relation between applied force, or load, and the elongation of the specimen is linear. The constant slope of this linear region is called as "Young's modulus" or "tensile modulus".

$$\text{Tensile Modulus } (E) = \frac{\Delta \text{Stress } (\sigma)}{\Delta \text{Strain } (\varepsilon)}$$

(2.1)

where stress is the force applied per unit area.

Stress $(\sigma) = F / A_0$

(2.2)

and strain is defined as the amount of deformation that the sample shows under stress. It is expressed as the ratio of the elongation to the original gage length.

$$\text{Strain } (\varepsilon) = \Delta L / L_0 \qquad\qquad (2.3)$$

Tensile strength is the force divided by the cross-sectional area of the specimen and expressed in terms of MPa.

$$\text{Tensile Strength} = \frac{\text{Force (F)}}{\text{Cross Sectional Area } (A_0)}$$

$$(2.4)$$

2.8.2.2 Flexural Test

The flexural test measures behavior of materials subjected to loading. There are two test types; 3-point and 4-point bending. The most common one for polymers is 3-point bending in which the specimen supported at both ends is loaded at midpoint as seen in Figure 2.11.
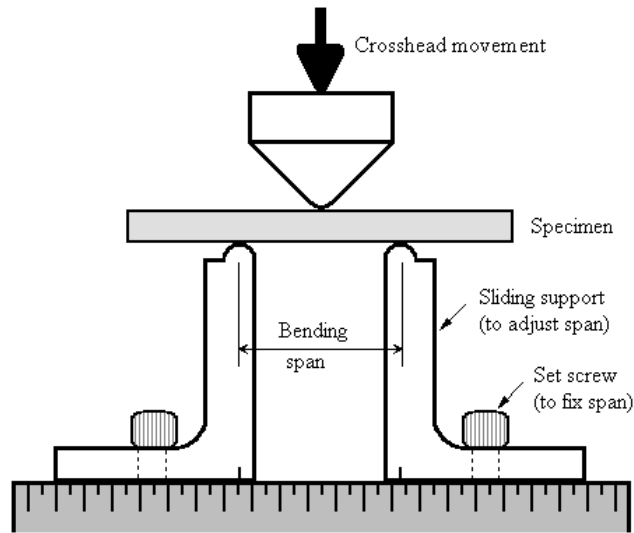
Figure 2.11 Flexural test set up [34]

In flexural test, the area of uniform stress is quite small and concentrated under the center loading point. The maximum stress (S) just before breaking shows the resistivity of the sample against bending force and is calculated by the following formula;

$$S = \frac{3FL}{2bd^2}$$

(2.5)

Where F is the force at given point on load-deflection curve, L is the length of support span, b and d are respectively the width and thickness of the specimen.
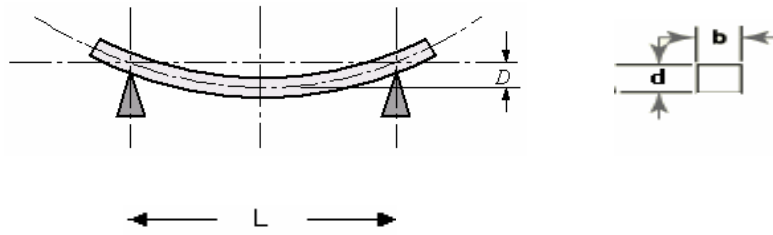
Figure 2.12 Maximum deflection (D) during flexure [34]

The maximum strain (r) due to bending is calculated as follows;

$$r = \frac{6Dd}{L^2}$$

(2.6)

D is the deflection at the center of beam showed in Figure 2.12, L is the length of support span and d is the thickness of the sample.

The flexural modulus or modulus of elasticity (E_B) is the ratio, within the elastic limit, of the applied stress to corresponding strain, and can be determined by using the slope (m) of the initial straight-line portion of the stress-strain curve in the following equation;

$$E_B = \frac{L^3 m}{4bd^3}$$

(2.7)

2.8.3 Thermal Analysis with DSC

Differential scanning calorimetry (DSC) is a thermo-analytical technique in which the difference in the amount of heat required to increase the temperature of a sample and reference are measured as a function of temperature [4]. DSC is the most common technique used to study the thermal transitions of a polymer, that is, the changes that take place in a polymer when heated. When thermal transition occurs in the sample, DSC provides a direct calorimetric measurement of the transition energy at the temperature of the transition [35].

A typical differential scanning calorimeter, as shown in Figure 2.13, consists of two sealed pans: a sample pan and a reference pan which is mostly left empty, using air as the reference. During the experiment, the sample and reference are both maintained at the same temperature. Usually, the computer program is set to increase the sample pan temperature linearly as a function of time.
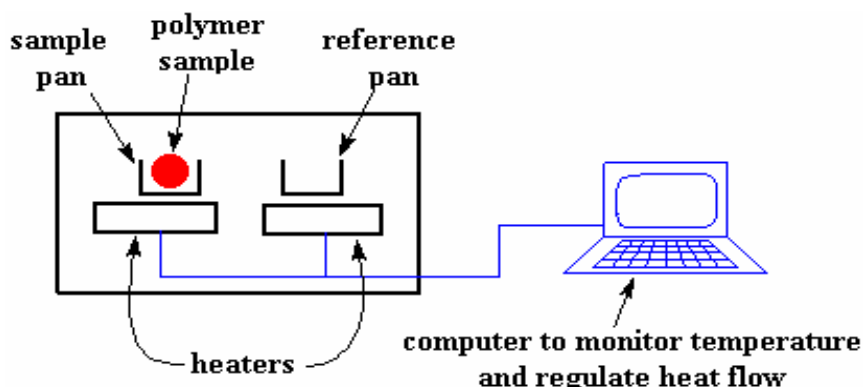
Figure 2.13 Schematic drawing of a DSC [36]

When the sample undergoes a physical transformation such as phase transitions, more (or less) heat will be transferred to it, than the reference to maintain both at the same temperature. During the experiment, the instrument detects differences in the heat flow between the sample and reference and this information is sent to an output device, mostly a computer. The basic principle underlying this technique is that, this information is expressed in a plot of the

differential heat flow between the reference and sample cell as a function of temperature. A sample plot is given in Figure 2.14.
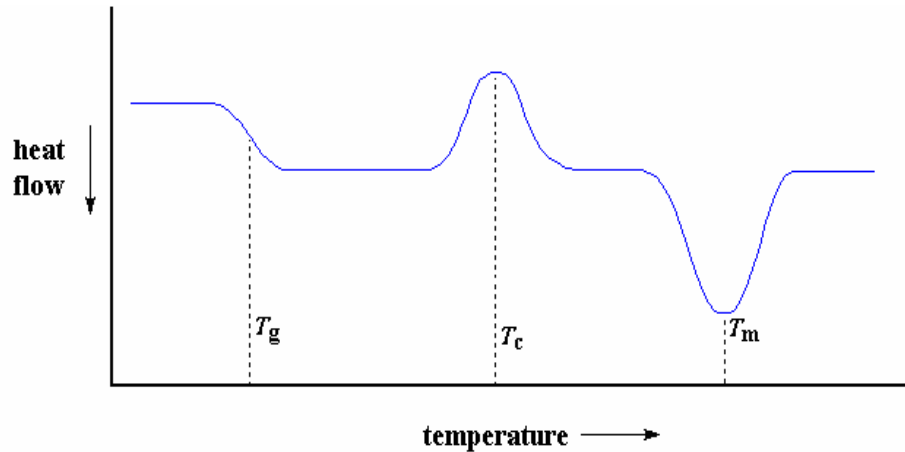
Figure 2.14 A schematic DSC curve demonstrating the appearance of several common features

This curve can be used to calculate enthalpies of transitions, such as the glass transition temperature (T_g), crystallization temperature (T_c) and melting point (T_m) and percent crystallization by using Equation 2.8.

$$\% \text{ Crystallinity} = \frac{\Delta H_{observed}}{\text{Weight fraction of polymer} \times \Delta H_{polymer}} \times 100$$

(2.8)

In this equation $\Delta H_{observed}$ is the enthalpy read from the DSC plot of the sample and ΔH_{LDPE} is the enthalpy of 100% crystalline LDPE.

The crystallization dip and the melting peak will only show up for polymers that can form crystals. Completely amorphous polymers won't show any

crystallization, or any melting either. But polymers with both crystalline and amorphous domains will show all the features seen in Figure 2.14.

2.8.4 Melt Viscosity Measurement with MFI

The Melt Flow Index (MFI) is a measure of the ease of melt thermoplastic polymer flow. The principle of this test is to determine the weight of polymer in grams flowing in 10 minutes through a capillary of specific dimensions. The pressure applied to push the melt is obtained with specific weights defined in related ASTM and ISO standards for alternative temperatures and polymers. The schematic drawing of MFI is given in Figure 2.15.
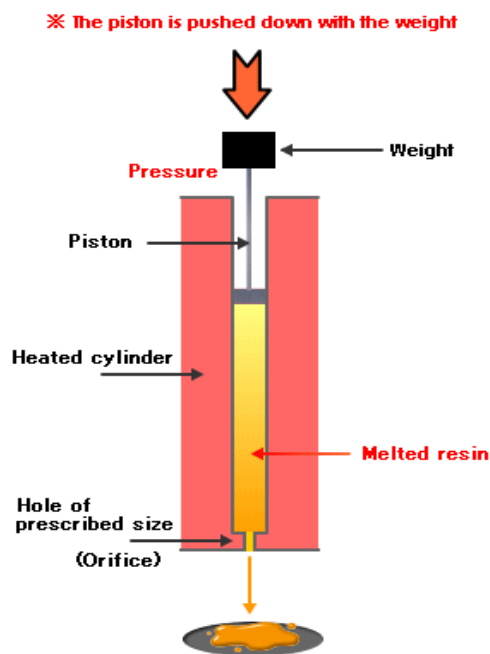
Figure 2.15 Schematic drawing of a melt flow indexer [37]

The melt flow rate is a measure of the ability of the material's melt to flow under pressure and it is inversely proportional to the viscosity of the melt at the conditions of the test.

Melt flow rate is very commonly used for polyolefins, polyethylene being measured at 190°C and polypropylene at 220 °C [20].

2.9 Previous Studies

Zhang et al. [38] worked on silica nanoparticles loaded PP composites prepared by industrial scale twin-screw extruder and injection molding machine. The results of tensile tests indicated that the nanoparticles provided PP with stiffening, strengthening and toughening effects at rather low filler content typically 0.5% by volume. They found that the presence of grafting polymers on the nanoparticles improves the tolerability of the composite and the tensile performance is highly dependent on loading rate.

Zhang et al. [9] studied the mechanical performance of nano-silica/PP composites. Unlike the fumed nano-silica used in the previous study, precipitated nano-silica is employed in this study. The nanoparticles were firstly compounded with PP with a two-roll and then mixed with neat PP through a twin-screw extruder before injection molded into dog-bone-shaped tensile bars. For carrying out the effective graft polymerization pretreatment onto the nano-silica particles; styrene, methyl methacrylate, ethyl acrylate and butyl acrylate, were used as grafting monomers. It is found that both treated and untreated nano-silica lead to an overall improvement of the composites' properties while grafted nanoparticles become more efficient to improve the strength and toughness of the composites among which acrylic polymers-grafted nano-silicas are more effective. The addition of nano-silica into PP results in reduced values of elongation-to-break and area under tensile stress–strain curve, no matter the particles have been treated or not. Comparing fumed and precipitated nano-silica, it is found that precipitated nano-silica of 10 nm gave higher results of impact strength and elongation values than the fumed nano-silica of 15 nm,

while fumed silica gave better result in tensile strength and Young's modulus values of both were almost same.

Rong et al. [39] reported the results of their study on nano-SiO_2/PP composites in relation to percolation mechanism. Nanoparticles of SiO_2 were grafted by styrene and melt mixed with PP in a single-screw extruder before compression molding. They found that, with a rise in filler content, the strength of the nanocomposites first increased and then remained unchanged. The critical filler volume content for a brittle-tough transition was determined to be around 1.03 vol.%. It was also found that, for a sufficient interfacial adhesion in case of brittle-tough transition, using smaller particles decreases required particle amount.

Karayannidis et al. [40] studied isotactic PP/SiO_2 nanocomposites with untreated and treated nanoparticles of 1, 2.5, 5, 7.5, and 10 wt.% SiO_2 prepared by melt mixing on a co rotating twin-screw extruder. Tensile and impact strength were found to be increased and affected mainly by the type and content of silica nanoparticles. They also determined that, increasing the amount of nanoparticles causes the formation of large agglomerates causing the reduction of mechanical properties with higher concentrations of SiO_2. Aggregates of surface-treated nanoparticles were observed to be larger, negatively affecting the mechanical properties. According to the results of DSC measurements, silica nanoparticles act as effective nucleating agents, increasing the crystallization rate and the degree of crystallinity of IPP.

Friedrich et al. [35] used isotactic PP homopolymer as the matrix and fumed silica as the fillers to prepare nanocomposites. To improve the reactivity, SiO_2 was pretreated by a g-methacryloxypropyl trimethoxy silane coupling agent, while commercial butyl acrylate was used as grafting monomer and trimethylolpropane triacrylate as crosslinking agent. The components were ground by a planetary ball before they were melt mixed in the mixer and injection molded. Comparison of effects of pretreated and untreated silicas, shows that the impact toughness and the tensile strength of the composites can be improved greatly when crosslinking agents are used, indicating that the nanoparticles indeed have toughening and reinforcing effects on PP due to the

enhanced interaction by the networks of cross-linked poly(butyl acrylate) and polypropylene phase.

Wu et al. [29] worked on acrylic-based polyurethane coatings with nano-silica and micro-silica. The results showed that, silicon atoms don't exist at the surfaces or the interfaces of coatings, reside inside the coatings. The tensile strength and modulus were enhanced with increasing content of nano-silica. However, the elongation at break decreased as nano-silica content increased. The performance of nano-silica was observed to be higher than that of micro-silica as a result of its greater specific surface area.

Xu et al [41] produced PE/maleic anhydride grafted PE/organic montmorillonite nanocomposites by melt blending and solution blending. According to their investigation, the intercalation of nanocomposites was enhanced by increasing the amount of the compatibilizer to certain extent and then decreased. Maximum tensile strength was obtained with 6% of compatibilizer concentration and maximum impact strength was obtained at 9% compatibilizer content.

Morawiec et al. [42] prepared LDPE nanocomposites containing 3 and 6 wt. % of organomodified montmorillonite clay and maleic anhydride grafted low density polyethylene as a compatibilizer by melt blending. As a result of this investigation it was found that the presence of the compatibilizer highly affects the mechanical properties. Maleic anhydride grafted polyethylene promotes the exfoliation of the clay and toughens the polymer matrix by increasing the adhesion.

CHAPTER 3

EXPERIMENTAL

3.1 Materials

3.1.1 Low Density Polyethylene

The matrix polymer used in this study was the low density polyethylene with the commercial name of Petilen G03-5 which is a product of Petkim Petrokimya Holding A.Ş, İzmir, Turkey. The chemical structure of LDPE is shown in Figure 3.1 and some properties of the used LDPE; Petilen G03-5 are given in Table 3.1.

Figure 3.1 Chemical structure of LDPE

Table 3.1 Properties of Petilen G 03-5 LDPE

Property	Value
Melt Flow Rate (2160 g, 190°C) ASTM D-1238, TS-1675	0.2-0.4 g/10 min
Density, 23°C ASTM D-1505, TS-1818	0.919-0.923 g/cm3

3.1.2 Fumed Silica

The filler used in this study was the fumed silica with a commercial name of Cab-o-sil® M5 which was purchased from Cabot Corporation, U.S.A. Amount of Cab-o-sil® was one of the process parameters. It was used as 2% and 5% in the composites. The chemical structure of fumed silica is SiO_2 which is shown in Figure 3.2. The properties of Cab-o-sil® M5, the fumed silica used are given in Table 3.2.
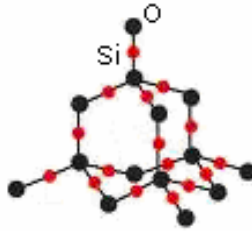
Figure 3.2 Chemical structure of SiO_2

Table 3.2 Properties of Cab-o-sil® M5 [15]

Property	Value
B.E.T. Surface Area	200 m^2/g
pH (4% aqueous slurry)	3.7–4.3
Specific Gravity	2.2
Bulk Density	50 g/L
Boiling Point	2230 °C
Melting Point	1700 °C

3.1.3 Compatibilizers

Three types of Lotader® resins named; Lotader® AX8840, Lotader® AX8900 and Lotader® 2210 were used as compatibilizers in this study which were purchased from Arkema Inc., France. These compatibilizers were selected since they are easy to use and can be blended with PE in various proportions. Lotader® resins are reactive polyethylenes including acrylic esters with a reactive functionality. This reactive group can be either maleic anhydride (MAH) which is very polar and give chemical reactions with -NH$_2$, -OH and epoxy groups, or glycidyl methacrylate (GMA) including acrylic and epoxy groups that can react on COOH, -OH, -NH$_2$. The acrylic ester that decreases the crystallinity of the polymer and improves its mechanical, thermal and flow properties can be methyl or butyl acrylate. Lotader® AX8840 is Ethylene – Glycidyl Methacrylate (E-GMA) copolymer and its chemical structure is shown in Figure 3.3. The chemical structures of Lotader® AX8900, which is Ethylene – Methyl Acrylate – Glycidyl Methacrylate (E-MA-GMA) terpolymer and Lotader® 2210, which is Ethylene – nButyl Acrylate – Maleic Anhydride (E-nBA-MAH) terpolymer, are shown in Figure 3.4 and Figure 3.5 respectively.
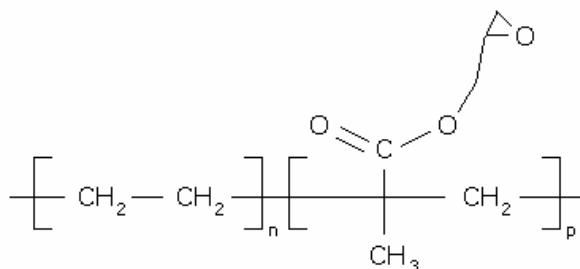
Figure 3.3 Chemical structure of Lotader® AX8840 (E-GMA)
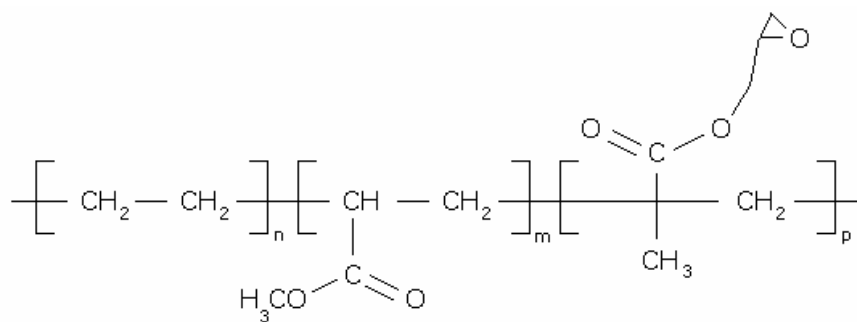
Figure 3.4 Chemical structure of Lotader® AX8900 (E-MA-GMA)
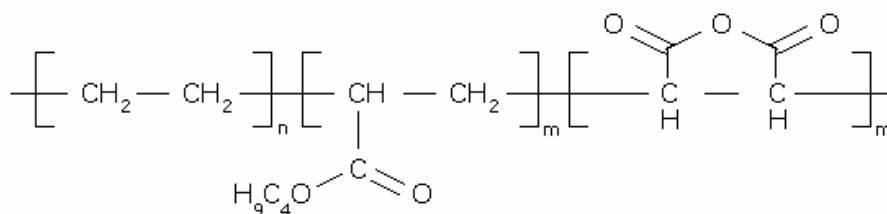
Figure 3.5 Chemical structure of Lotader® 2210 (E-nBA-MAH)

These compatibilizers have excellent thermal stability and thus, no corrosion occurs during processing. The properties of these Lotader® resins are given in Table 3.3.

Table 3.3 Properties of compatibilizers

Lotader® / Property	AX8840 (E-GMA)	AX8900 (E-MA-GMA)	2210 (E-nBA-MAH)
Melt Index (g/10 min.) (190°C, 2.1kg, ASTM 1238)	5	6	3
Melting Point (°C) (DSC)	105	60	107
Vicat Point (°C) (ASTM1525-1kg)	87	<40	80
Methyl Acrylate Content (W%)	-	25	-
GMA Content (W%)	8	8	0
nBA Content (W%)	-	-	6
Maleic Anhydride Content (W%)	-	-	3
Tensile Strength at Break (MPa) (ASTM D638)	8	4	12
Elongation at Break (%) (ASTM D638)	420	1100	600

3.2 Experimental Procedure

3.2.1 Melt Compounding

In this study, the nanocomposites were prepared by melt intercalation method, using Thermoprism TSE 16 TC co-rotating twin screw extruder. The L/D ratio of this extruder is 24, with barrel length of 384 mm and screw diameter of 16 mm. Figure 3.6 shows the extruder with the control panel and its screws.
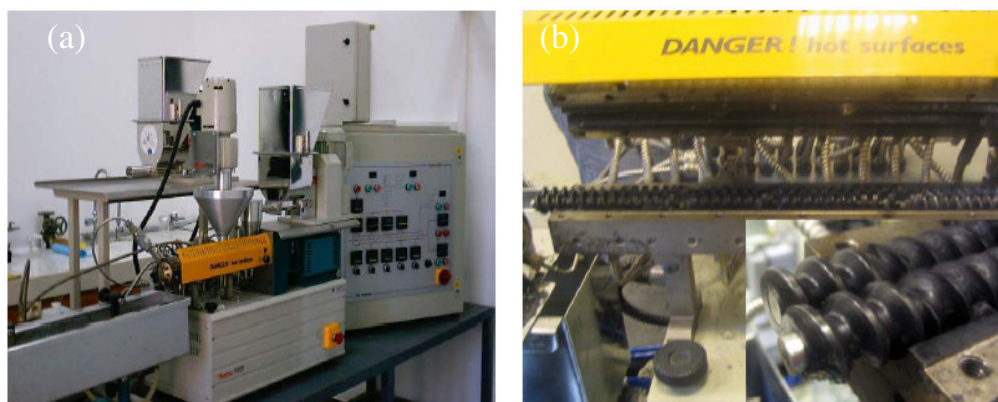
Figure 3.6 Thermoprism TSE 16 TC co-rotating twin screw extruder(a) and its screws(b)

The materials were dried at temperatures as given in Table 3.4 before the extrusion to avoid the unwanted side effects of residual moisture.

Table 3.4 Drying conditions of materials

		Material	Temperature	Time
Pre-1st Extrusion		LDPE	—	—
		Lotader® AX8840	40 °C	12 h
		Lotader® AX8900		
		Lotader® 2210		
		Cab-o-sil®	120 °C	4 h
Pre-2nd Extrusion		LDPE	100 °C	12 h
		LDPE + Lotader® + Cab-o-sil®		
		LDPE + Lotader®		
		LDPE + Cab-o-sil®		
		Lotader® + Cab-o-sil®	40 °C	
Pre-Injection		All samples	100 °C	12 h

The nanocomposites prepared were extruded twice, all with the same extrusion parameters at a flow rate of 10 g/min with 200 rpm/min screw speed. The extrusion temperatures of inlet, three mixing zones and die were set as shown in Table 3.5.

Table 3.5 Extrusion temperatures

	Temperatures($°C$)				
	Inlet	Mixing Zones			Die
Systems including LDPE	170	210	210	210	220
Lotader® + Cab-o-sil® Systems	170	190	190	190	200

The flow chart of the experimental process is given in Figure 3.7.
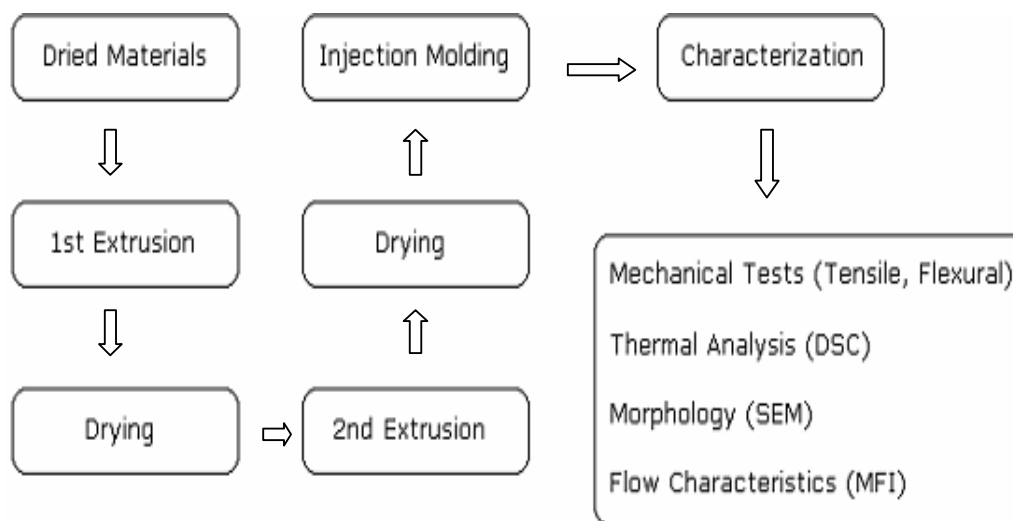
Figure 3.7 Flow chart of the experimental process

The temperatures and screw speed were adjusted from the control panel before the experiments and the feed rates of the first and second feeders were calibrated according to the raw material proportions of the composites. LDPE and compatibilizer were fed from the main feeder and the fumed silica was fed from the side feeder. Hot molten mixture obtained was passed through the cold water bath. Cooled solid product was dried with an air blower and pelletized.

3.2.1.1 Feeding Order of Components

Feeding order of the components was one of the parameters during the experiments. In the first run, all components were fed simultaneously. Afterwards, two of the components were blended and the third component was added at the second extrusion. Four different feeding orders were performed during experiments. Sets were performed with 2 and 5% of silica for 5% of the three types of compatibilizers.

In the first set of experiments, all components were fed at the same time. LDPE and Lotader$^®$ were mixed and fed from the main feeder while silica was fed simultaneously from the side feeder. This simultaneous feeding process is abbreviated as SF.

For the second set of experiments, LDPE and Lotader$^®$ were mixed at desired ratio and fed from the main feeder. In the second part of this set, the pellets obtained from the first extrusion were fed from the main feeder while fumed silica was fed from the side feeder. This experiment set is represented by FO1.

In the third set of experiments, LDPE fed from the main feeder was mixed with the silica fed from the side feeder. Pellets of this product were mixed with Lotader$^®$ and this mixture was fed from the main feeder for the second extrusion. Similarly this set is called FO2.

The fourth set of experiments, which will be represented by FO3, could only be carried out with 2% of silica and 5% of Lotader$^®$ 2210. In this set, the compatibilizer was fed from the main feeder and the silica was fed from the side feeder in the first extrusion. Afterwards, LDPE was added to the pellets of the

first extrusion and the mixture was fed from the main feeder. For 5% silica, compatibilizer amount was insufficient and the extruder was choked. The same problem occurred during the experiments with Lotader® AX 8840 and Lotader® AX 8900 with 2% silica, thus those sets could not be prepared either.

The addition order of the components and their proportions are given in Table 3.6. The components in parenthesis were extruded in the first part and the other component is added in the second extrusion.

Table 3.6 Feeding order of components and their proportions

Run	Abbreviation	Feeding Order	Proportions Used
1	SF	(LDPE + Lotader® + Cab-o-sil®)	(93% + 5% + 2%)
			(90% + 5% + 5%)
2	FO1	(LDPE + Lotader®) + Cab-o-sil®	(93% + 5%) + 2%
			(90% + 5%) + 5%
3	FO2	(LDPE + Cab-o-sil®) + Lotader®	(93% + 2%) + 5%
			(90% + 5%) + 5%
4[*]	FO3	(Lotader® + Cab-o-sil®) + LDPE	(5% + 2%) + 93%
			—

[*]This set was achieved only for Lotader® 2210

3.2.2 Sample Preparation

Samples were prepared with DSM Micro 10cc injection molding machine, seen in Figure 3.8. The temperatures of the process are given in Table 3.7 while the pressure profile and application periods are given in Table 3.8. Injection molding machine was set to these parameters and all samples were held for 2 minutes to melt before the injection process.

Figure 3.8 Injection molding machine

Table 3.7 Injection molding temperatures

Parameter	Value
Mold Temperature	30 °C
Melt Temperature	220 °C

Table 3.8 Pressures applied during injection molding process

	Pressure (bar)	Time (sec)
Step 1	5.0	0.0
Step 2	5.0	5.0
Step 3	15.0	0.0
Step 4	15.0	14.0
Step 5	0.0	0.0

3.3 Characterization

Morphological, mechanical, thermal properties and flow characteristics of the nanocomposites were determined in order to investigate the effect of different amounts of fumed silica, compatibilizer and their addition order on their properties.

3.3.1 Morphological Analysis

The morphology of the samples were investigated by scanning electron microscopy (SEM). The fractured surfaces of the samples were obtained by cracking them after liquid nitrogen application. The surfaces of these samples were coated with a thin gold layer in order to obtain a conductive surface. The micrographs of the samples were taken by JEOL JSM-6400 low vacuum SEM shown in Figure 3.9 at magnifications of ×250 and ×3000.

Figure 3.9 JEOL JSM-6400 low vacuum SEM

3.3.2 Mechanical Analysis

Tensile and flexural tests of the specimens were performed at room temperature by Lloyd LS 5000, computer controlled mechanical testing machine , which is

shown in Figure 3.10. For each composition, at least five samples were tested and the average and standard deviations of the sets were calculated.

Figure 3.10 Lloyd LS 5000, computer controlled mechanical testing machine

3.3.2.1 Tensile Tests

Tensile tests of the dog bone shaped specimens were performed according to ASTM D638M-91a (Standard Test Method for Tensile Properties of Plastics). The shape and dimensions of the specimens are given in Figure 3.9. The crosshead speed of 0.43 cm/min was calculated according to the ASTM standard with a strain rate of 0.1 min^{-1}. Tensile strength, Young's modulus and strain at break values of the specimens were calculated. The shape and dimensions of tensile test specimens are given in Figure 3.11 and Table 3.9 respectively.
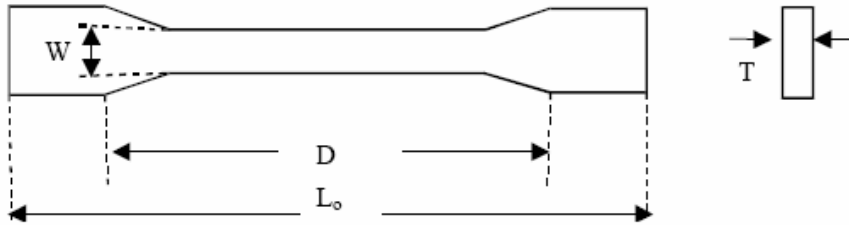
Figure 3.11 Tensile test specimen

Table 3.9 Tensile test specimen dimensions

Symbol	Dimensions (mm)
L_0: Specimen length	80
D: Distance between grips	43
W: Width of narrow section	4
T: Thickness	2

3.3.2.2 Flexural Tests

Three-point bending tests were performed on rectangular specimens according to, Test-Method 1 Procedure A of ASTM D790M-92 (Standard Test Methods for Flexural Properties of Unreinforced and Reinforced Plastics and Electrical Insulating Materials). The shape and dimensions of the specimens are given in Figure 3.12, where the support span length (L) is determined as 64 mm and the rate of crosshead motion is calculated as 17 mm/min. The strain rate corresponding to these conditions is, 0.1 min^{-1}.
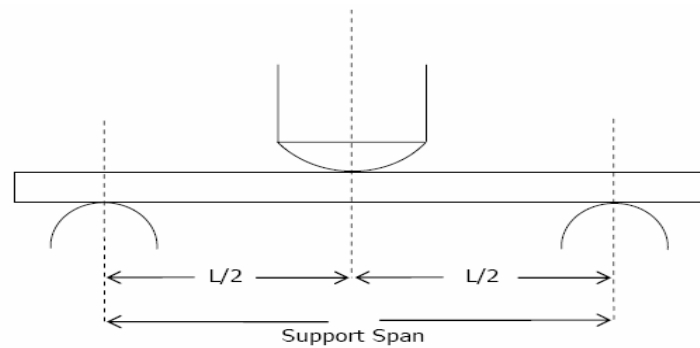
Figure 3.12 3-Point bending flexural test diagram

3.3.3 Thermal Analysis

The thermal properties of the nanocomposites were investigated by General V4.1.C DuPont 2000 differential scanning calorimeter (DSC). The measurements were carried out between 30-300°C temperature range with a heating rate of 10°C/min under nitrogen atmosphere. The effect of the filler content, compatibilizers and preparation method of the composites were investigated according to the changes in T_m. Melting points of samples were determined by using DSC curves and the degree of crystallinity values were calculated according to Equation 2.8, taking the heat of fusion (ΔH) for 100 % crystalline LDPE as 293 J/g [42].

3.3.4 Flow Characteristics

The flow characteristics of the nanocomposites were investigated by melt flow index (MFI) test using Omega Melt Flow Indexer shown in Figure 3.13. The tests were performed at 190°C with a 5kg load according to ISO 1133:1991 (E) standard. The mass flow rates of the samples were determined as g/10 min.

Figure 3.13 Omega melt flow indexer

CHAPTER 4

RESULTS AND DISCUSSION

4.1 Morphological Analysis with SEM

In order to examine the effect of fumed silica nanofiller and compatibilizer on the morphology of the LDPE, scanning electron microscopy (SEM) analysis were performed on the fractured surfaces of the samples prepared by liquid nitrogen. Each sample is discussed with two SEM images of different magnifications as x250 and x3000.

In the SEM micrographs of nanocomposites, fumed silica nanoparticles and agglomerates can easily be observed and it is also seen that the compatibilizer has an important role in dispersion of the silica throughout the polymer matrix.

Figure 4.1 shows the fractured surfaces of pure LDPE at x250 and x3000 magnifications where few crack propagation lines can be observed. These SEM images showing the smooth surface of twice extruded LDPE are used as reference for the investigation of the morphological changes.
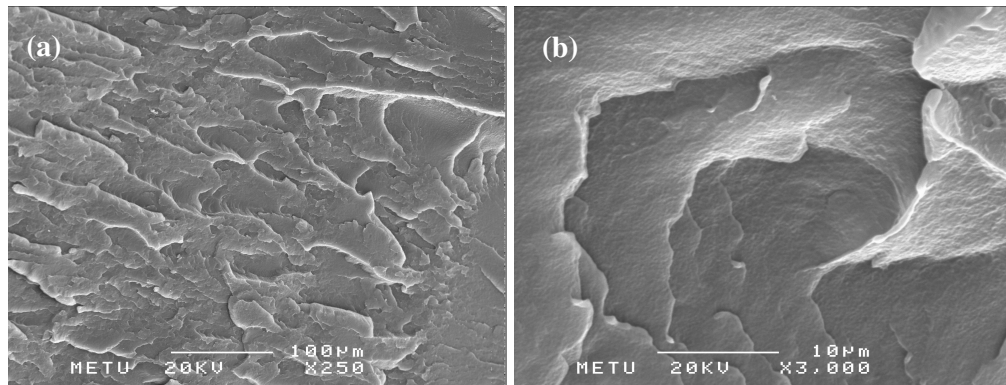
Figure 4.1 SEM micrographs of pure LDPE at (a) x250 (b) x3000 magnifications.

Figure 4.2 shows the fractured surfaces of LDPE/Cabosil® M5 nanocomposites containing 2 and 5 weight per cent of fumed silica. It is observed that the smooth surface of the LDPE disappears with the addition of fumed silica.

The x250 magnification of 5 wt.% silica containing nanocomposite shows almost straight and more ordered crack propagation lines than the x250 magnification of 2 wt.% silica containing nanocomposite. Comparing the x3000 magnifications of two nanocomposites, smaller nanoparticles can be seen in nanocomposite containing 2 wt.% silica, while an agglomerate can be observed in 5 wt.% silica containing nanocomposite.
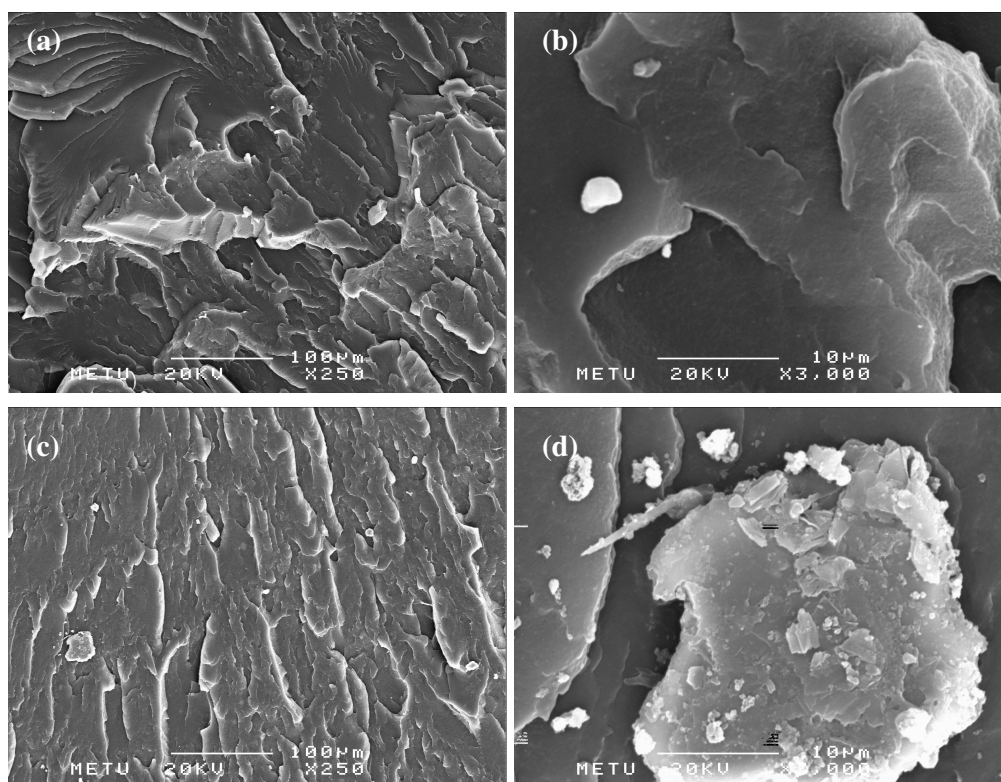
Figure 4.2 SEM micrographs of LDPE/Cabosil® M5 nanocomposites containing fumed silica (a) 2 wt.% x250 (b) 2 wt.% x3000 (c) 5 wt.% x250 (d) 5 wt.% x3000.

Figures 4.3, 4.4 and 4.5 show the SEM micrographs of LDPE/E-nBA-MAH, LDPE/E-GMA and LDPE/E-MA-GMA blends respectively with 5 wt.% compatibilizer composition at magnifications of x250, and x3000. The compatibility of the compatibilizers with LDPE is observed by the continuous phases seen in these images.
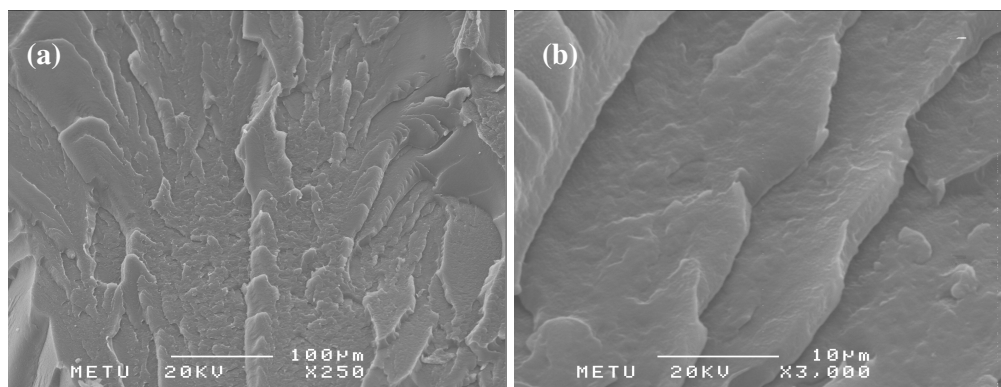
Figure 4.3 SEM micrographs of LDPE/Lotader® 2210 (E-nBA-MAH) blend containing 5 wt.% compatibilizer at (a) x250 (b) x3000.
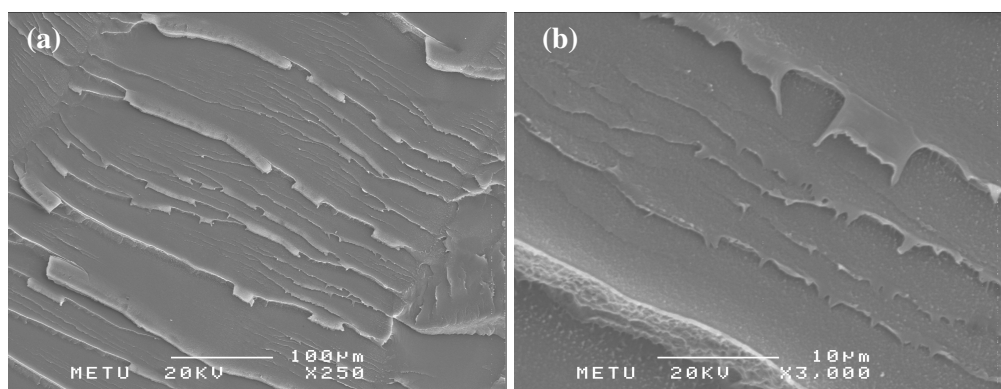
Figure 4.4 SEM micrographs of LDPE/Lotader® AX 8840 (LDPE/E-GMA) blend containing 5 wt.% compatibilizer at (a) x250 (b) x3000.
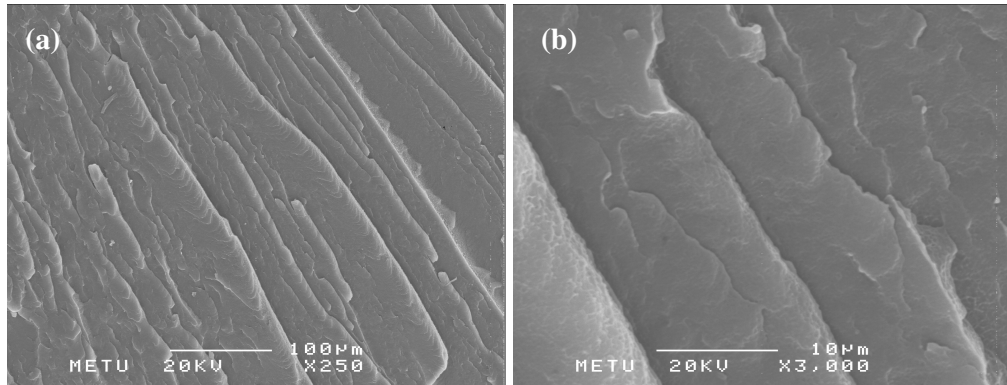
Figure 4.5 SEM micrographs of LDPE/Lotader® AX 8900 (LDPE/E-MA-GMA) blend containing 5 wt.% compatibilizer at (a) x250 (b) x3000.

In Figures 4.6 to 4.8, SEM micrographs of fracture surfaces of simultaneously fed ternary LDPE/compatibilizer/fumed silica nanocomposites are given, in which all the components are fed to the extruder at the same time and extruded twice. The images belong to LDPE/Lotader® 2210/Cabosil® M5, LDPE/Lotader® AX8840/Cabosil® M5 and LDPE/Lotader® AX8900/Cabosil® M5 nanocomposites respectively with 2 and 5% of fumed silica. Comparing with SEM micrographs of LDPE/Cabosil® M5 nanocomposites, the addition of compatibilizer increases the miscibility of materials resulting in improved mechanical properties.

Typical fumed silica agglomerate with its grape-like particulate structure can be observed in Figure 4.7 (a) and (b) with x250 and x3000 magnifications respectively. High level of agglomeration of nanoparticles decreases the mechanical properties. Agglomerates are the weak points in a material and can not resist to a stress applied. Also, as agglomerates are larger than primary particles, they produce weaker materials than composites containing dispersed particles [1].
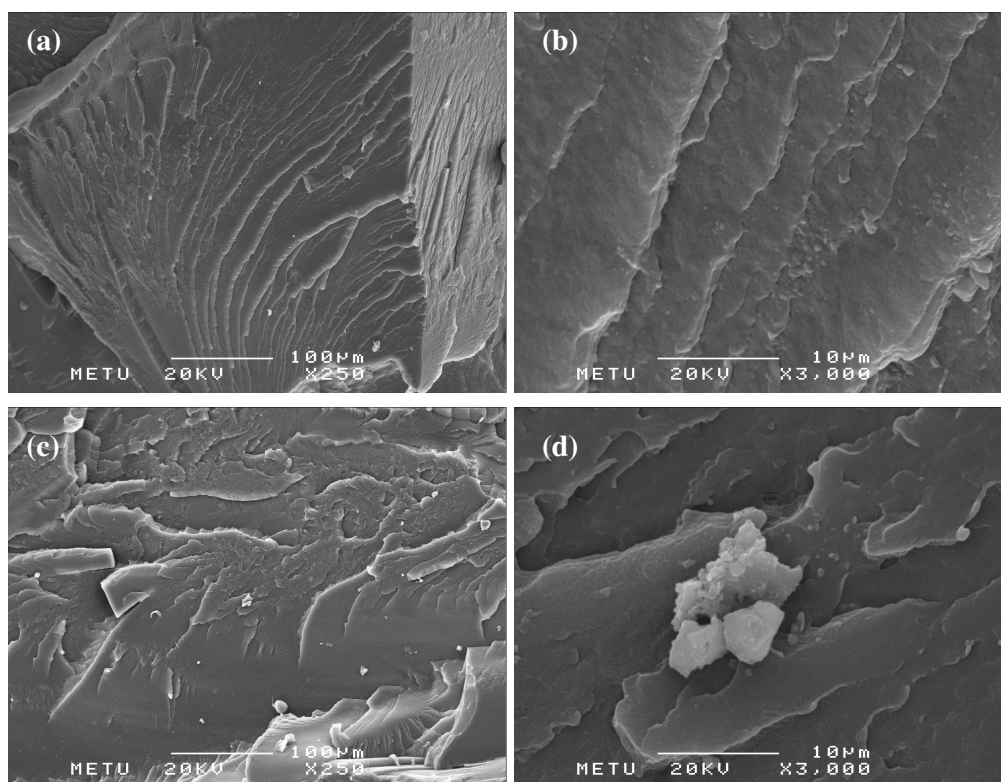
Figure 4.6 SEM micrographs of LDPE/Lotader® 2210/Cabosil® M5 nanocomposites having filler ratios of (a) 2 wt.% x250 (b) 2 wt.% x3000 (c) 5 wt.% x250 (d) 5 wt.% x3000.
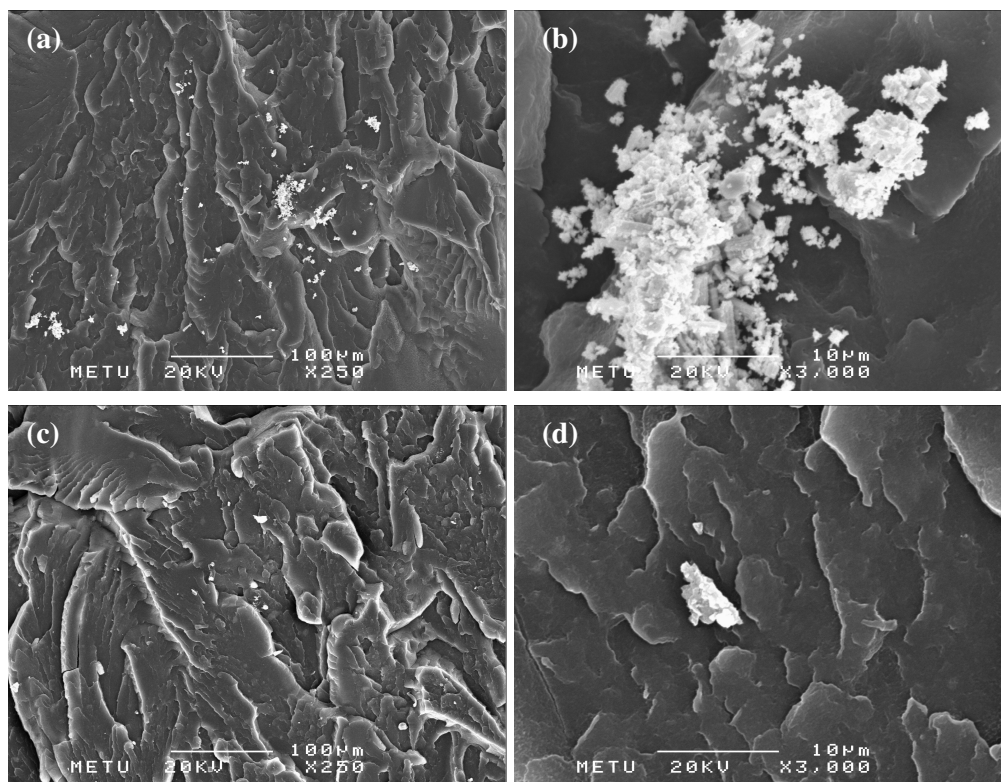
Figure 4.7 SEM micrographs of LDPE/Lotader® AX 8840/Cabosil® M5 nanocomposites having filler ratios of (a) 2 wt.% x250 (b) 2 wt.% x3000 (c) 5 wt.% x250 (d) 5 wt.% x3000.
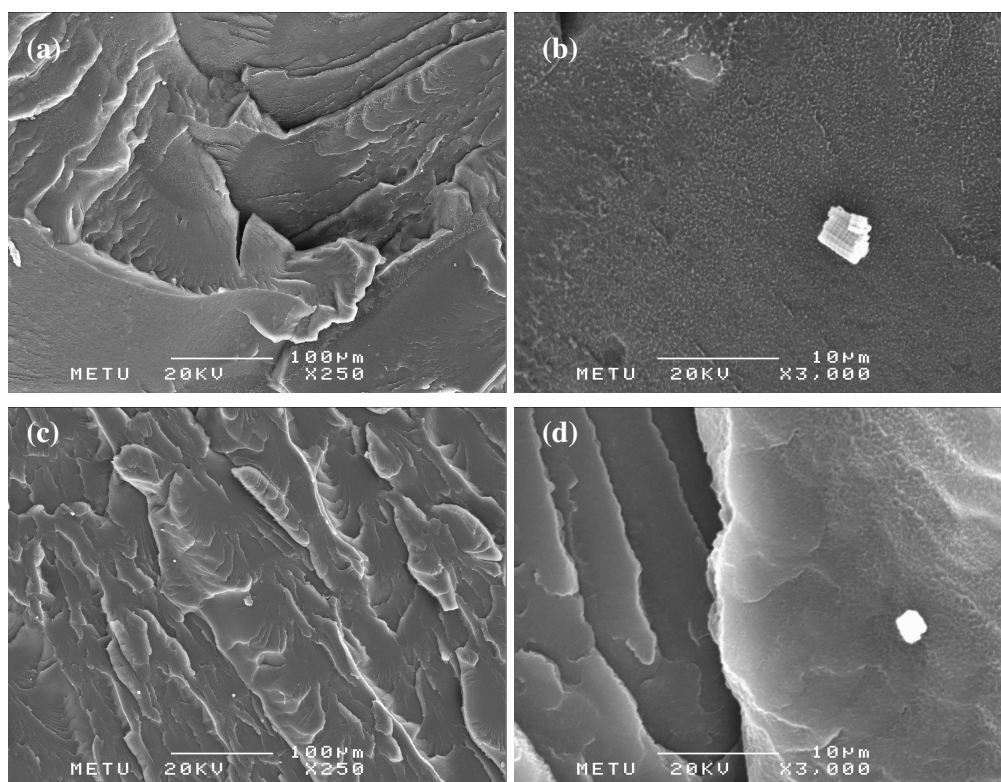
Figure 4.8 SEM micrographs of LDPE/Lotader® AX 8900/Cabosil® M5 nanocomposites having filler ratios of (a) 2 wt.% x250 (b) 2 wt.% x3000 (c) 5 wt.% x250 (d) 5 wt.% x3000.

From Figure 4.9 to Figure 4.14, the SEM micrographs belong to the LDPE/compatibilizer/fumed silica ternary nanocomposites prepared by different feeding orders.

Figures 4.9 and 4.10 represent the ternary nanocomposites with the compatibilizer Lotader® 2210 (E-nBA-MAH) having 2 wt.% and 5 wt.% fumed silica respectively. Images of nanocomposites prepared by feeding order 2 (FO2) and feeding order 3 (FO3), where silica is extruded twice, show more tortuous surfaces and better dispersion. As the amount of compatibilizer was not sufficient to be mixed with fumed silica during extrusion FO3 could only be achieved for Lotader® 2210.
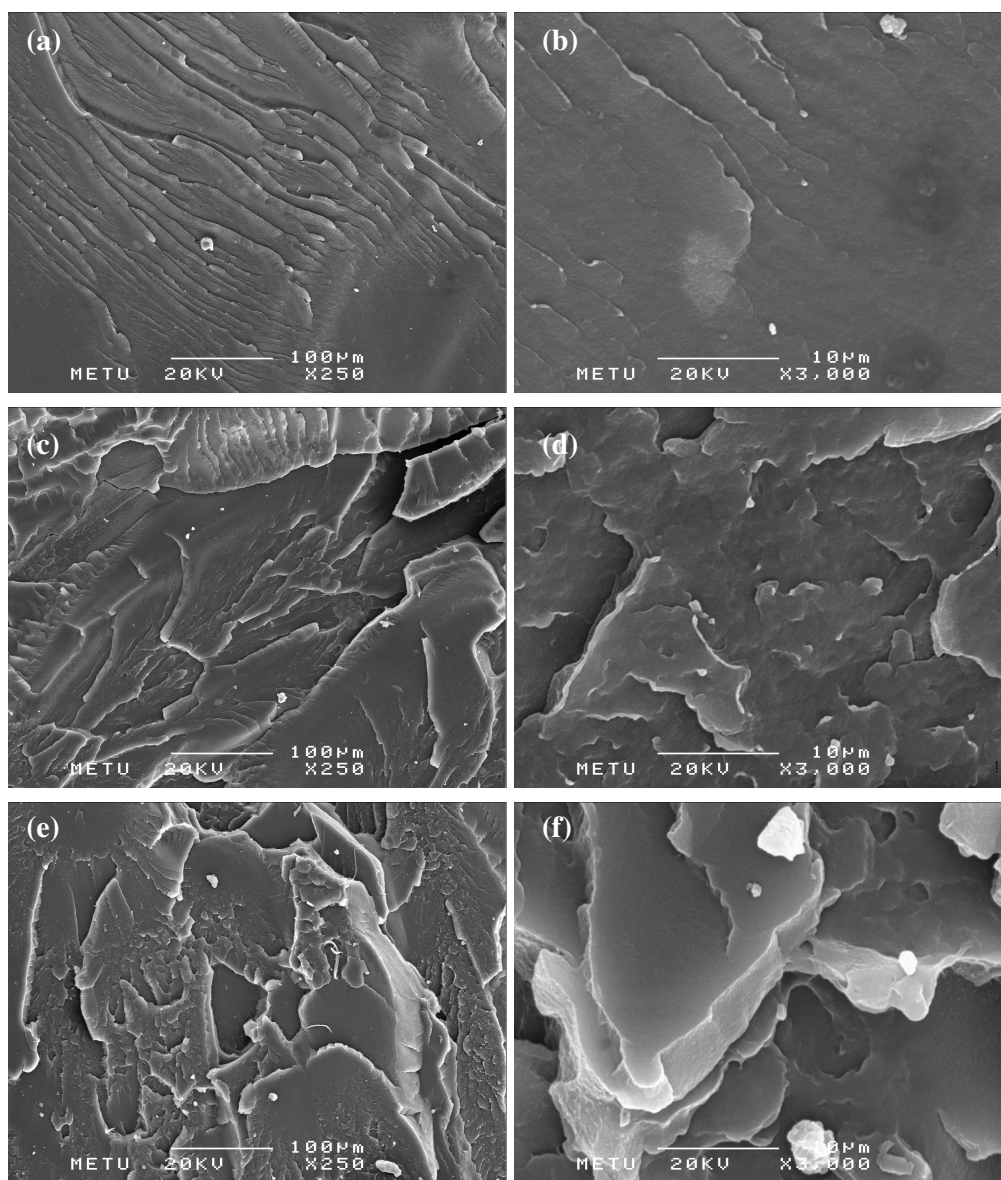
Figure 4.9 SEM micrographs of LDPE/Lotader[®] 2210/Cabosil[®] M5 nanocomposites having 5 wt.% compatibilizer and 2 wt.% fumed silica, produced by (a) FO1 x250 (b) FO1 x3000 (c) FO2 x250 (d) FO2 x3000 (e) FO3 x250 (f) FO3 x3000.
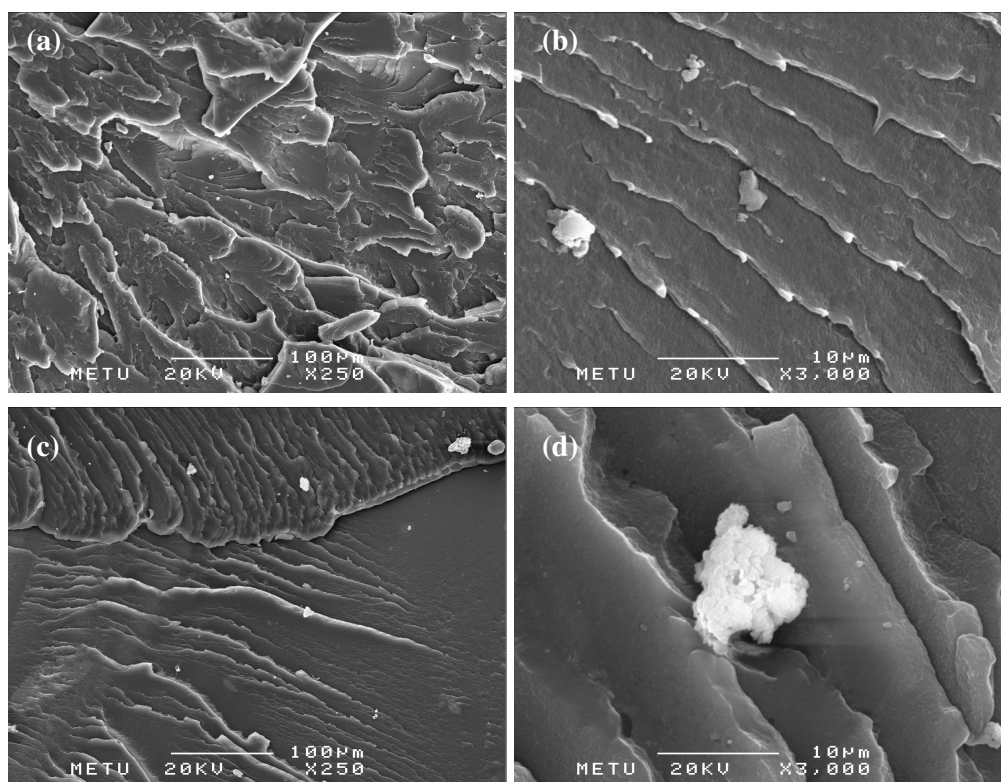
Figure 4.10 SEM micrographs of LDPE/Lotader® 2210/Cabosil® M5 nanocomposites having 5 wt.% compatibilizer and 5 wt.% fumed silica produced by (a) FO1 x250 (b) FO1 x3000 (c) FO2 x250 (d) FO2 x3000.

In Figures 4.11 and 4.12, the ternary nanocomposites prepared with Lotader® AX 8840 (E-GMA) are shown respectively with 2 and 5 wt.% of fumed silica. The images showing nanocomposites with 2wt.% silica show more tortuous surfaces yielding better mechanical properties.

Figures 4.13 and 4.14 belonging to the ternary nanocomposites prepared with Lotader® AX 8900 (E-MA-GMA), respectively show the nanocomposites having 2 and 5 wt.% fumed silica. The tortuous surfaces can also be examined in these images.
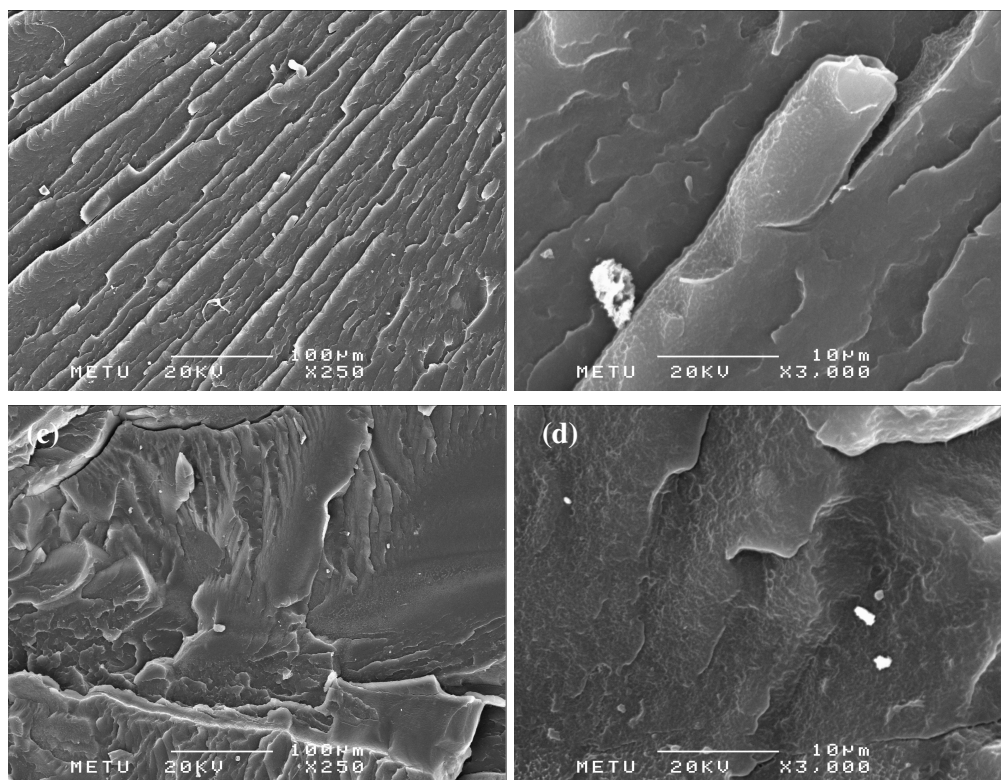
Figure 4.11 SEM micrographs of LDPE/Lotader® AX 8840/Cabosil® M5 nanocomposites having 5 wt.% compatibilizer and 2 wt.% fumed silica produced by (a) FO1 x250 (b) FO1 x3000 (c) FO2 x250 (d) FO2 x3000.
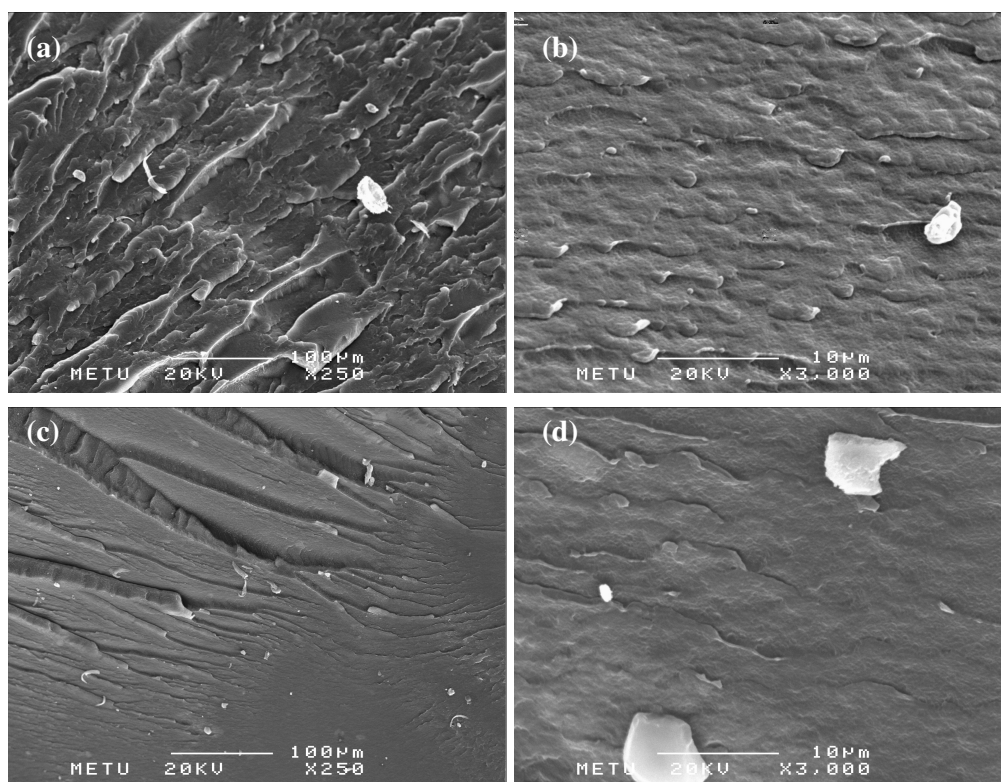
Figure 4.12 SEM micrographs of LDPE/Lotader® AX 8840/Cabosil® M5 nanocomposites having 5 wt.% compatibilizer and 5 wt.% fumed silica produced by (a) FO1 x250 (b) FO1 x3000 (c) FO2 x250 (d) FO2 x3000.
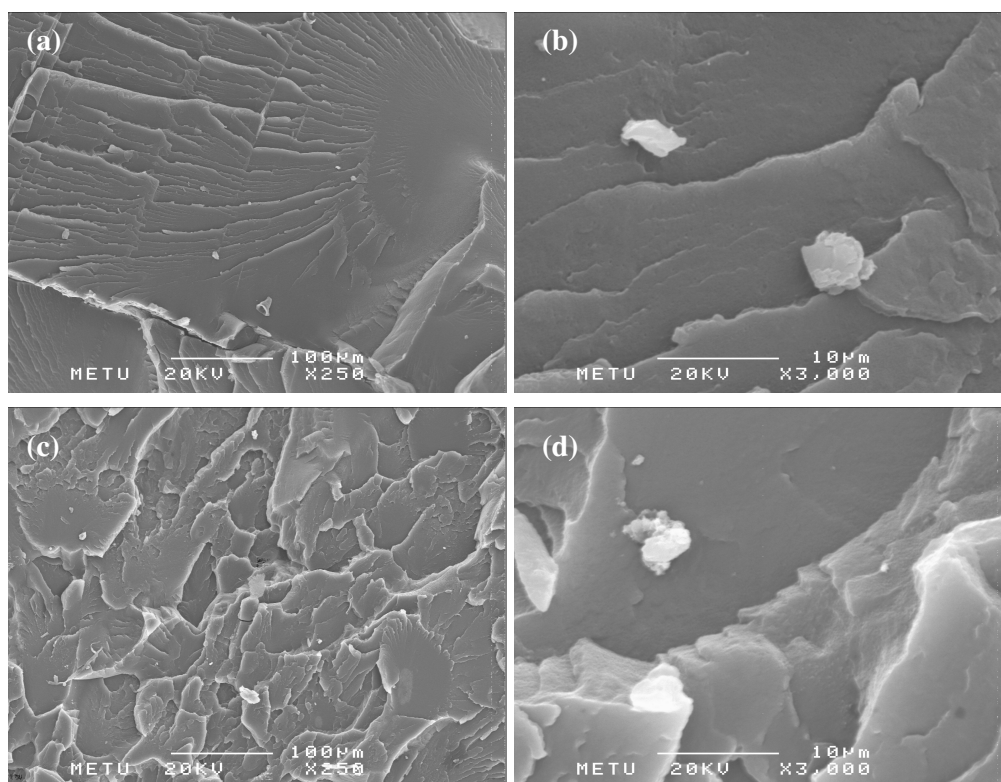
Figure 4.13 SEM micrographs of LDPE/Lotader® AX 8900/Cabosil® M5 nanocomposites having 5 wt.% compatibilizer and 2 wt.% fumed silica produced by (a) FO1 x250 (b) FO1 x3000 (c) FO2 x250 (d) FO2 x3000.
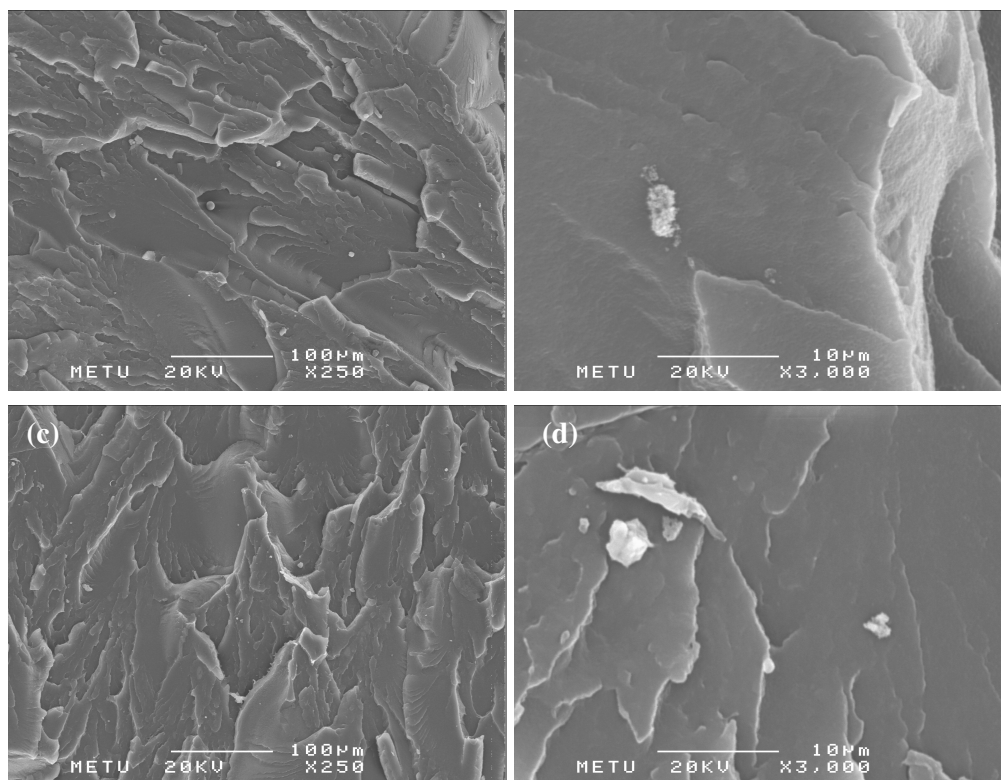
Figure 4.14 SEM micrographs of LDPE/Lotader® AX 8900/Cabosil® M5 nanocomposites having 5 wt.% compatibilizer and 5 wt.% fumed silica produced by (a) FO1 x250 (b) FO1 x3000 (c) FO2 x250 (d) FO2 x3000.

4.2 Mechanical Analysis

Tensile and flexural tests were performed on injection molded specimens of nanocomposites produced in order to investigate the effects of the fumed silica, compatibilizer type and feeding order of materials on the mechanical properties. All mechanical properties were measured on at least five samples and the test results given are defined as the average values of tested samples for each composition.

All the mechanical tests were performed on twice extruded LDPE, LDPE/Compatibilizer blends, LDPE/Cabosil® M5 binary nanocomposites and LDPE/Cabosil® M5/Compatibilizer ternary nanocomposites prepared with

different feeding order of materials. The test results are compared with each other and the individual effects of components and feeding orders are determined.

4.2.1 Tensile Properties

The tensile tests performed on LDPE/Compatibilizer blends were compared with twice extruded LDPE in order to observe the effect of the compatibilizer on pure LDPE. These results are shown in Figures 4.15 to 4.17. Since compatibilizers have lower mechanical properties, all the mechanical properties have been negatively affected from their addition. The tensile strength and tensile modulus values of the blends decreased slightly, while the strain at break values decreased by almost 50%.
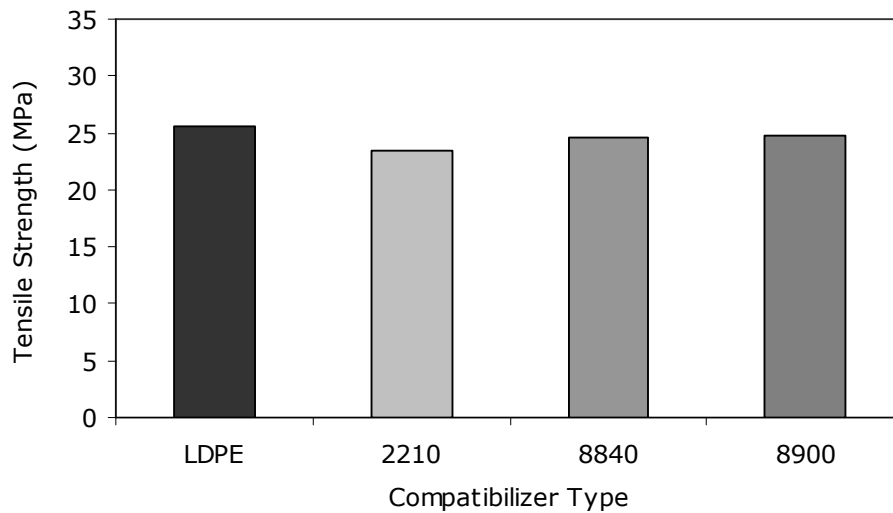
Figure 4.15 Tensile strength values of LDPE/compatibilizer blends.
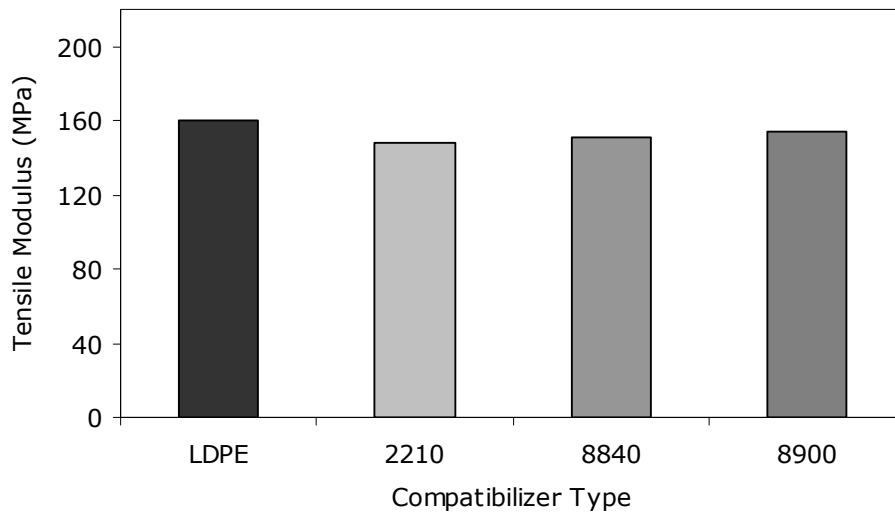
Figure 4.16 Tensile modulus values of LDPE/compatibilizer blends.
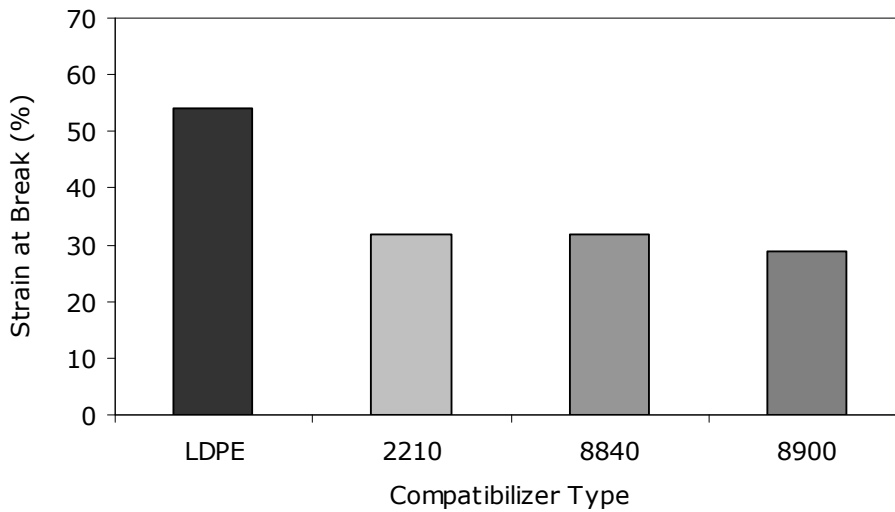
Figure 4.17 Strain at break values of LDPE/compatibilizer blends.

Figures 4.18 to 4.20 show the mechanical properties of LDPE/Cabosil® M5 nanocomposites. It is observed that all the mechanical properties of twice extruded pure LDPE decreased with the addition of fumed nanosilica. It shows

that, the nanosilica particles are not compatible with LDPE and change the continuous structure of LDPE causing weakness.
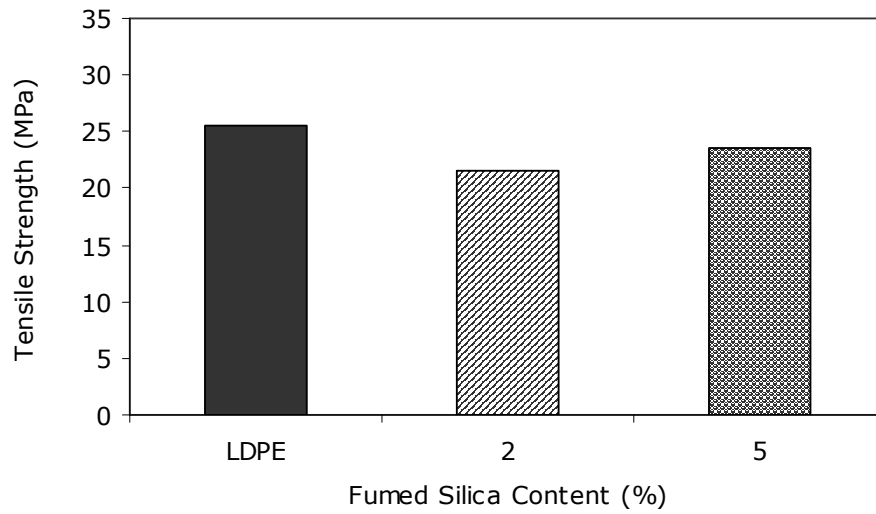
Figure 4.18 Tensile strength values of LDPE/fumed silica nanocomposites.
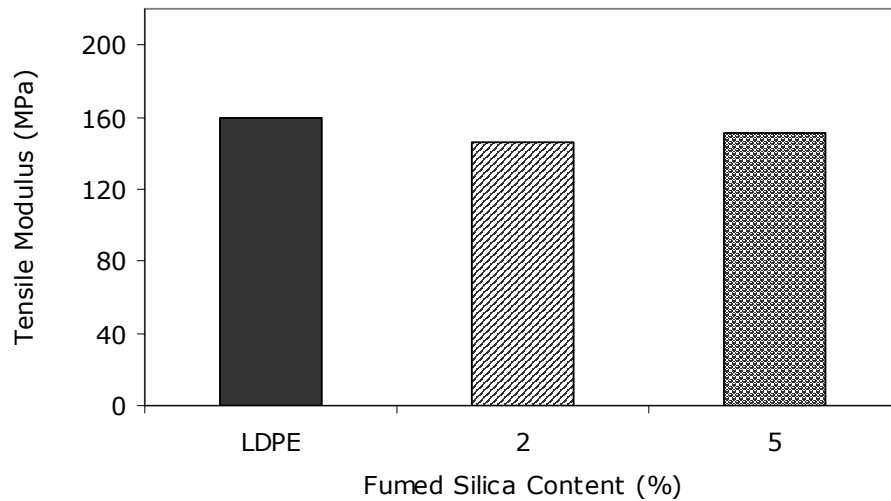
Figure 4.19 Tensile modulus values of LDPE/fumed silica nanocomposites.
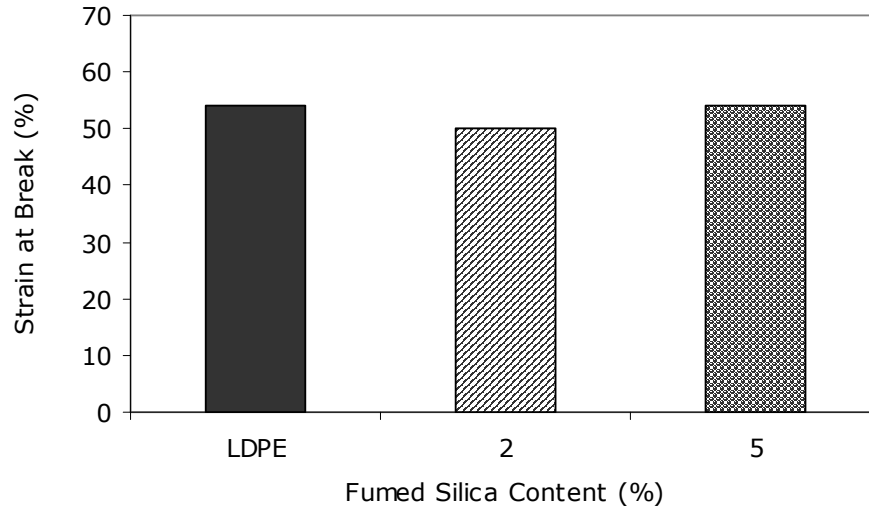
Figure 4.20 Strain at break values of LDPE/fumed silica nanocomposites.

In figures 4.21 to 4.23, the mechanical properties of ternary nanocomposites prepared by simultaneous feeding with different compatibilizers are shown. It is observed that tensile strength values of nanocomposites increased with increasing fumed silica content, the highest strength is observed with 5 wt.% fumed silica and compatibilizer Lotader®AX 8840. There were no significant change in tensile modulus values of the ternary nanocomposites with the addition of 2 wt.% fumed silica while they increased with addition of 5 wt.% fumed silica. But strain at break values of the simultaneously fed ternary nanocomposites increased with 2 wt.% silica addition and decreased with the increasing amount of silica nanoparticles.

Different than binary systems, samples of ternary systems show improved mechanical properties. This shows that, the improving effect of silica on mechanical properties can only be observed when its compatibility is increased with an appropriate compatibilizer. Otherwise, silica shows a negative effect on the mechanical properties because of the agglomeration and incompatibility.
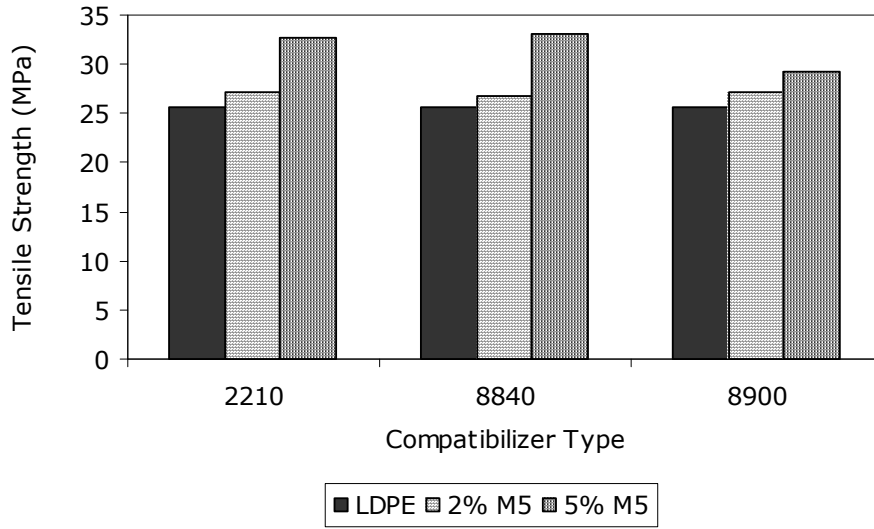
Figure 4.21 Tensile strength values of ternary LDPE/compatibilizer/fumed silica nanocomposites.
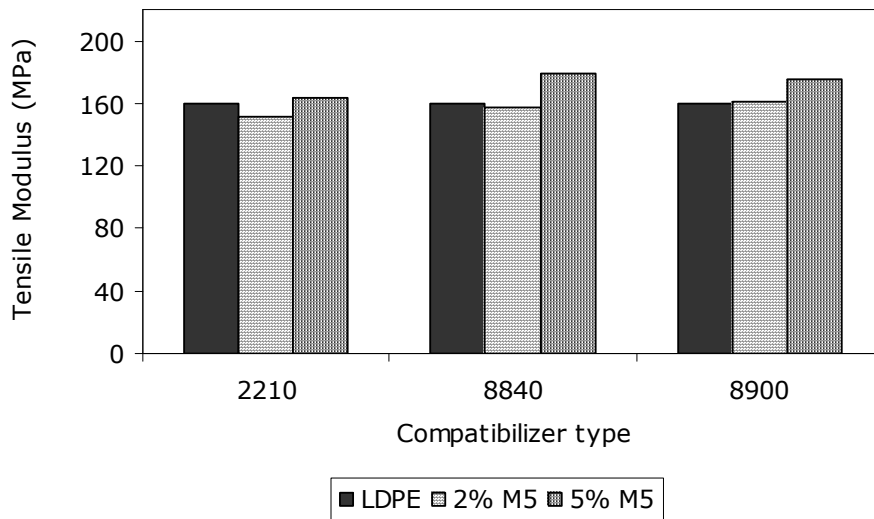
Figure 4.22 Tensile modulus values of ternary LDPE/compatibilizer/fumed silica nanocomposites.
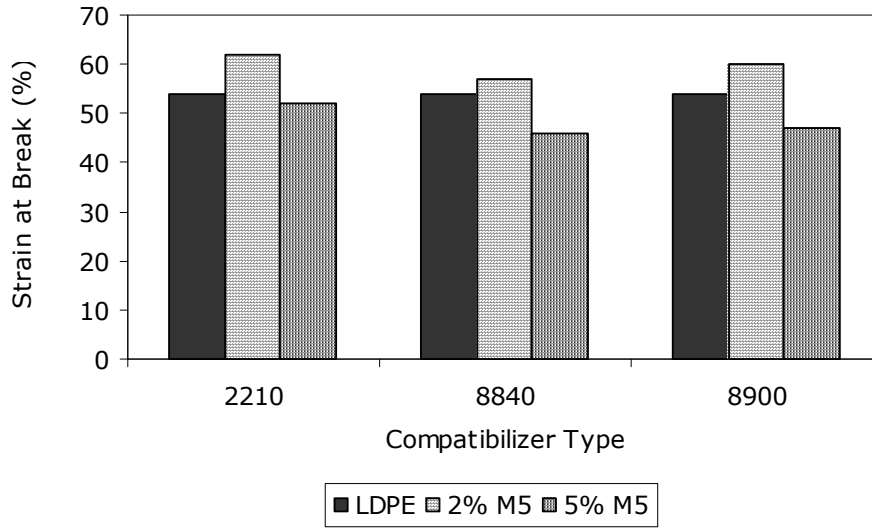
Figure 4.23 Strain at break values of ternary LDPE/compatibilizer/fumed silica nanocomposites.

From Figure 4.24 to Figure 4.41, mechanical properties of ternary nanocomposites are given, which are prepared by three different compatibilizers as; Lotader® 2210 (E-nBA-MAH), Lotader® AX 8840 (E-GMA), Lotader® AX 8900 (E-MA-GMA) and different feeding orders as FO1 [(PCo)M5], FO2 [(PM5)Co], FO3 [(CoM5)P].

Tensile strength and modulus of the composites prepared by FO1 are improved or remain nearly unchanged with increasing amount of fumed silica, while these properties decrease when prepared by FO2 mixing order. This difference appears because, in FO2, LDPE and fumed silica are first mixed together. They are poor in miscibility owing to the hydrophobic nature of LDPE. But in FO1, LDPE and compatibilizer are first mixed together, forming a compatible mixture for fumed silica.

Mixing order FO3 could only be achieved for compatibilizer Lotader® 2210 and 2 wt.% silica, as the compatibilizer amount was not sufficient for forming a fluid mixture and extrusion process was interrupted by pressure alarm. Since the elastomer with polar groups was directly mixed with silica, FO3 seemed the most appropriate situation for the reactions to happen and its test results were

expected to give the best results. The test results of this sequence are given in Figures 4.24 to 4.26.
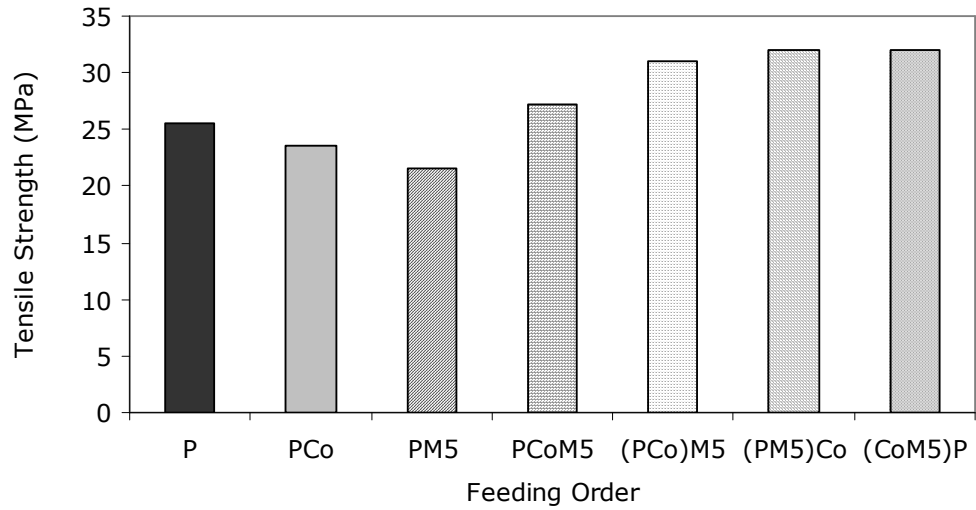
Figure 4.24 Effect of feeding order on tensile strength of LDPE/E-nBA-MAH/fumed silica nanocomposites having 2% Cabosil M5 fumed silica.
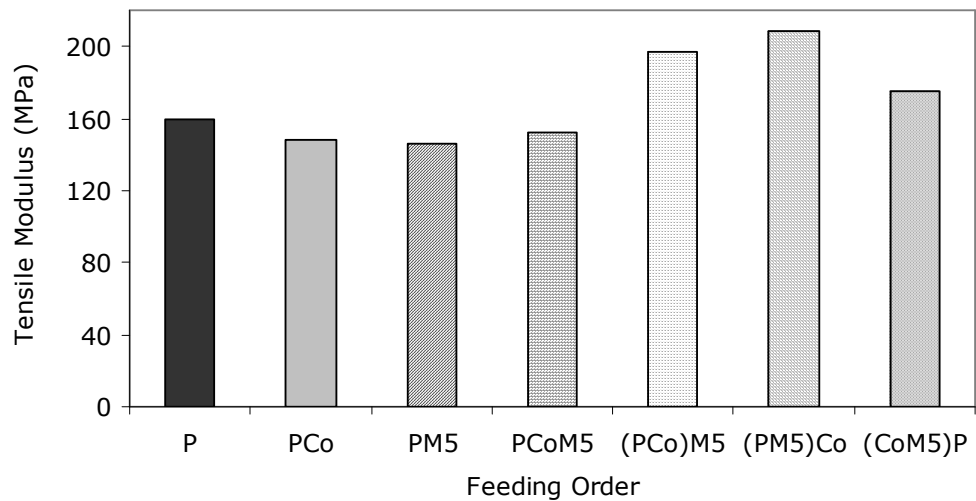
Figure 4.25 Effect of feeding order on tensile modulus of LDPE/E-nBA-MAH/fumed silica nanocomposites having 2% Cabosil M5 fumed silica.
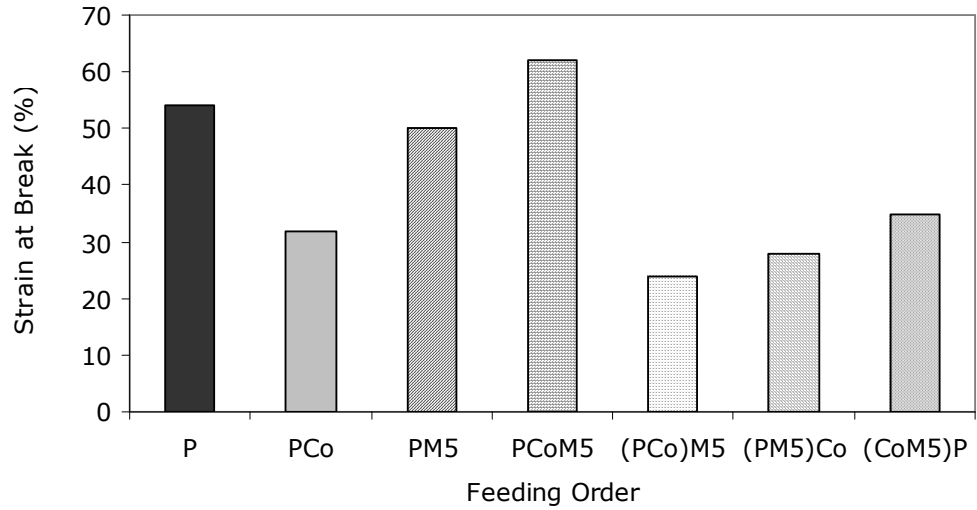
Figure 4.26 Effect of feeding order on strain at break value of LDPE/E-nBA-MAH/fumed silica nanocomposites having 2% Cabosil M5 fumed silica.

Unexpectedly FO3 addition type gave lower results than the other Lotader[®] 2210 compatibilized composites of FO1 and FO2 addition orders. This is due to the agglomeration of fumed silica, arising from the deficient mixing of elastomer with silica during extrusion.

In Figures 4.27 to 4.29, tensile test results of Lotader[®] 2210 compatibilized ternary nanocomposites with 5% nanosilica are given. At 5 wt.% silica loading, tensile modulus value shows a significant improvement in FO1 type nanocomposite, while its strain at break value seems to be low.
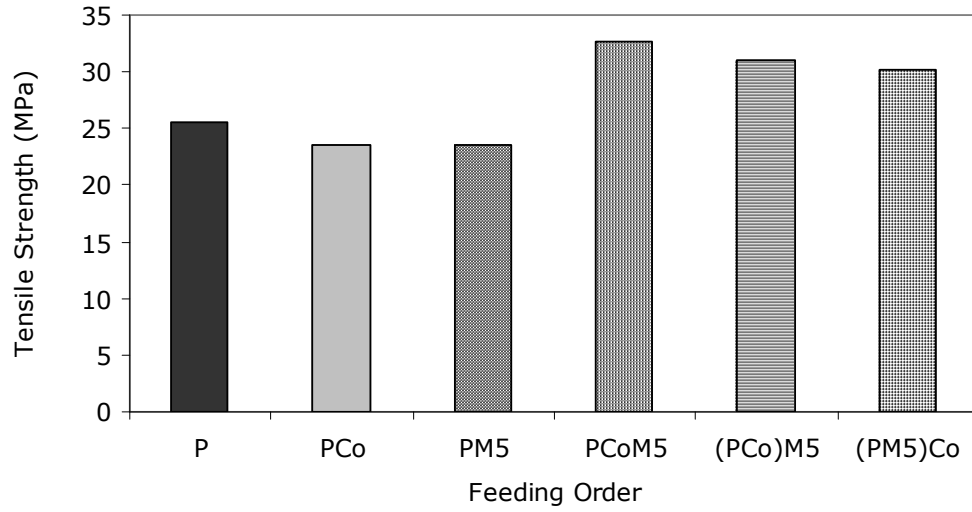
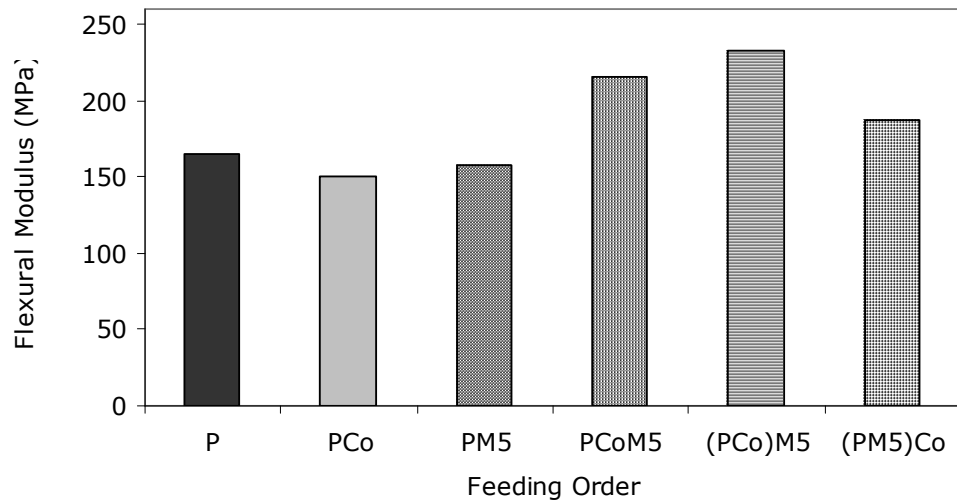**Figure 4.27** Effect of feeding order on tensile strength of LDPE/E-nBA-MAH/fumed silica nanocomposites having 5% Cabosil M5 fumed silica.
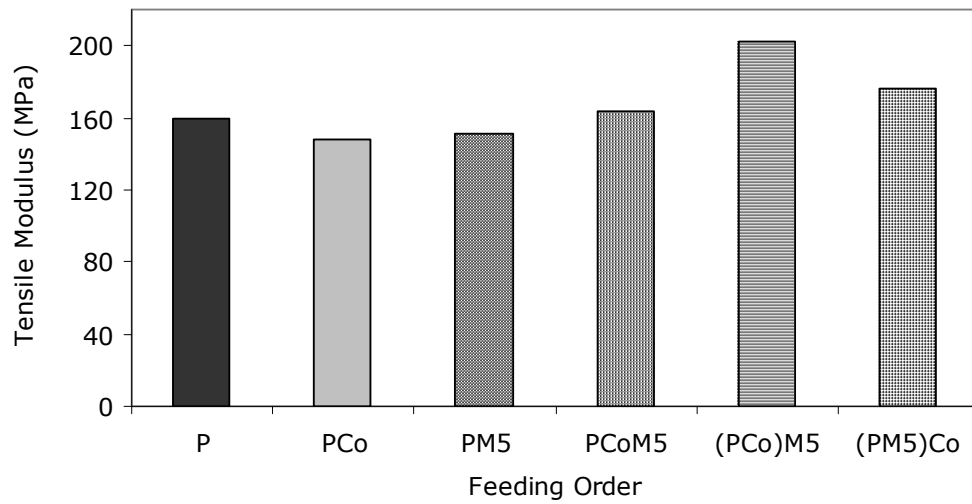
Figure 4.28 Effect of feeding order on tensile modulus of LDPE/E-nBA-MAH/fumed silica nanocomposites having 5% Cabosil M5 fumed silica.
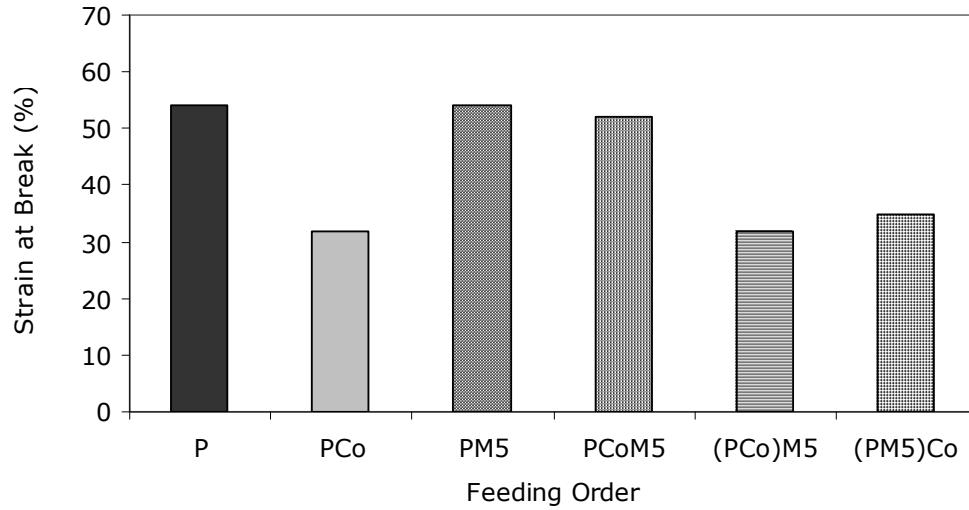
Figure 4.29 Effect of feeding order on strain at break value of LDPE/E-nBA-MAH/fumed silica nanocomposites having 5% Cabosil M5 fumed silica.

From Figures 4.30 to 4.35, tensile test results of Lotader® AX 8840 compatibilized ternary nanocomposites are given. Among the nanocomposites prepared with this compatibilizer, best result is obtained by FO2 mixing type with 2 wt.% fumed silica and FO1 mixing type with 5 wt% fumed silica.
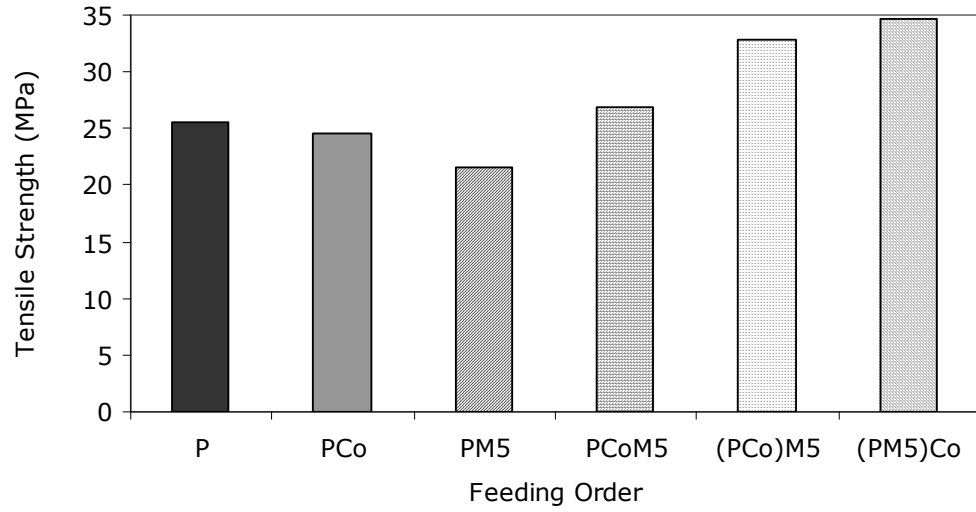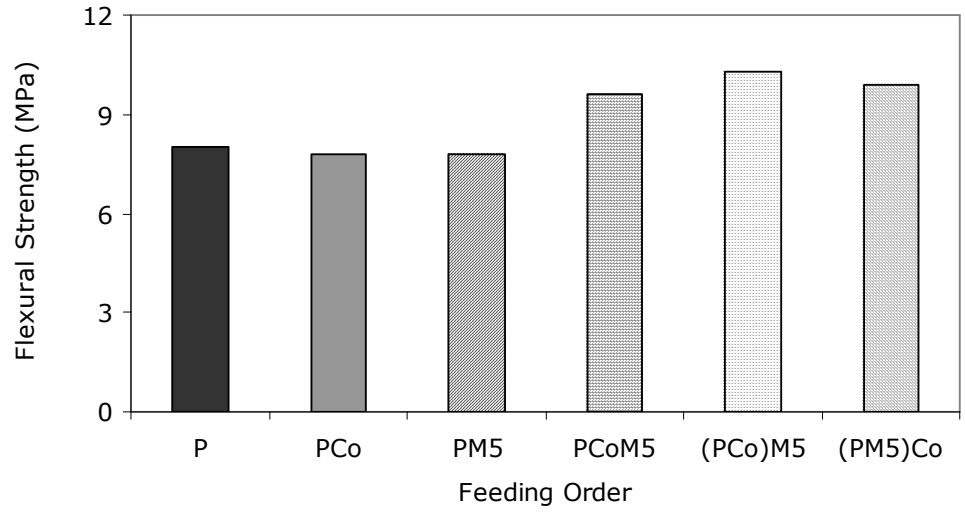
Figure 4.30 Effect of feeding order on tensile strength of LDPE/E-GMA/fumed silica nanocomposites having 2% Cabosil M5 fumed silica.
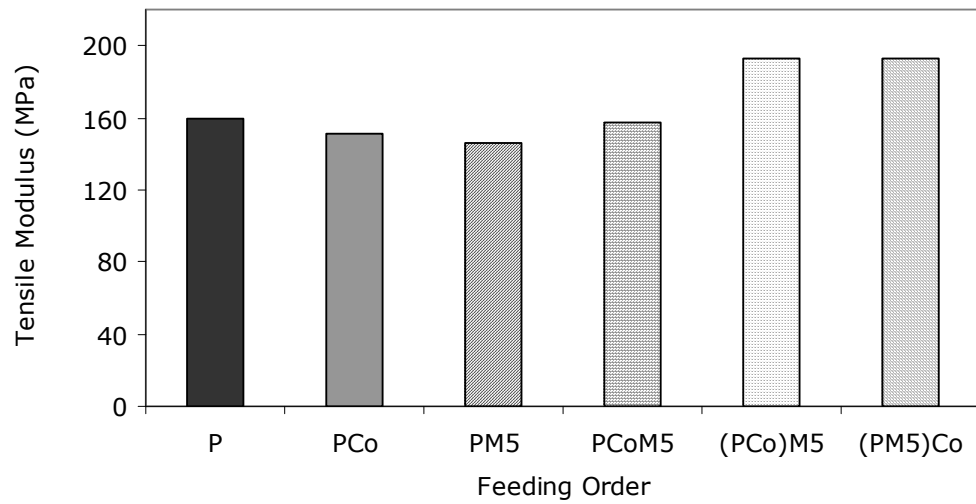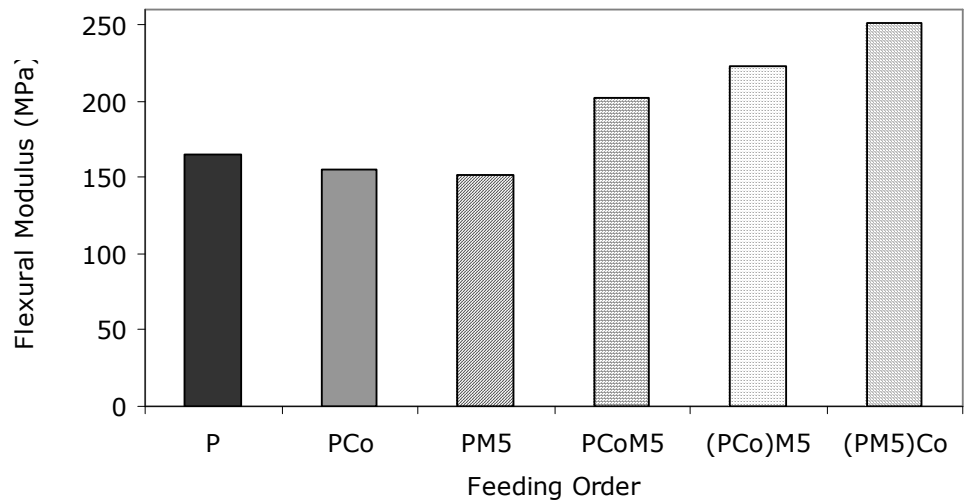

Figure 4.31 Effect of feeding order on tensile modulus of LDPE/E-GMA/fumed silica nanocomposites having 2% Cabosil M5 fumed silica.
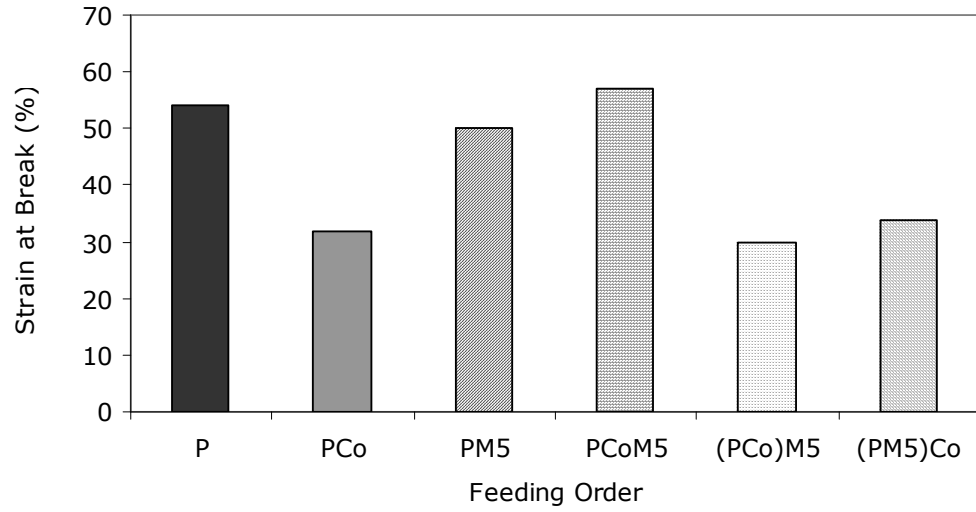
Figure 4.32 Effect of feeding order on strain at break value of LDPE/E-GMA/fumed silica nanocomposites having 2% Cabosil M5 fumed silica.
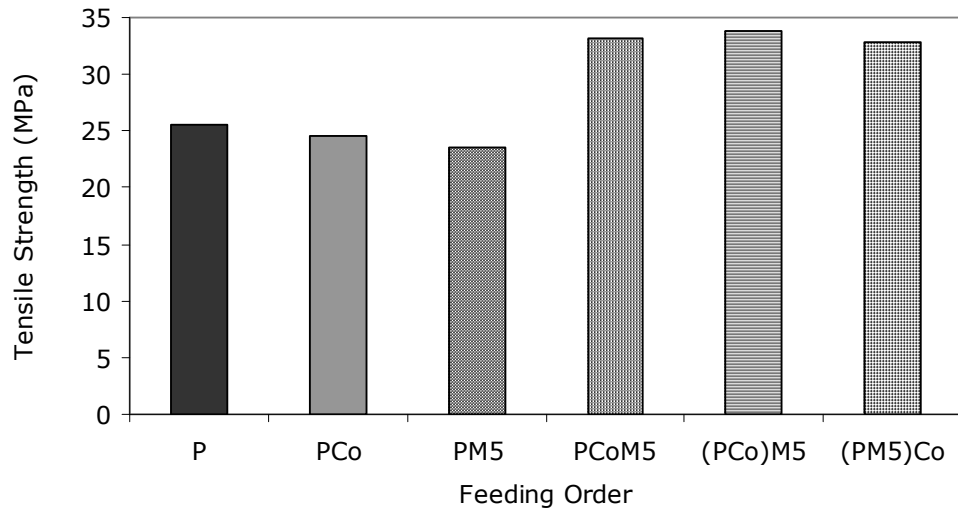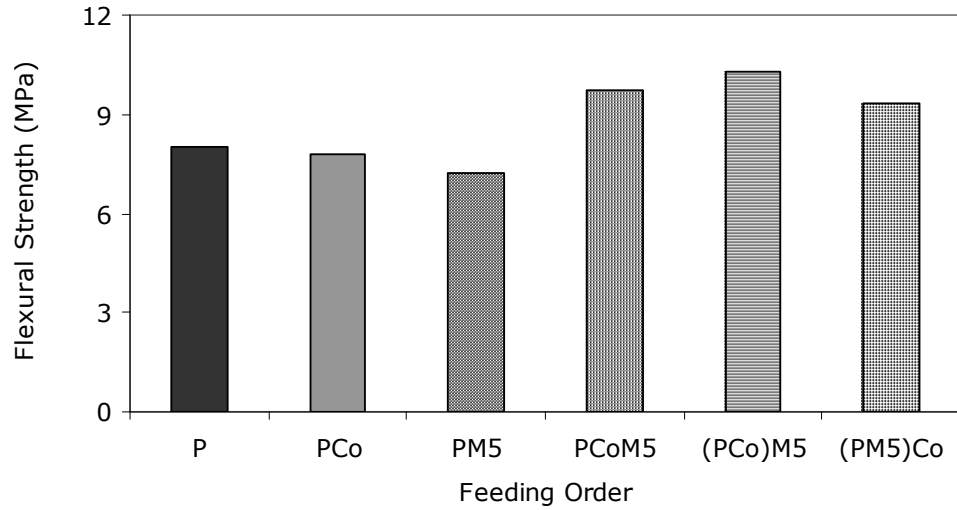

Figure 4.33 Effect of feeding order on tensile strength of LDPE/E-GMA/fumed silica nanocomposites having 5% Cabosil M5 fumed silica.
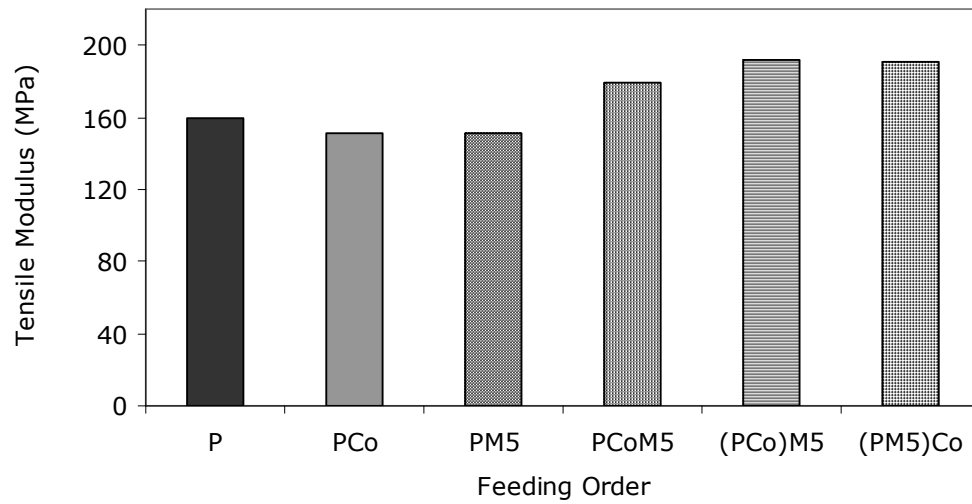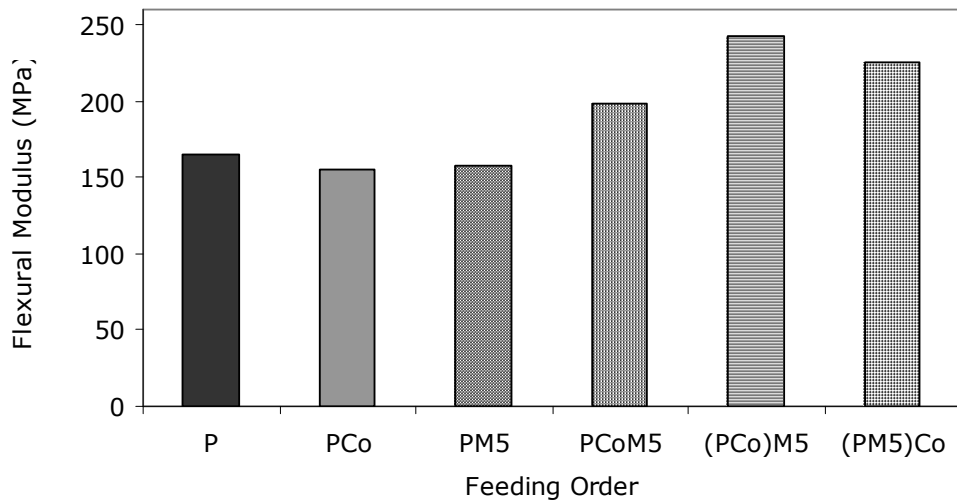
Figure 4.34 Effect of feeding order on tensile modulus of LDPE/E-GMA/fumed silica nanocomposites having 5% Cabosil M5 fumed silica.
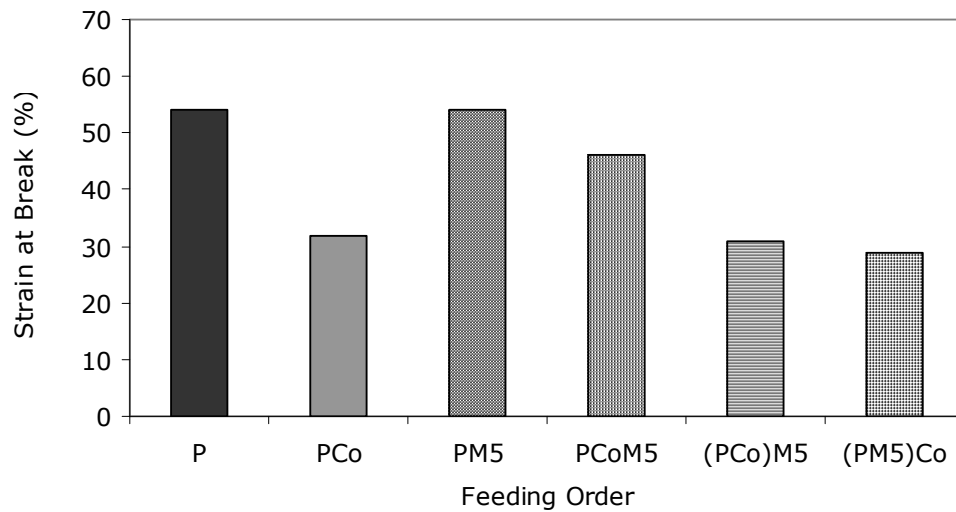
Figure 4.35 Effect of feeding order on strain at break value of LDPE/E-GMA/fumed silica nanocomposites having 5% Cabosil M5 fumed silica.

From Figure 4.36 to 4.41, tensile test results of ternary nanocomposites prepared with the compatibilizer Lotader® AX 8900 are given. With this

compatibilizer type, the best results are obtained by FO1 mixing order for both 2 and 5 wt.% fumed silica.
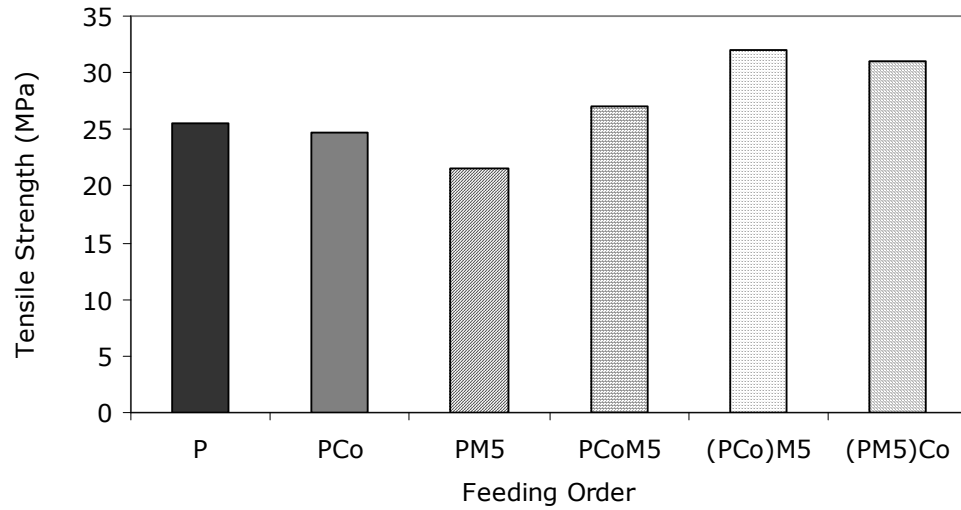
Figure 4.36 Effect of feeding order on tensile strength of LDPE/E-MA-GMA/fumed silica nanocomposites having 2% Cabosil M5 fumed silica.
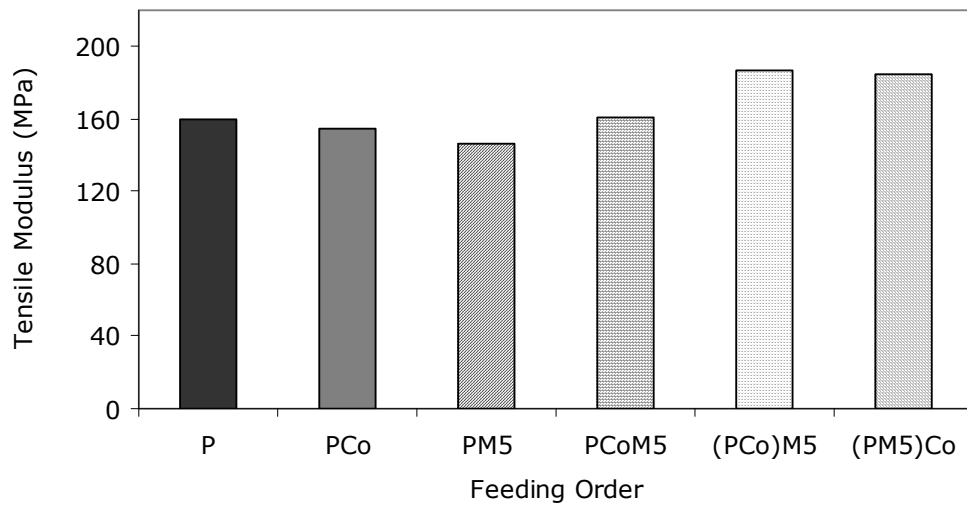
Figure 4.37 Effect of feeding order on tensile modulus of LDPE/E-MA-GMA/fumed silica nanocomposites having 2% Cabosil M5 fumed silica.
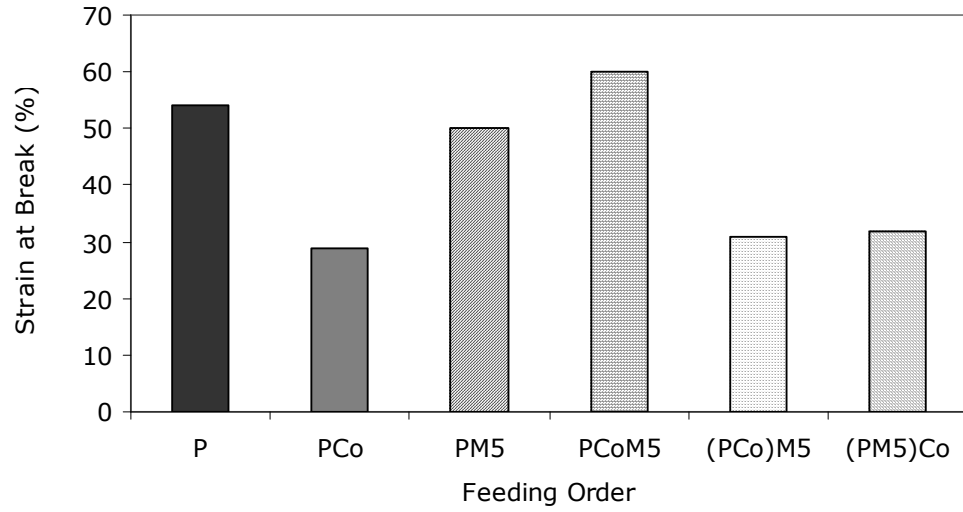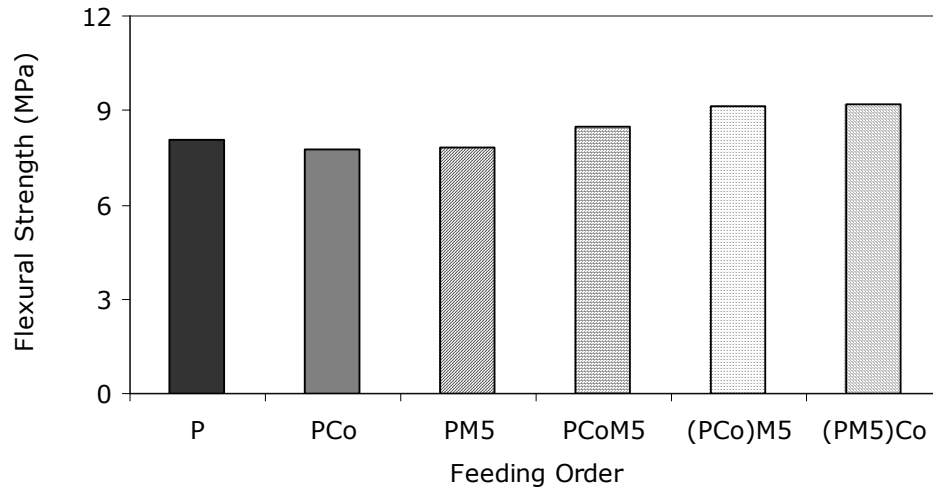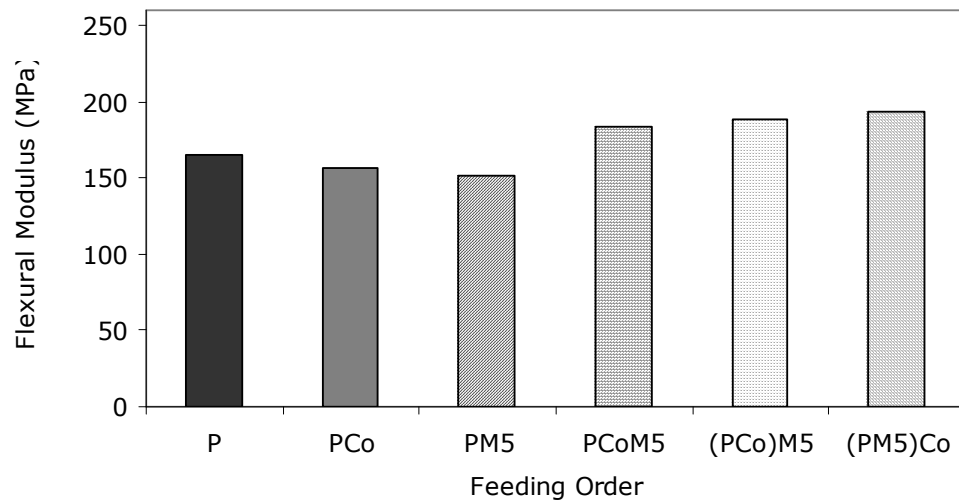
Figure 4.38 Effect of feeding order on strain at break value of LDPE/E-MA-GMA/fumed silica nanocomposites having 2% Cabosil M5 fumed silica.
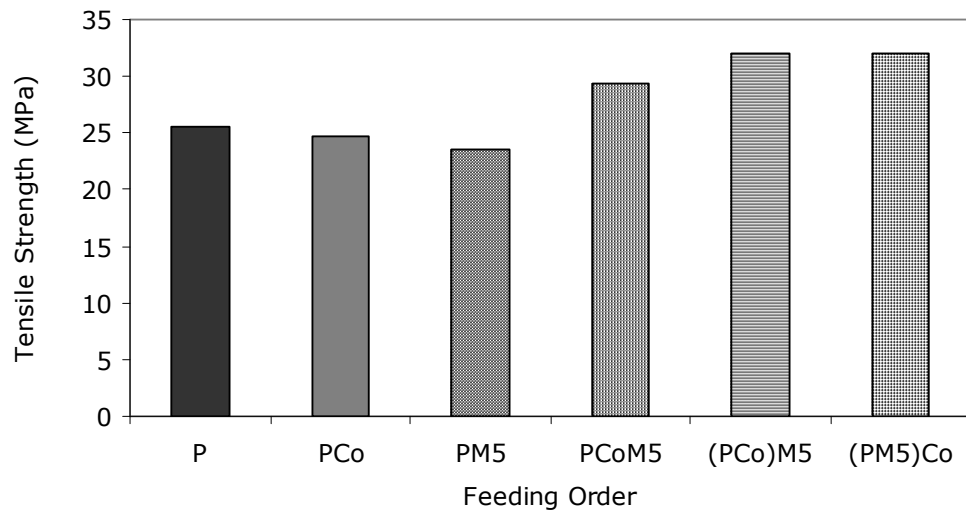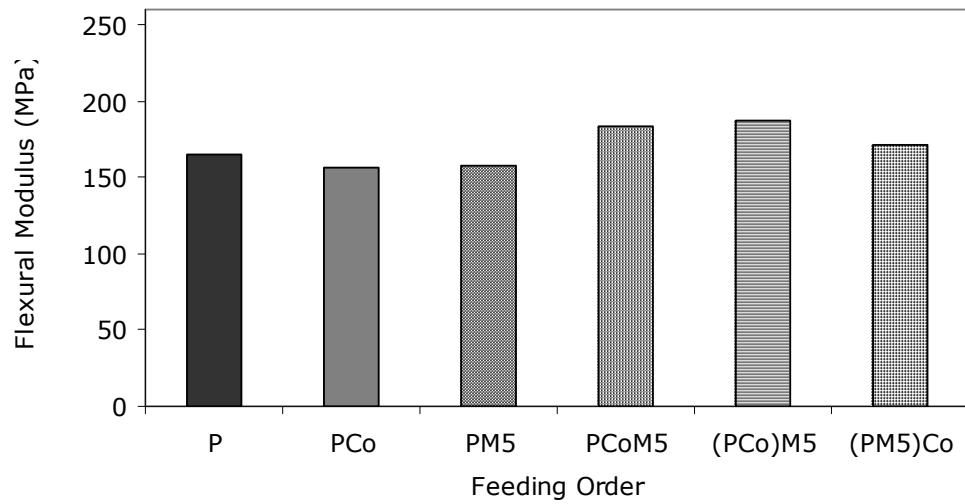

Figure 4.39 Effect of feeding order on tensile strength of LDPE/E-MA-GMA/fumed silica nanocomposites having 5% Cabosil M5 fumed silica.
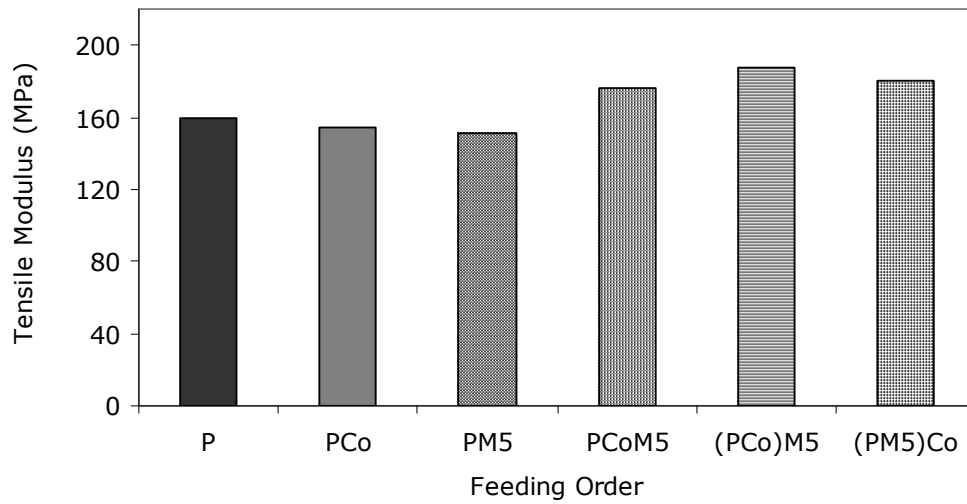
Figure 4.40 Effect of feeding order on tensile modulus of LDPE/E-MA-GMA/fumed silica nanocomposites having 5% Cabosil M5 fumed silica.
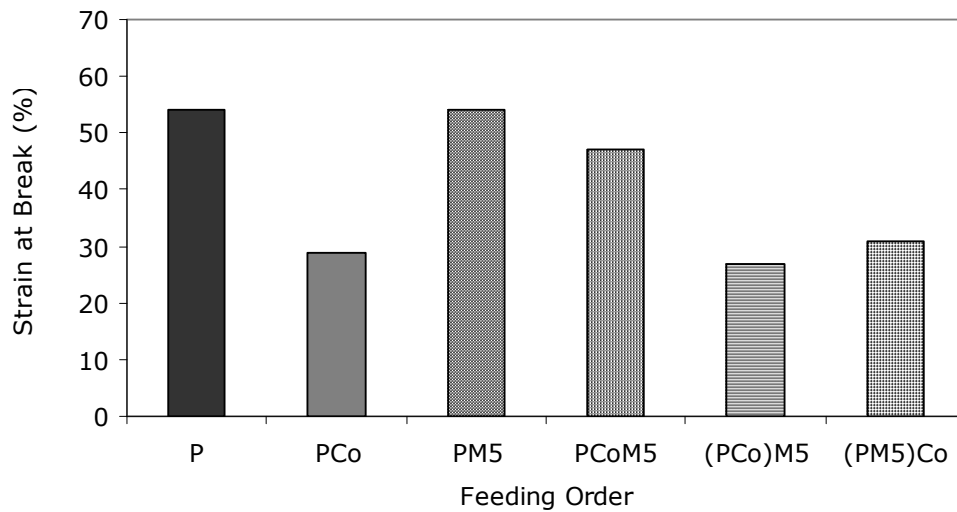
Figure 4.41 Effect of feeding order on strain at break value of LDPE/E-MA-GMA/fumed silica nanocomposites having 5% Cabosil M5 fumed silica.

It is concluded that; by changing the feeding order of the materials, higher tensile strength and tensile modulus values can be obtained in comparison to the

results obtained by simultaneous feeding process. The strain at break values are significantly lower than that of simultaneously fed composites. Increasing amount of fumed silica slightly increased modulus and strength values in FO1 but decreased in FO2 mixing order. This shows that, more efficient mixing is required for FO2 addition sequence.

4.2.2 Flexural Properties

The flexural test, measured by three-point bending, involves both tension and compression of the specimen. The upper surface is compressed while the bottom surface is under tension which is expected to result in crack formation. However, as a result of the elastic behavior of LDPE, crack formation could not be observed in the flexural tests of samples. During the tests, there was no failure and the tests were manually stopped after the maximum in the force was observed.

Since the compressive strength is greater than the tensile strength, flexural strength and modulus tend to show greater values than tensile strength and modulus [1]. However, since the specimens did not fail in flexural tests, it was observed that, although flexural modulus values are significantly higher than tensile modulus values, flexural strength values were lower than tensile strength for all samples.

The results of flexural tests are generally in agreement with tensile test results. Addition of compatibilizer to LDPE decreased the flexural modulus and strength due to low mechanical properties of elastomers.
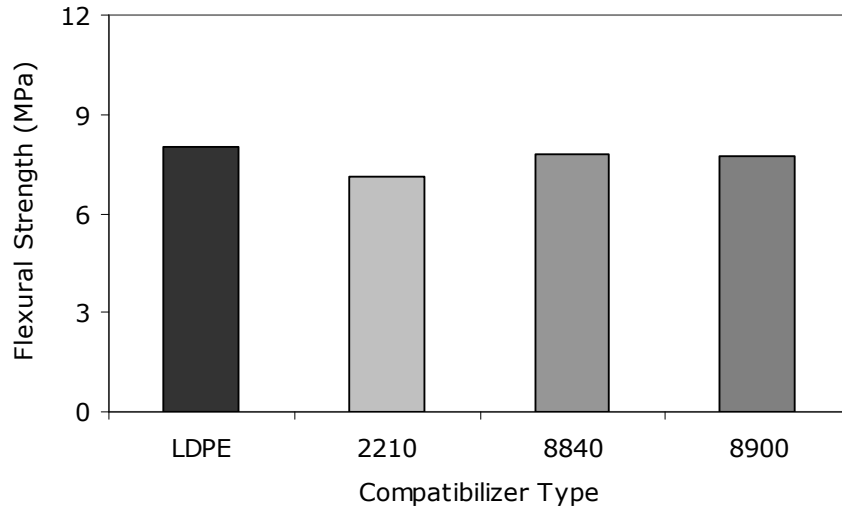
Figure 4.42 Flexural strength values of LDPE/compatibilizer blends.
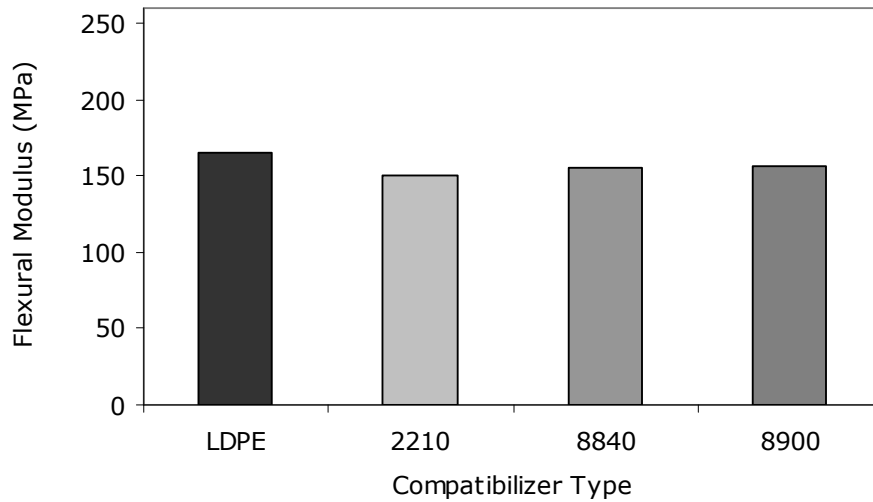
Figure 4.43 Flexural modulus values of LDPE/compatibilizer blends.

Also like tensile properties, flexural properties of LDPE-silica binary nanocomposites are worse than pure LDPE, while the properties of LDPE-silica-compatibilizer ternary nanocomposites are better owing to the increase in miscibility of silica in LDPE.
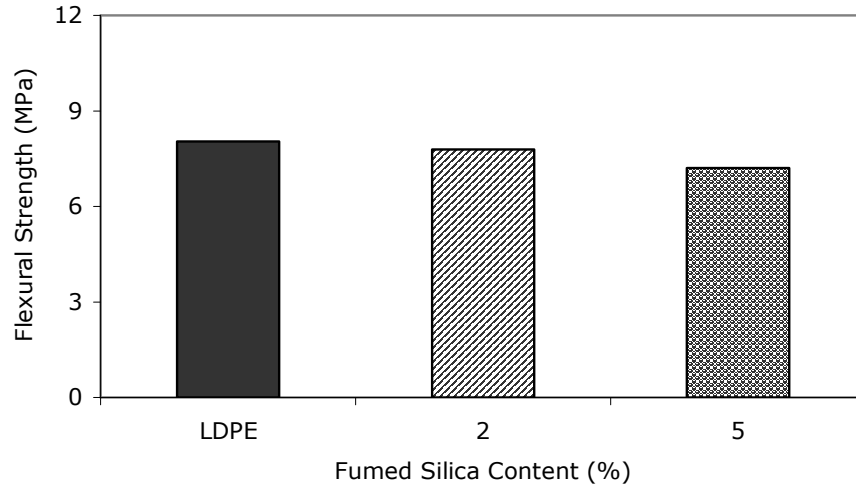
Figure 4.44 Flexural strength values of LDPE/fumed silica nanocomposites.
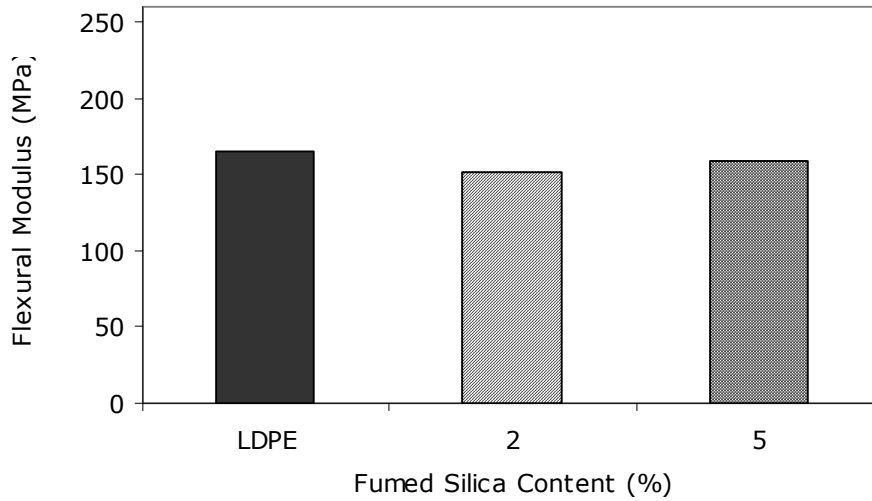
Figure 4.45 Flexural modulus values of LDPE/fumed silica nanocomposites.

In simultaneously fed samples, as the amount of fumed silica is increased, the flexural properties are improved or remained unchanged as a result of well dispersion of materials during twice extrusion. The improved flexural properties in ternary nanocomposites show that; the significant effect of fumed silica can only be observed when the required compatibility with the polymer is provided.
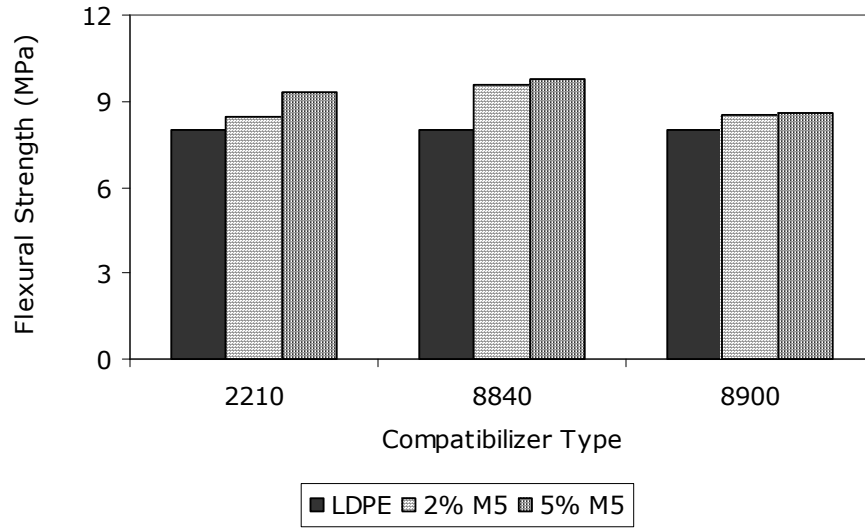
Figure 4.46 Flexural strength values of ternary LDPE/compatibilizer/fumed silica nanocomposites.
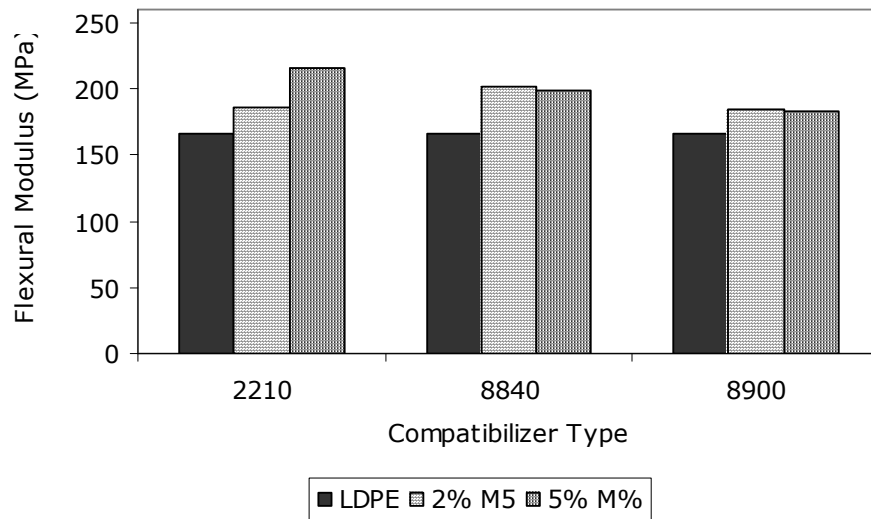
Figure 4.47 Flexural modulus values of ternary LDPE/compatibilizer/fumed silica nanocomposites.

The flexural test results of samples prepared by different addition orders also imply similar behavior to their tensile test counterparts. The flexural strength

and modulus increased with increasing amount of fumed silica in FO1 and significantly decreased in FO2. Also, counter to expected, flexural properties of FO3 samples were less than those of other feeding orders of Lotader® 2210.
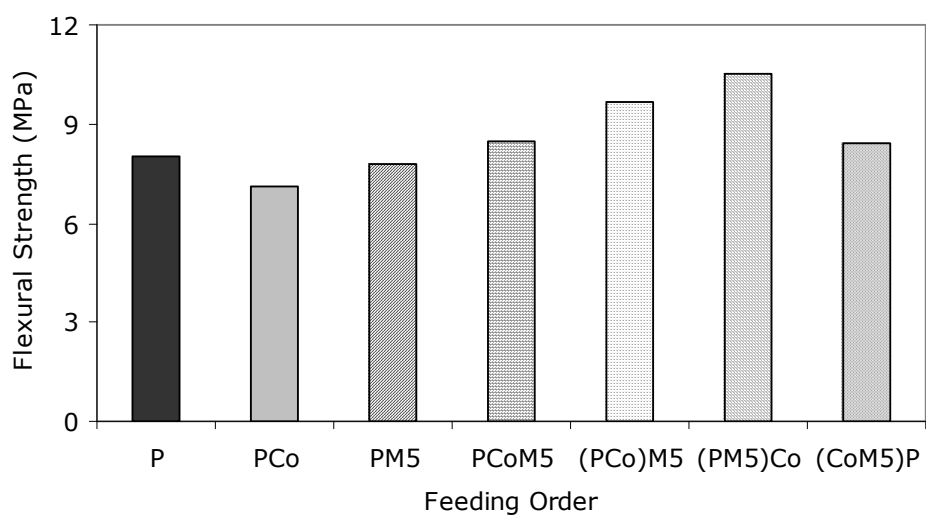
Figure 4.48 Effect of feeding order on flexural strength of LDPE/E-nBA-MAH/fumed silica nanocomposites having 2% Cabosil M5 fumed silica.
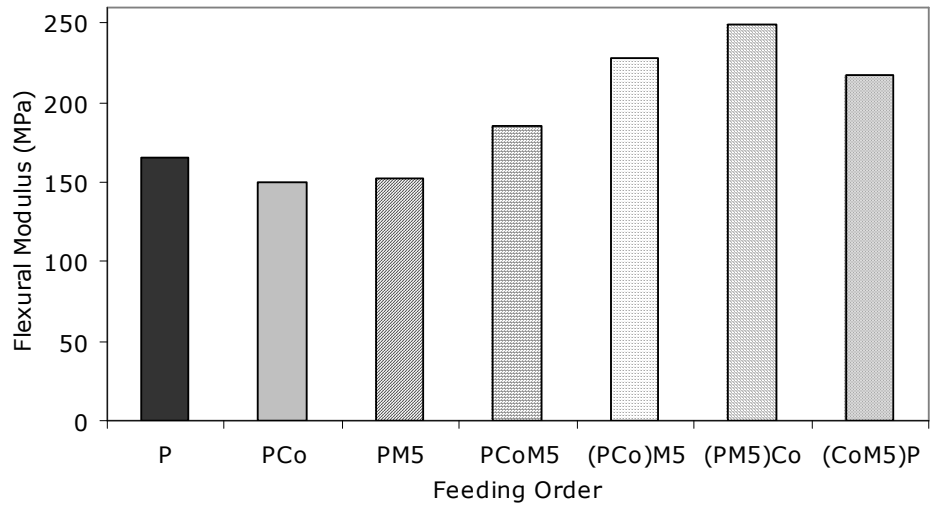
Figure 4.49 Effect of feeding order on flexural modulus of LDPE/E-nBA-MAH/fumed silica nanocomposites having 2% Cabosil M5 fumed silica.
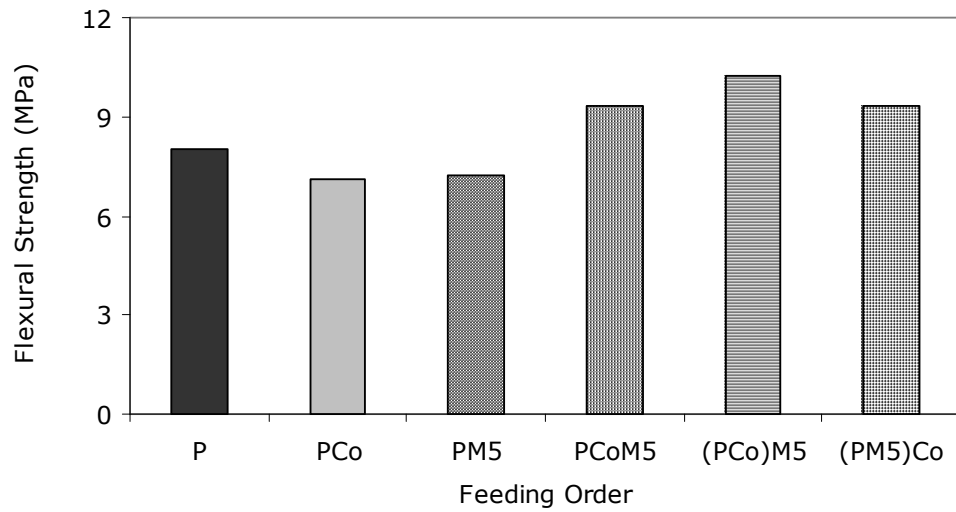
Figure 4.50 Effect of feeding order on flexural strength of LDPE/E-nBA-MAH/fumed silica nanocomposites having 5% Cabosil M5 fumed silica.

Figure 4.51 Effect of feeding order on flexural modulus of LDPE/E-nBA-MAH/fumed silica nanocomposites having 5% Cabosil M5 fumed silica.

From Figure 4.52 to 4.55 flexural test results of Lotader® AX 8840 compatibilized ternary nanocomposites prepared by different mixing orders are given. It is observed that, the increase in fumed silica content increased flexural modulus only with FO2 preparation type but there were not significant changes in flexural strength values.

Figure 4.52 Effect of feeding order on flexural strength of LDPE/E-GMA/fumed silica nanocomposites having 2% Cabosil M5 fumed silica.

Figure 4.53 Effect of feeding order on flexural modulus of LDPE/E-GMA/fumed silica nanocomposites having 2% Cabosil M5 fumed silica.

Figure 4.54 Effect of feeding order on flexural strength of LDPE/E-GMA/fumed silica nanocomposites having 5% Cabosil M5 fumed silica.

Figure 4.55 Effect of feeding order on flexural modulus of LDPE/E-GMA/fumed silica nanocomposites having 5% Cabosil M5 fumed silica.

From Figure 4.56 to 4.59 the graphics belong to the test results of Lotader[®] AX 8900 compatibilized ternary nanocomposites prepared by different mixing

orders. The increase in fumed silica content negatively affected the flexural modulus values but slightly improved flexural strength values.

Figure 4.56 Effect of feeding order on flexural strength of LDPE/E-MA-GMA/fumed silica nanocomposites having 2% Cabosil M5 fumed silica.

Figure 4.57 Effect of feeding order on flexural modulus of LDPE/E-MA-GMA/fumed silica nanocomposites having 2% Cabosil M5 fumed silica.
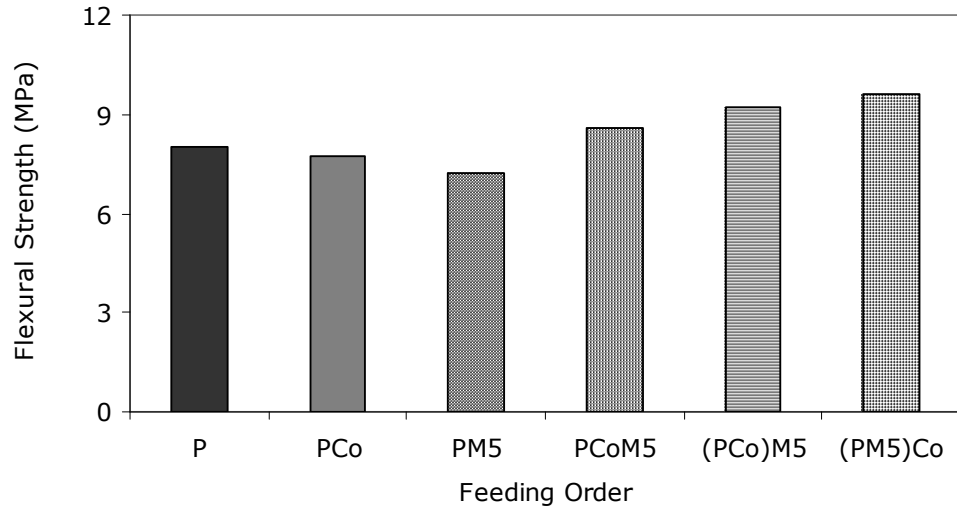
Figure 4.58 Effect of feeding order on flexural strength of LDPE/E-MA-GMA/fumed silica nanocomposites having 5% Cabosil M5 fumed silica.

Figure 4.59 Effect of feeding order on flexural modulus of LDPE/E-MA-GMA/fumed silica nanocomposites having 5% Cabosil M5 fumed silica.

4.3 Thermal Analysis with DSC

DSC analysis were performed in order to investigate the effect of compatibilizer and fumed silica content on thermal properties of nanocomposites in terms of melting temperature and crystallization. The results are presented in Table 4.1 and DSC diagrams are given in Appendix A.

The glass transition temperature of the components were not detected by DSC since T_g of LDPE and compatibilizers are below the room temperature. Significant change in melting points of samples was not observed. The melting points of compatibilizers E-nBA-MAH, E-GMA and E-MA-GMA are 107°C, 105 °C and 60°C respectively. Since they have melting points lower than LDPE, T_m values of LDPE/Compatibilizer blends are slightly lower than that of LDPE. The variation of melting point is only 1-3 °C showing that fumed silica and compatibilizer addition does not have much effect on the melting behavior of the compositions.

The crystallinity of the samples support the mechanical test results. LDPE/M5 nanocomposites which are prepared without compatibilizer show lower crystallinity with increasing silica content, resulting in a negative effect on mechanical properties. Percent crystallinity values of the ternary nanocomposites are higher than LDPE percent crystallinity value. An increase in crystallinity results in increases in modulus and yield strength but decrease in elongation at break [1].

Table 4.1 DSC results of samples

Composition	LDPE wt.%	M5 wt.%	ΔH (j/g)	% crystallinity	T_m (°C)
LDPE	100	—	79.47	27	112.2
LDPE+M5	98	2	57.49	20	114.8
LDPE+M5	95	5	49.91	18	114.5
LDPE+2210	95	—	80.76	29	110.8
LDPE+8840	95	—	80.25	29	111.2
LDPE+8900	95	—	83.24	30	110.9
LDPE/ Lotader® 2210/ Cabosil® M5					
SF:(LDPE+Co+M5)	93	2	81.85	30	113.0
	90	5	76.58	29	113.7
FO1:(LDPE+Co)+M5	93	2	78.01	29	113.4
	90	5	78.97	30	112.3
FO2:(LDPE+M5)+Co	93	2	75.34	28	114.8
	90	5	76.14	29	111.8
FO3:(Co+M5)+LDPE	93	2	82.41	30	110.6
LDPE/ Lotader® AX8840/ Cabosil® M5					
SF:(LDPE+Co+M5)	93	2	81.23	30	111.0
	90	5	81.00	31	110.7
FO1:(LDPE+Co)+M5	93	2	78.72	29	113.9
	90	5	80.84	31	113.4
FO2:(LDPE+M5)+Co	93	2	80.29	29	115.6
	90	5	87.42	33	111.2
LDPE/ Lotader® AX8900/ Cabosil® M5					
SF:(LDPE+Co+M5)	93	2	83.14	31	111.1
	90	5	78.31	30	112.6
FO1:(LDPE+Co)+M5	93	2	75.21	28	114.4
	90	5	75.02	28	114.2
FO2:(LDPE+M5)+Co	93	2	78.91	29	114.0
	90	5	76.11	29	113.3

4.4 Flow Characteristics

Melt flow index measurements were carried out in order to understand the flow behavior of the samples under a specified load of 5 kg and a specified temperature of 190°C according to ISO 1133:1991 (E) standard.

Melt flow index is inversely related to the melt viscosity which changes according to the molecular weight of the material. Besides molecular weight, there are other factors that affect the MFI results, such as the degree of chain branching, heat transfer in polymer processing and presence of co-monomers.

MFI values of pure materials are given in Table 4.2. The MFI value of pure LDPE increased as a result of the extrusion process. This may be due to the decrease in the molecular weight of the LDPE due to the applied shear during extrusion.

Table 4.2 Flow properties of pure materials

Material	MFI (g/10 min)
LDPE (not extruded)	0.74
LDPE (twice extruded)	1.43
Lotader® 2210 (E/nBA/MAH)	21.88
Lotader® AX8840 (E/GMA)	16.47
Lotader® AX8900 (E/MA/GMA)	7.96

The MFI values of LDPE-fumed silica binary nanocomposites are given in Table 4.3. This table can be considered as a general view of MFI experiments' results since all the ternary nanocomposites showed similar results, for decreasing MFI with the increasing value of fumed silica. Here, dispersed silica particles cause an increase in the viscosity as they display the role of preventing the flow of the polymer chains. This expected behavior was also observed in the study of Tam et al. [44] investigating the effect of nano-silica on rheological properties of PP.

They found that, the addition of hydrophilic fumed silica causes an increase in the viscosity of PP matrix.

Table 4.3 Flow properties of LDPE/fumed silica nanocomposites

Composition	Fumed Silica (wt%)	MFI (g/10 min)
LDPE+ Cabosil® M5	2	0.65
LDPE+ Cabosil® M5	5	0.46

The MFI values of LDPE-compatibilizer blends can be seen in Table 4.4. Because of the high MFI of compatibilizers, the addition of compatibilizers to LDPE improved its flow property. The amount of increase seems to be directly proportional with the MFI values of the compatibilizers.

Table 4.4 Flow properties of LDPE/compatibilizer blends

Composition	MFI (g/10 min)
LDPE+ Lotader® 2210	1.98
LDPE+ Lotader® AX8840	1.86
LDPE+ Lotader® AX8900	1.70

Simultaneously fed LDPE/compatibilizer/fumed silica ternary nanocomposites are seen in Table 4.5. Also a comparison of the nanocomposites prepared by different feeding orders can be found in Table 4.6. Following the same trend, it is observed that, increasing the amount of fumed silica dramatically decreases the flow properties of all samples prepared by different feeding orders.

Table 4.5 Flow properties of LDPE/compatibilizer/fumed silica ternary nanocomposites prepared by simultaneous feeding process

Composition	Fumed Silica (wt%)	MFI (g/10 min)
LDPE+ Lotader® 2210+ Cabosil® M5	2	1.10
	5	0.51
LDPE+ Lotader® AX8840+ Cabosil® M5	2	1.03
	5	0.57
LDPE+ Lotader® AX8900+ Cabosil® M5	2	1.02
	5	0.56

Table 4.6 Flow properties of LDPE/compatibilizer/fumed silica ternary nanocomposites prepared by different feeding order processes

Feeding Order	Fumed Silica (wt%)	MFI (g/10 min)
LDPE/ Lotader® 2210/ Cabosil® M5		
SF:(LDPE+Co+M5)	2	1.10
	5	0.51
FO1:(LDPE+Co)+M5	2	0.73
	5	0.23
FO2:(LDPE+M5)+Co	2	1.10
	5	0.75
FO3:(Co+M5)+LDPE	2	1.22
LDPE/ Lotader® AX8840/ Cabosil® M5		
SF:(LDPE+Co+M5)	2	1.03
	5	0.57
FO1:(LDPE+Co)+M5	2	0.66
	5	0.25
FO2:(LDPE+M5)+Co	2	0.82
	5	0.69
LDPE/ Lotader® AX8900/ Cabosil® M5		
SF:(LDPE+Co+M5)	2	1.02
	5	0.56
FO1:(LDPE+Co)+M5	2	0.58
	5	0.36
FO2:(LDPE+M5)+Co	2	0.64
	5	0.54

CHAPTER 5

CONCLUSIONS

Ternary nanocomposites of low density polyethylene were prepared by means of melt compounding method at 2 and 5 weight % fumed silica loadings with three types of compatibilizers at 5 wt %. Effects of fumed silica, compatibilizer and the feeding order of the components on morphological, mechanical and thermal properties, as well as flow behavior were investigated.

SEM analyses show that the addition of fumed silica and compatibilizer changed the smooth fracture surface of neat LDPE. SEM micrographs of LDPE/compatibilizer blends exhibit continuous and interpenetrated phases indicating their compatibility. In binary and ternary nanocomposites, the crack propagation lines seem to be rather short, close and generally not straight. Also the grape-like particulate structure of fumed silica agglomerates can easily be seen in the SEM micrographs. Larger agglomerates of fumed silica nanoparticles are observed in 5% filler loaded nanocomposites. The effect of compatibilizer type and feeding order of materials can not be observed in SEM images, since the surfaces don't show any significant difference.

DSC analyses show that percent crystallinity and melting temperature of LDPE did not remarkably change with fumed silica and compatibilizer addition. This result indicates that neither the compatibilizer nor the fumed silica has significant nucleation activity on LDPE.

As a result of the poor mechanical properties of compatibilizers, their blends with LDPE have low tensile and flexural properties. Also, the addition of silica decreases the properties of LDPE due to agglomeration of silica and its incompatibility with LDPE.

Different than binary systems, samples of ternary systems show improved mechanical properties. This shows that, for obtaining the improving effect of silica on mechanical properties its compatibility must be increased with an appropriate compatibilizer. Otherwise, silica shows a negative effect on the mechanical properties because of the agglomeration and incompatibility.

Nanocomposites prepared by different feeding orders show remarkable results. The mechanical test results of the ternary nanocomposites prepared by different feeding orders show improved properties in comparison to the properties of simultaneously fed samples. Comperatively poor results of some samples are thought to be the result of high agglomeration and poor dispersion of fumed silica nanoparticles.

The best results are obtained with FO1 feeding order [(LDPE+Co)+M5] and FO2 feeding order [(LDPE+M5)+Co] only with 2% silica. In terms of the compatibilizer, nanocomposites having E-nBA-MAH terpolymer shows the highest mechanical test results. The best result among all samples is obtained with this compatibilizer, including 2 % silica and prepared by FO2 mixing order.

MFI value of LDPE increases with the addition of compatibilizers owing to their high MFI. The addition of fumed silica decreases the MFI (increase the viscosity) of LDPE. Higher quantities of silica resulted in lower MFI values (higher viscosity) as expected, owing to the filler effect. This filler effect on MFI was also observed in ternary composites; in which increasing amount of silica exhibited lower MFI. The effect of silica was so dominant that, the increasing effect of compatibilizer could only slightly improve MFI values.

It can be concluded that in fumed silica nanocomposites, high level of adhesion and well-dispersion of nanoparticles have an important role in promoting mechanical and flow properties. The intrinsic high strength of fumed silica aggregates offer higher strength for the composites subjected to applied stress, only if its compatibility with the polymer could be increased. Suitable polymeric additives play an important role in increasing the compatibility and yield to improved properties at low fumed silica content.

REFERENCES

1. Mazumdar S.K., "Composites Manufacturing; Materials, Product, and Process Engineering", CRC Press, USA, 2002.

2. Akovali G., "Handbook of Composite Fabrication", Rapra Technology Ltd., England, 2001.

3. Nielsen L.E. and Landel R.F., "Mechanical Properties of Polymers and Composites", 2nd ed., Marcel Dekker, Inc., New York, 1994.

4. "Concise Encyclopedia of Polymer Science and Engineering", John Wiley and Sons Inc., New York, 1990.

5. Schwartz M.M., "Composite Materials Handbook", McGraw-Hill, USA, 1984.

6. Chung D.D.L., "Composite Materials: Functional Materials for Modern Technologies", Springer, USA, 2003.

7. www.nanocompositech.com/review-nanocomposite.htm, 2006.

8. "Encyclopedia of Polymer Science and Technology", 3rd ed., vol. 12, Wiley-Interscience, 2003.

9. Wu C.L., Zhang M.Q., Rong M.Z. and Friedrich K., "Silica Nanoparticles Filled Polypropylene: Effects of Particle Surface Treatment, Matrix Ductility and Particle Species on Mechanical Performance of the Composites", Composites Science and Technology, vol. 65, 635-645, 2005.

10. Nielsen L.E., "Simple Theory of Stress–Strain Properties of Filled Polymer" Journal of Applied Polymer Science, vol.10, 97–103, 1966.

11. Nicolais L and Narkis M., "Stress–Strain Behavior of Styrene–Acrylonitrile/Glass Bead Composites in the Glassy Region" Polymer Engineering Science, vol. 11, 194–199, 1971.

12. "Kirk-Othmer Encyclopedia of Chemical Technology", 4th ed., vol. 7, John Wiley and Sons Inc., New York, 1993.

13. "Ullman's Encyclopedia of Industrial Chemistry", 5th ed. vol A23, VCH Publishers, USA, 1992.

14. "Fumed Silica Interactive Learning Module", Product Research and Development Brochure, Cabot Corporation.

15. "CAB-O-SIL$^®$ M5 Untreated Fumed Silica", Product Form, Cabot Corporation.

16. Khavryutchenko V., Khavryutchenko Al. and Barthel H., "Fumed Silica Synthesis: Influence of Small Molecules on the Particle Formation Process", Wiley-VCH, Macromolecular Symposia, 169, 1-5, 2001.

17. "CAB-O-SIL$^®$ Untreated Fumed Silica: Properties & Functions", Product Brochure, Cabot Corporation.

18. http://www.uwplatt.edu/~sundin/114/image/l1439_a.gif, 2006.

19. http://www.britannica.com/ebc/article-9375583, 2006

20. http://en.wikipedia.org, 2006

21. "Kirk-Othmer Encyclopedia of Chemical Technology", 4th ed., vol. 17, John Wiley and Sons Inc., New York, 1993.

22. "Encyclopedia of Polymer Science and Technology", 3rd ed., vol. 2, Wiley-Interscience, 2003.

23. Behzad M., Tajvidi M., Ehrahimi G. and Falk R.H., "Dynamic Mechanical Analysis of Compatibilizer Effect on the Mechanical Properties Of Wood Flour – High density Polyethylene Composites", IJE Transactions B: Applications, vol. 17, 95–104, 2004.

24. Torres N., Robin J.J. and Boutevin B., "Study of Compatibilization of HDPE–PET Blends by Adding Grafted or Statistical Copolymers", Journal of Applied Polymer Science, vol. 81, 2377–2386, 2001.

25. "Encyclopedia of Polymer Science and Technology", 3rd ed., vol. 1, Wiley-Interscience, 2003.

26. http://www.dow.com/acrylic/function/gmafunc.html, 2006

27. "Encyclopedia of Polymer Science and Technology", 3rd ed., vol. 11, Wiley-Interscience, 2003.

28. "Encyclopedia of Polymer Science and Technology", 3rd ed., vol. 3, Wiley-Interscience, 2003.

29. Zhou S., Wu L., Sun J. and Shen W., "The Change of the Properties of Acrylic –Based Polyurethane via Addition of Nano-Silica", Progress in Organic Coatings, Elsevier, vol.45, 33-42, 2002.

30. http://acept.la.asu.edu/PiN/rdg/elmicr/elmicrs.html, 2006

31. Sampson A.R. "Scanning Electron Microscopy", Advanced Research Systems, 1996.

32. http://www.plasticsmag.com/article_images/Tensile%20Test.JPG, 2006

33. http://hekabe.kt.dtu.dk/~vigild/2005_04_melitek/tensile_test.htm, 2006

34.http://www.polial.polito.it/Mercurio/Polymer/mercurio_mechpro/Image81.gif, 2006

35. Friedrich K., Ruan W.H. and Zhang M.Q., "Structure-Property Relationships of In-situ Crosslinking Modified Nano-silica Filled Polypropylene Composites", Proceeding of the 8th Polymers for Advanced Technologies International Symposium, Budapest, Hungary, September 2005.

36. http://www.pslc.ws/mactest/dsc.htm, 2006

37. http://www.polyplastics.com/ch/support/Tecin/methods/image/mv1.gif, 2006

38. Wu C.L., Zhang M.Q., Rong M.Z. and Friedrich K., "Tensile Performance Improvement of Low Nanoparticles Filled Polypropylene Composites", Composites Science and Technology vol. 62, 1327-1340, 2002.

39. Rong M.Z., Zhang M.Q., Zheng Y.X., Zeng H.M. and Friedrich K., "Improvement of Tensile Properties of Nano-SiO$_2$/PP Composites in Relation to Percolation Mechanism", Polymer, vol. 42, 3301-3304, 2001.

40. Bikiaris D.N., Papageorgiou G.Z., Pavlidou E., Vouroutzis N., Palatzoglou P. and Karayannidis G.P., "Preparation by Melt Mixing and Characterization of Isotactic Polypropylene/SiO$_2$ Nanocomposites Containing Untreated and Surface-Treated Nanoparticles ", Journal of Applied Polymer Science, vol.100, 2684-2696, 2006.

41. Liang G., Xu J., Bao S. and Xu W., "Polyethylene / Maleic Anhydride Grafted Polyethylene / Organic-Montmorillonite Nanocomposites. I. Preparation, Microstructure and Mechanical Properties", Journal of Applied Polymer Science, vol.91, 3974-3980, Wiley Periodicals Inc., 2004.

42. Morawiec J., Pawlak A., Slouf M., Galeski A., Piorkowska E. and Krasnikowa N., "Preparation and Properties of Compatibilized LDPE/Organo-modified Montmorillonite Nanocomposites", European Polymer Journal, vol.41, 1115-1122, 2005.

43. www.atofinachemicals.com, 2006

44. Zhang L., Tam K.C., Gan L.H., Yue C.Y., Lam Y.C. and Hu X., "Effect of Nano-Silica Filler on the Rheological and Morphological Properties of Polypropylene/Liquid-Crystalline Polymer Blends", Journal of Applied Polymer Science, vol. 87, 1484-1492, 2003.

45. "Modern Plastics Encyclopedia", McGraw Hill, New York, 1995.

46. Billmeyer J. and Fred W., "Textbook of Polymer Science", 3rd Edition, John Wiley & Sons, Inc., 1984.

47. Garcia M., Vliet G.V., Jain S., Schrauwen B.A.G., Sarkissov A., Zyl W.E.V and Boukamp B. "Polypropylene/SiO$_2$ Nanocomposites with Improved Mechanical Properties", Reviews on Advanced Materials Science, vol. 6, 169-175, 2004.

48. Donnet J.B., "Nano and Microcomposites of Polymers, Elastomers and their Reinforcement", Composites Science and Technology, vol. 63, 1085-1088, 2003.

Appendix A

DSC Thermograms

Sample: SET1 Pe%100 F.ISIK 21.3.05   DSC   File: MAR21.01
Size: 10.9000 mg
Method: RAMP 10C/MIN; 30-180 C   Run Date: 21-Mar-05 13:40
Comment: N2: 75 CC/MIN

100.44°C
79.47J/g

112.18°C

Temperature (°C)   General V4.1C DuPont 2000
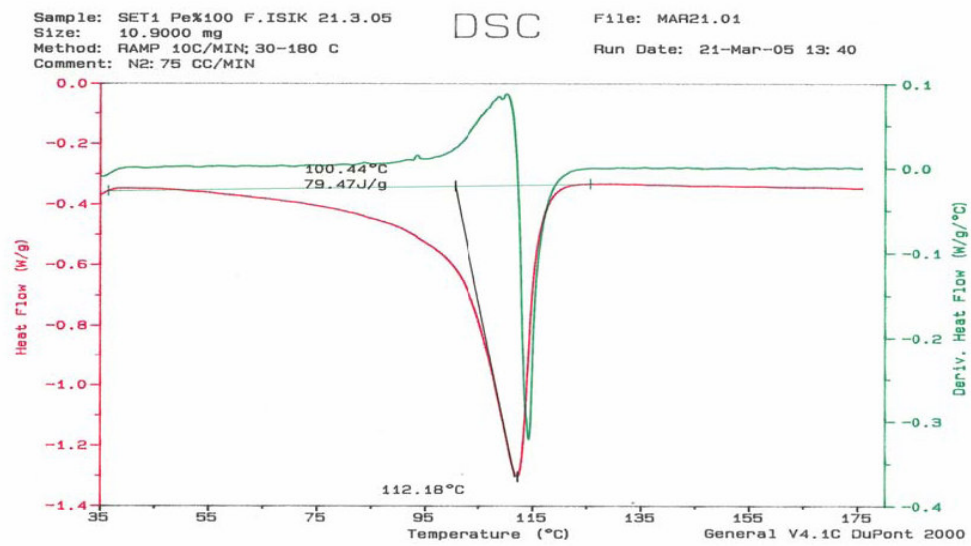
Figure A.1 DSC thermogram of pure LDPE.
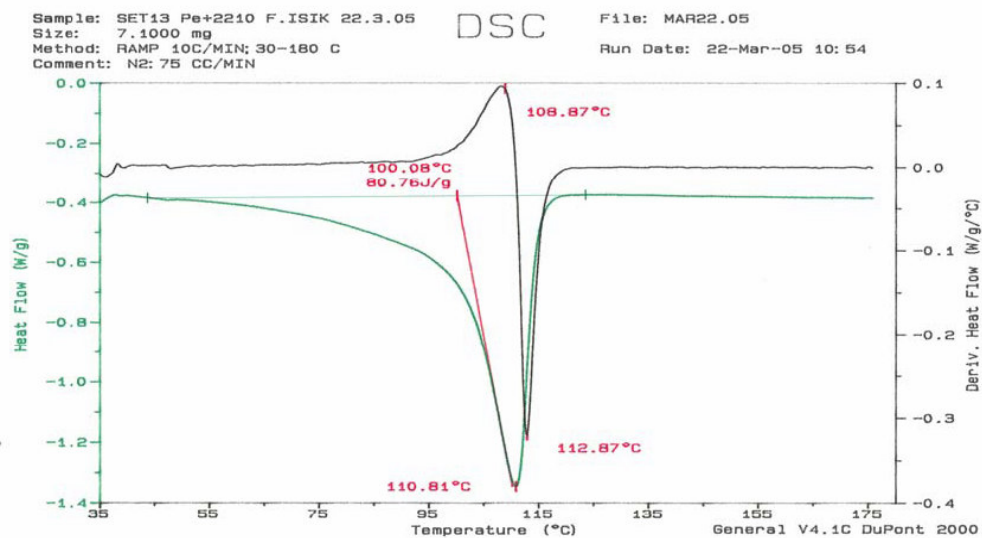
Figure A.2 DSC thermogram of LDPE/ Lotader® 2210 blend.
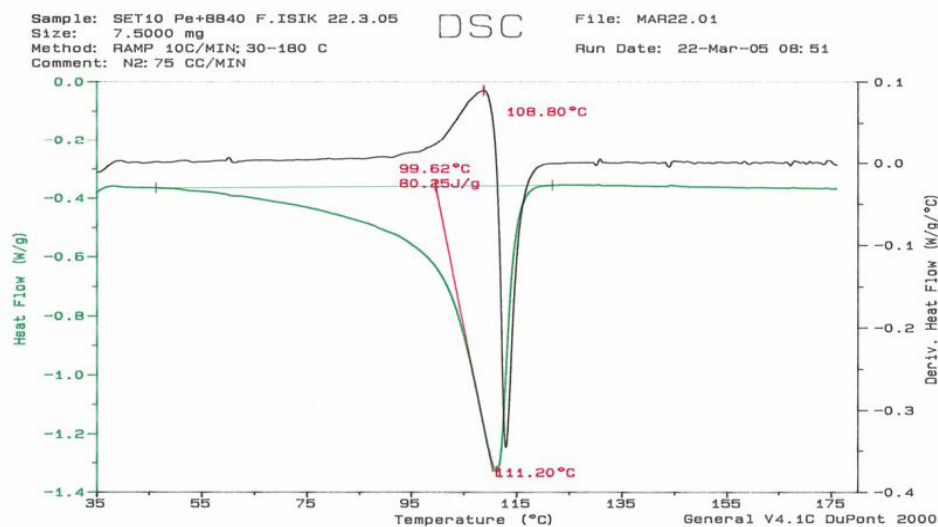
Figure A.3 DSC thermogram of LDPE/ Lotader® AX 8840 blend.
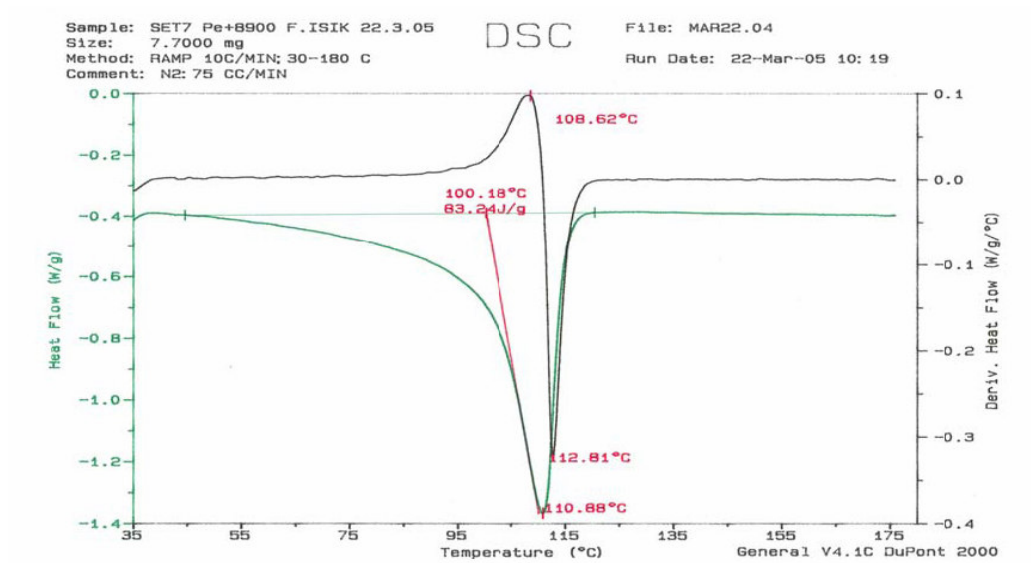
Figure A.4 DSC thermogram of LDPE/ Lotader® AX 8900 blend.
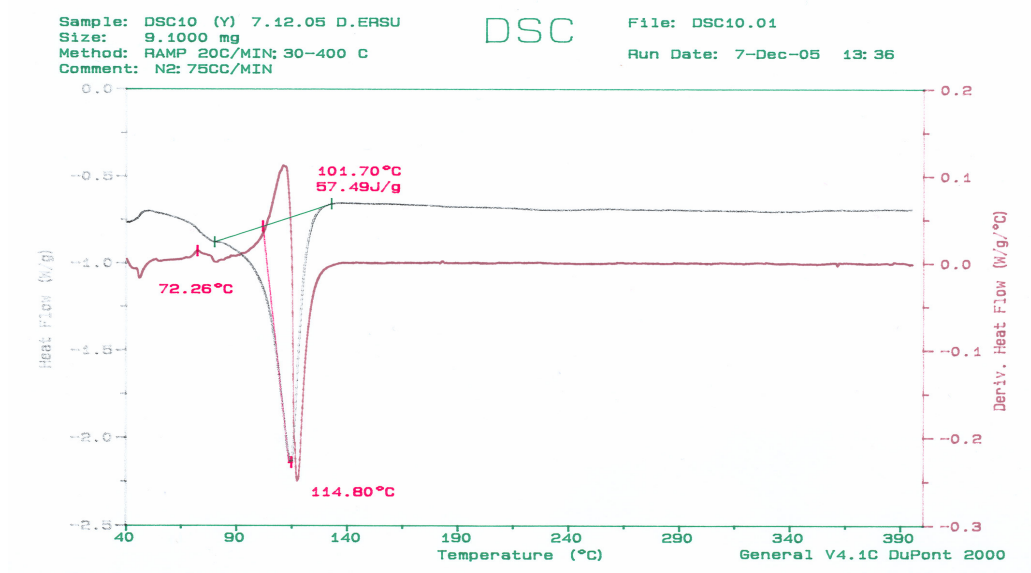
Figure A.5 DSC thermogram of simultaneously fed LDPE/Cabosil® M5 binary nanocomposite including 2 wt.% silica.
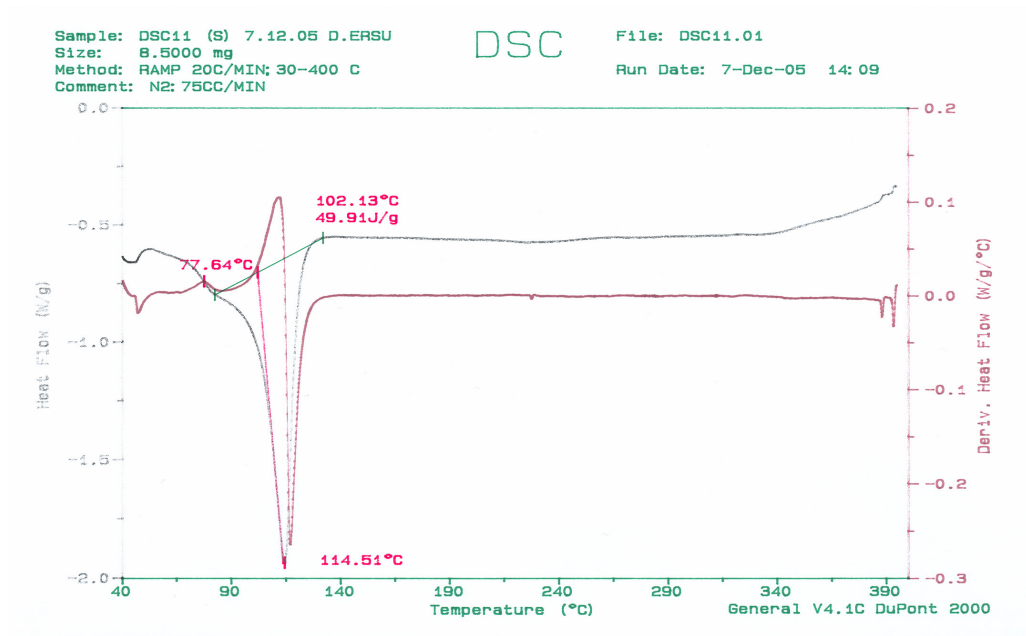
Figure A.6 DSC thermogram of simultaneously fed LDPE/Cabosil® M5 binary nanocomposite including 5 wt.% silica.
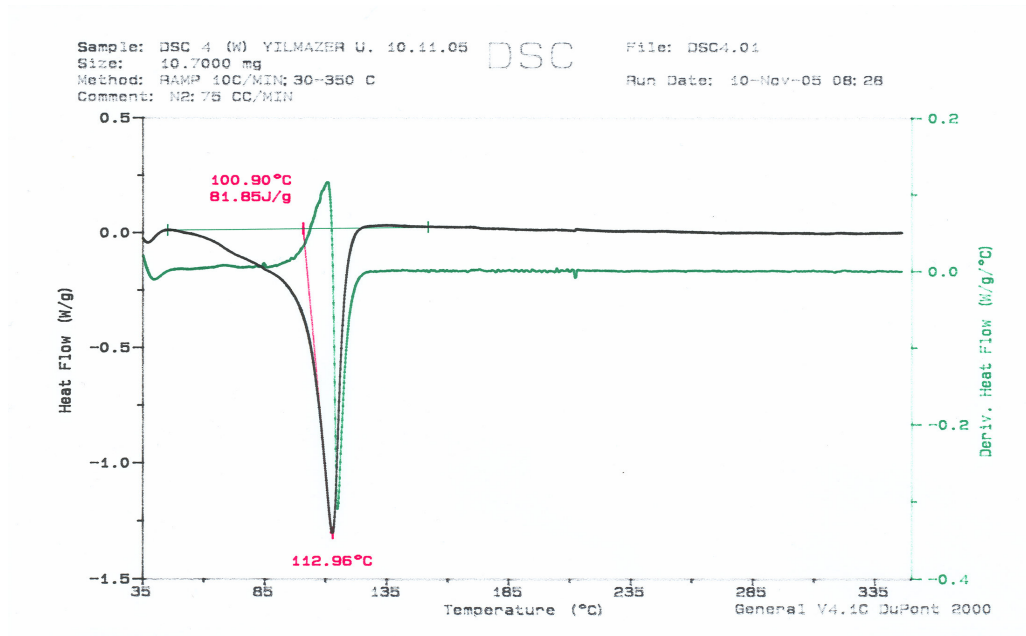
Figure A.7 DSC thermogram of simultaneously fed LDPE/Cabosil® M5/Lotader® 2210 ternary nanocomposite including 2 wt.% silica.
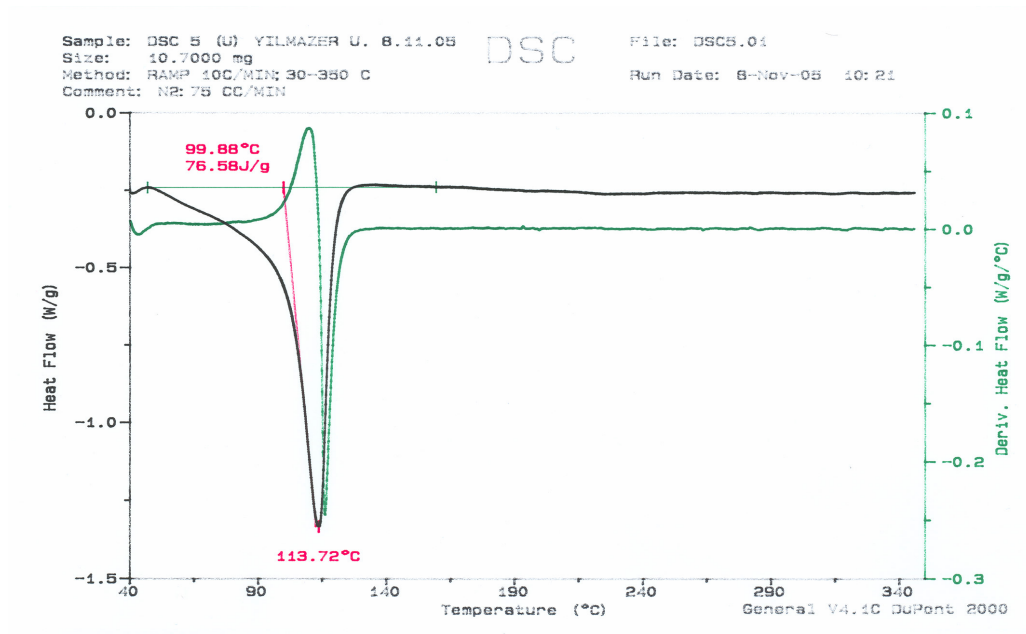
Figure A.8 DSC thermogram of simultaneously fed LDPE/Cabosil® M5/Lotader® 2210 ternary nanocomposite including 5 wt.% silica.
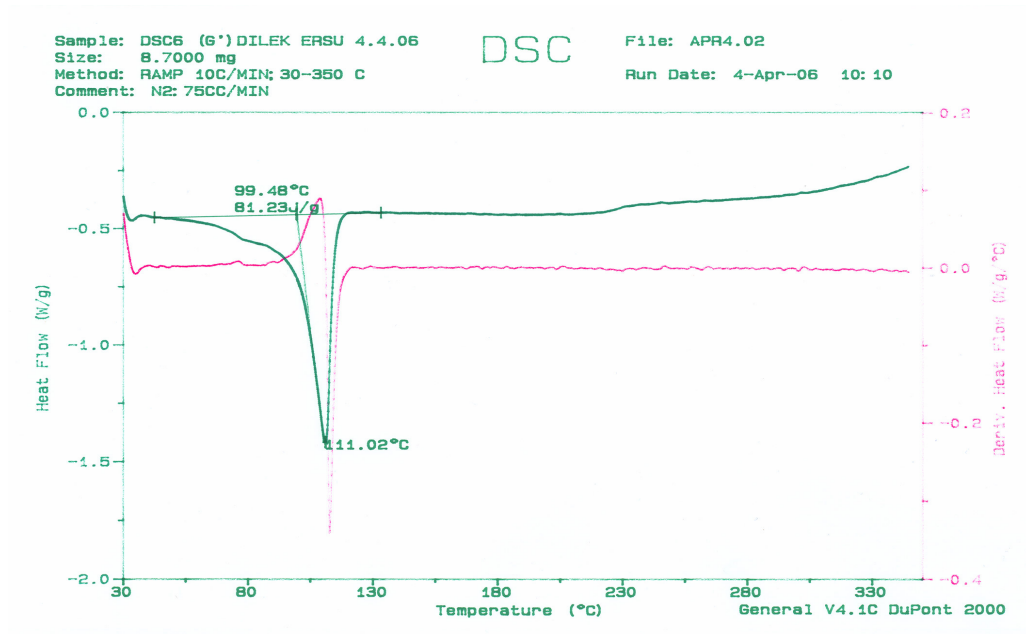
Figure A.9 DSC thermogram of simultaneously fed LDPE/Cabosil® M5/Lotader® AX 8840 ternary nanocomposite including 2 wt.% silica.
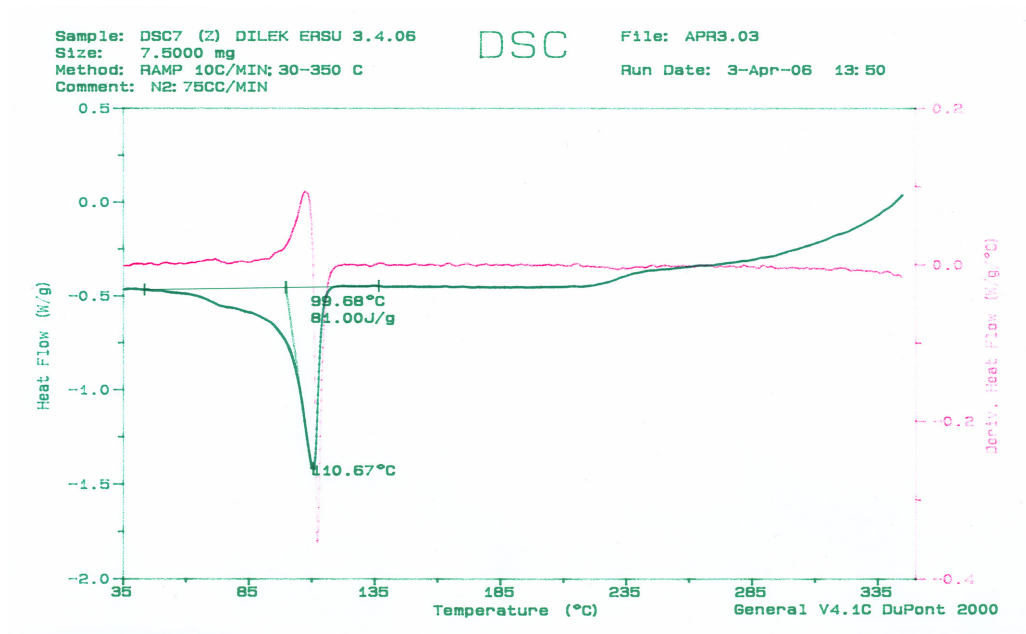
Figure A.10 DSC thermogram of simultaneously fed LDPE/Cabosil®
M5/Lotader® AX 8840 ternary nanocomposite including 5 wt.% silica.
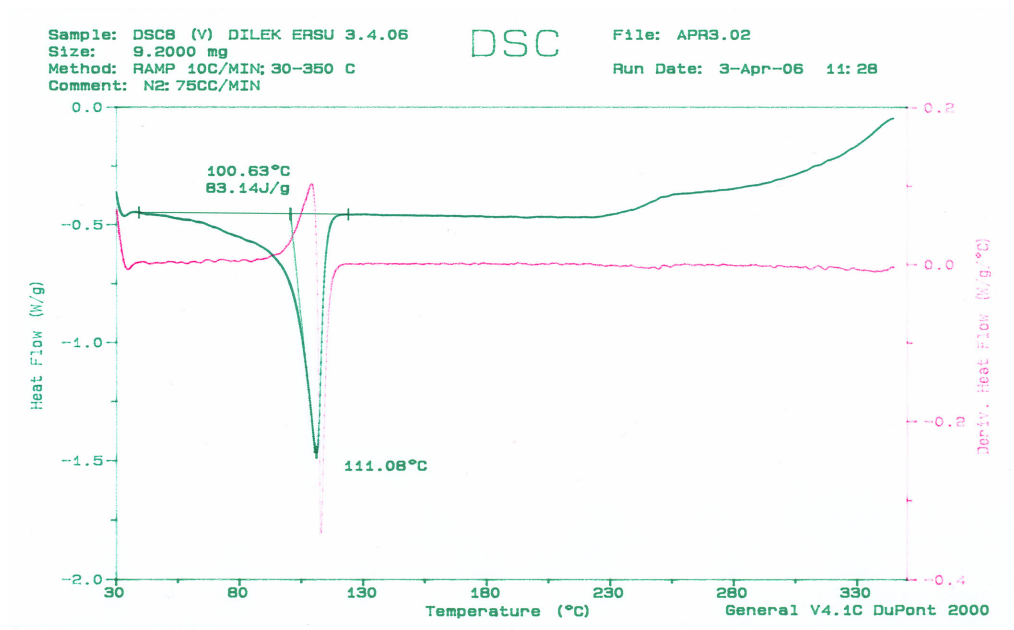
Figure A.11 DSC thermogram of simultaneously fed LDPE/Cabosil®
M5/Lotader® AX 8900 ternary nanocomposite including 2 wt.% silica.
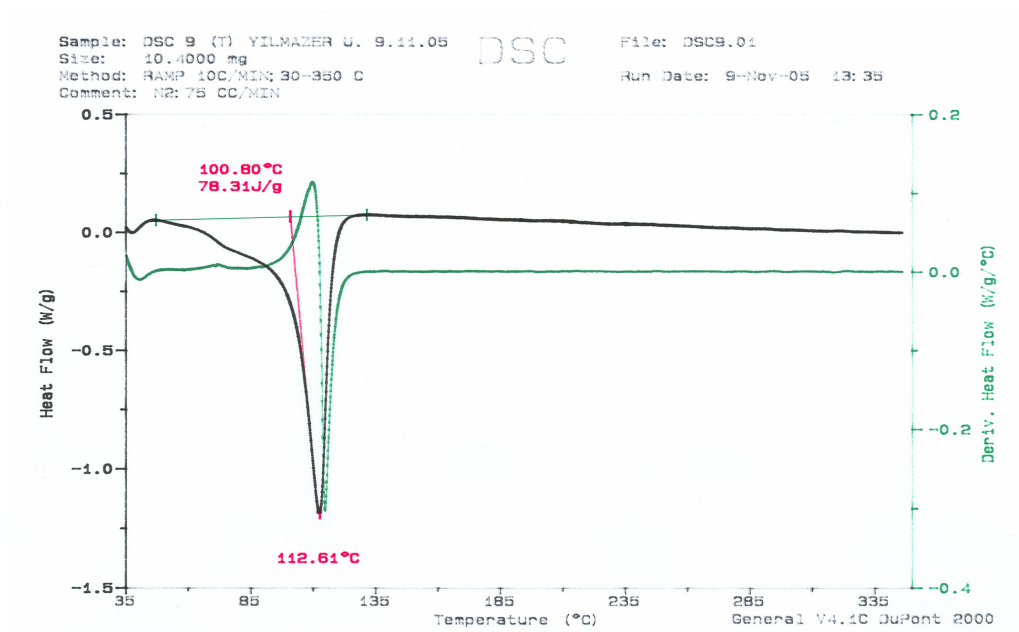
Figure A.12 DSC thermogram of simultaneously fed LDPE/Cabosil®
M5/Lotader® AX 8900 ternary nanocomposite including 5 wt.% silica.
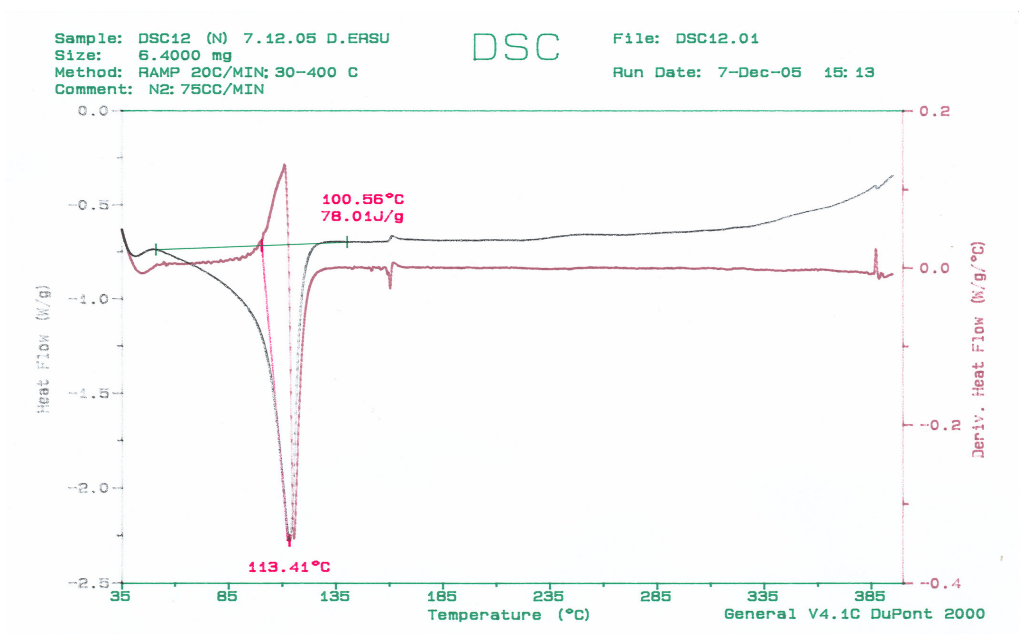
Figure A.13 DSC thermogram of LDPE/Cabosil® M5/Lotader® 2210 ternary
nanocomposite prepared by FO1 mixing order and including 2 wt.% silica.
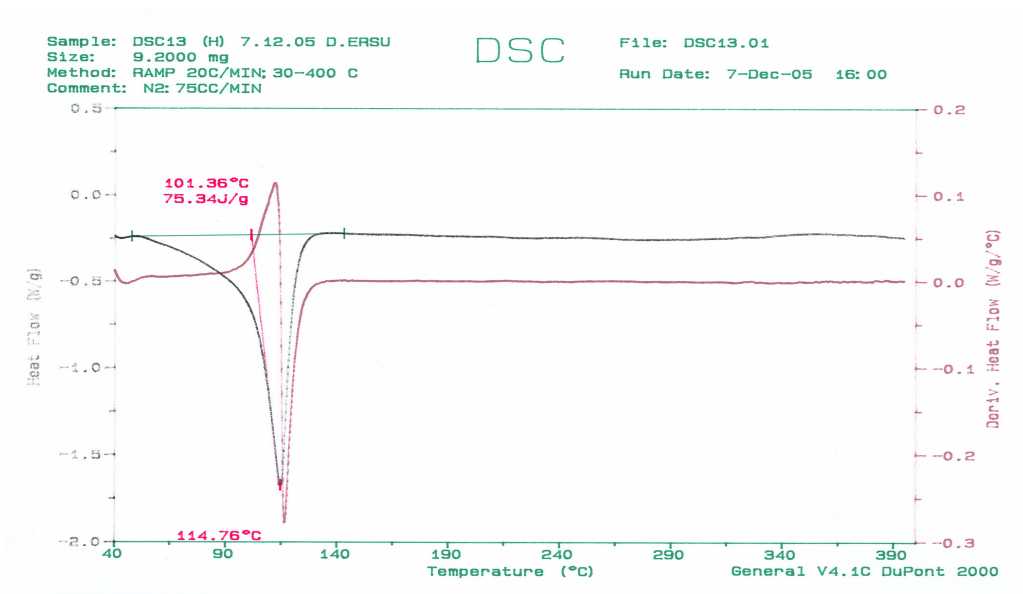
Figure A.14 DSC thermogram of LDPE/Cabosil® M5/Lotader® 2210 ternary nanocomposite prepared by FO2 mixing order and including 2 wt.% silica.
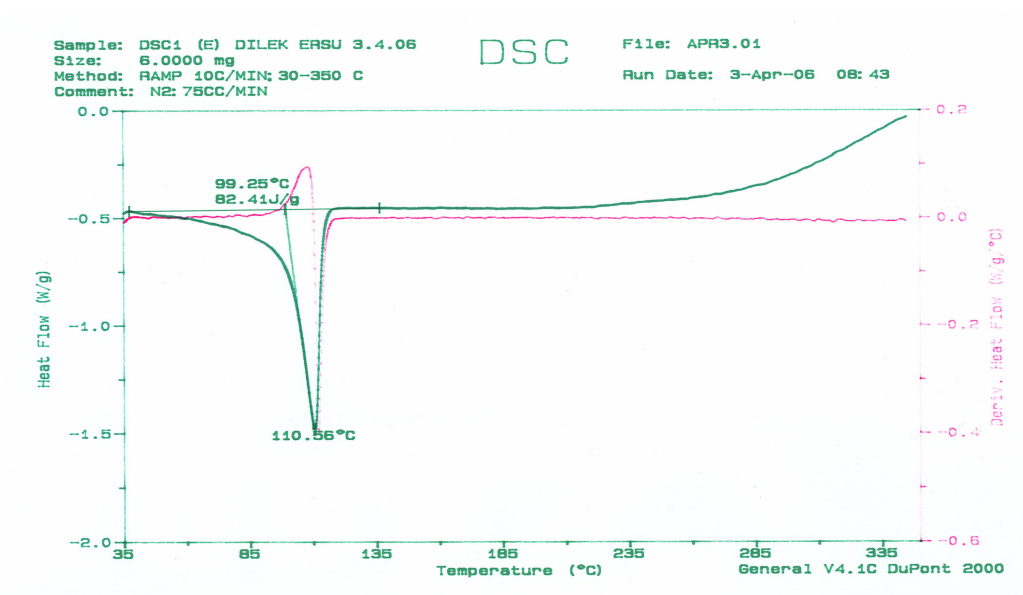
Figure A.15 DSC thermogram of LDPE/Cabosil® M5/Lotader® 2210 ternary nanocomposite prepared by FO3 mixing order and including 2 wt.% silica.
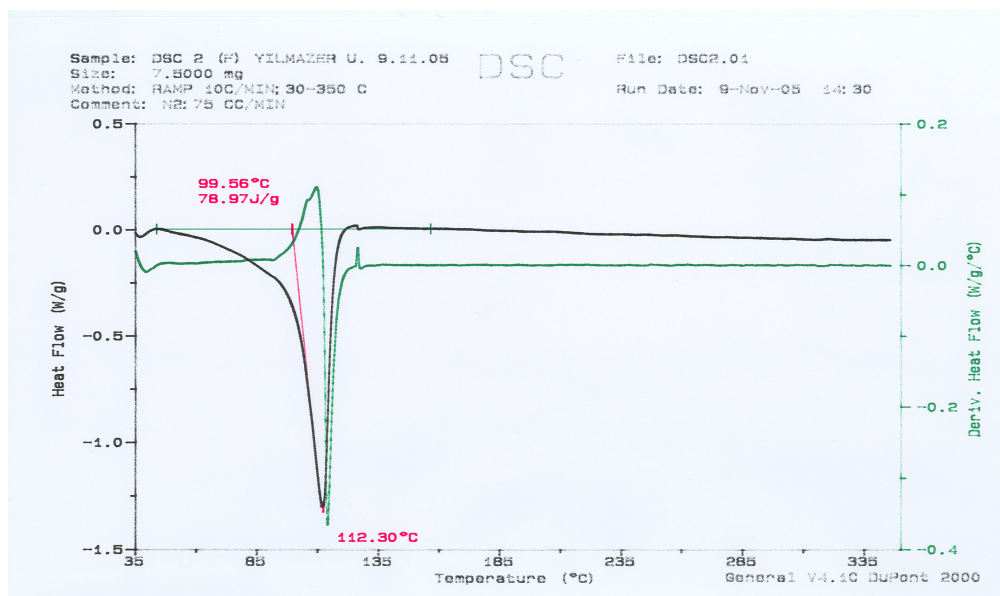
Figure A.16 DSC thermogram of LDPE/Cabosil® M5/Lotader® 2210 ternary nanocomposite prepared by FO1 mixing order and including 5 wt.% silica.
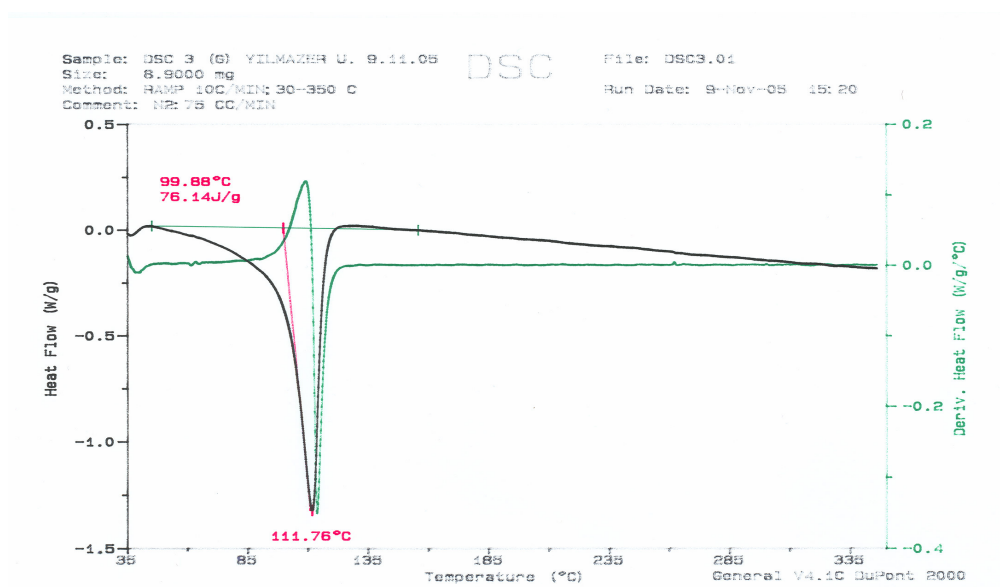
Figure A.17 DSC thermogram of LDPE/Cabosil® M5/Lotader® 2210 ternary nanocomposite prepared by FO2 mixing order and including 5 wt.% silica.
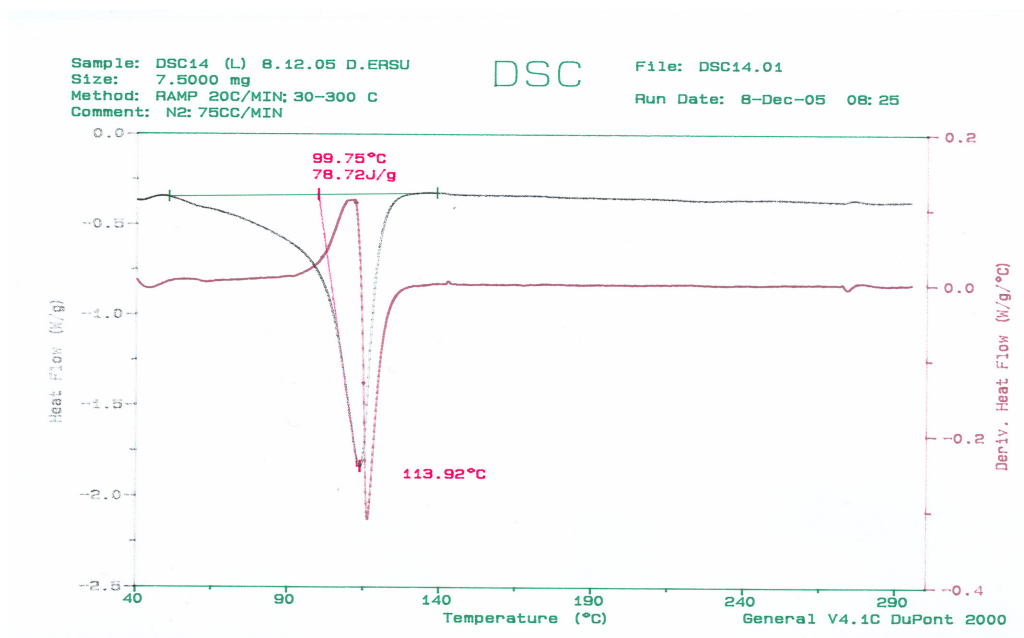
Figure A.18 DSC thermogram of LDPE/Cabosil® M5/Lotader® AX 8840 ternary nanocomposite prepared by FO1 mixing order and including 2 wt.% silica.
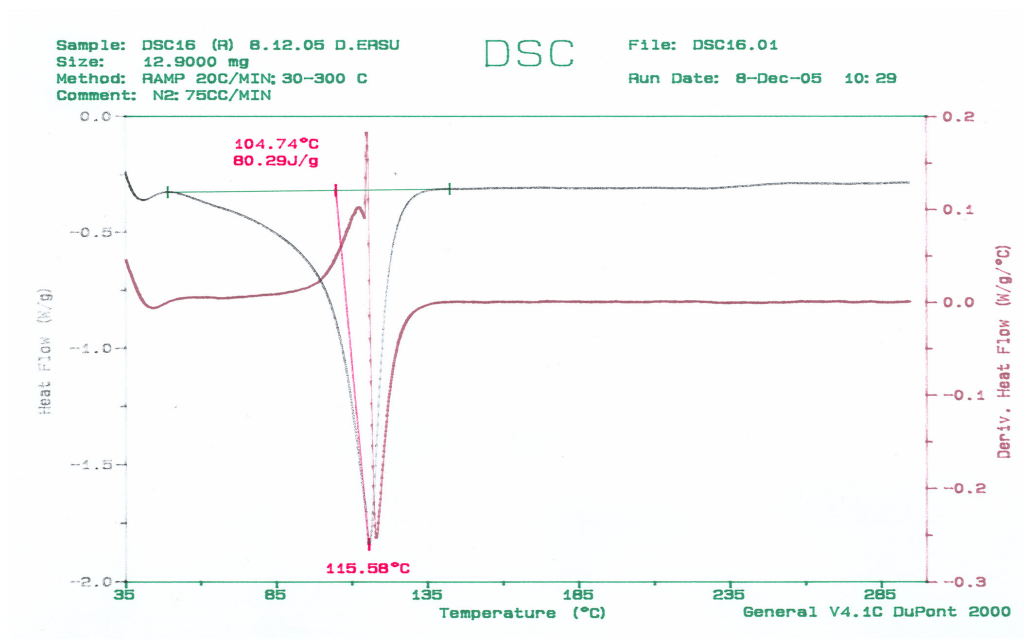
Figure A.19 DSC thermogram of LDPE/Cabosil® M5/Lotader® AX 8840 ternary nanocomposite prepared by FO2 mixing order and including 2 wt.% silica.
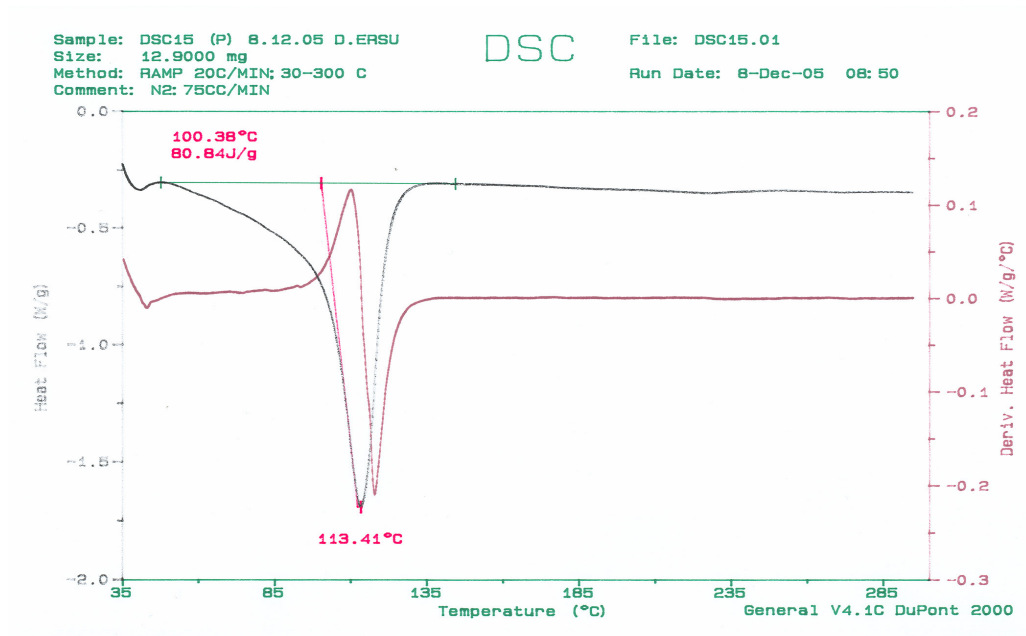
Figure A.20 DSC thermogram of LDPE/Cabosil® M5/Lotader® AX 8840 ternary nanocomposite prepared by FO1 mixing order and including 5 wt.% silica.
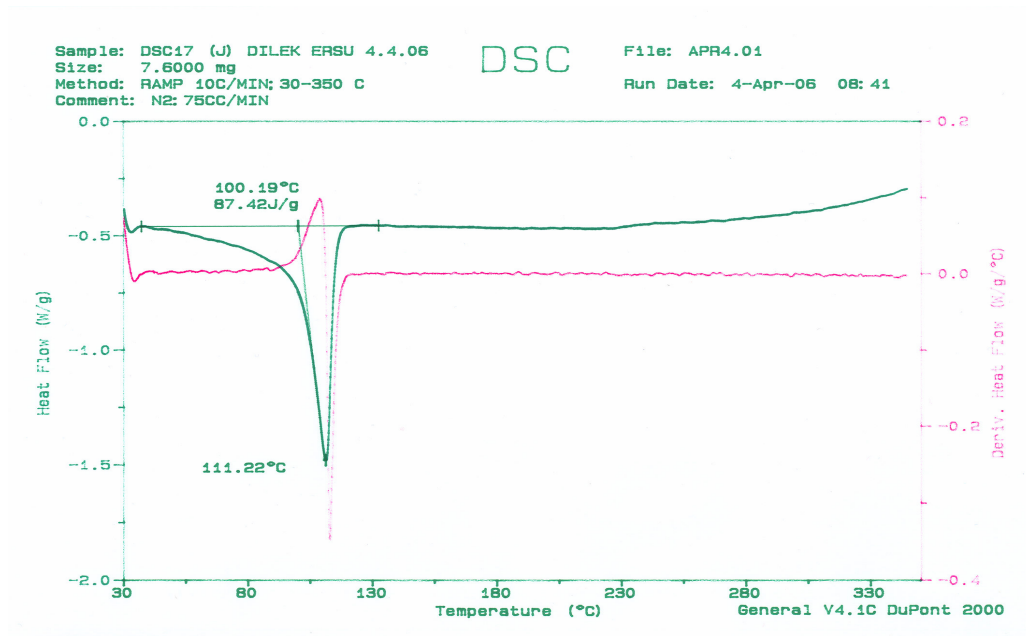
Figure A.21 DSC thermogram of LDPE/Cabosil® M5/Lotader® AX 8840 ternary nanocomposite prepared by FO2 mixing order and including 5 wt.% silica.
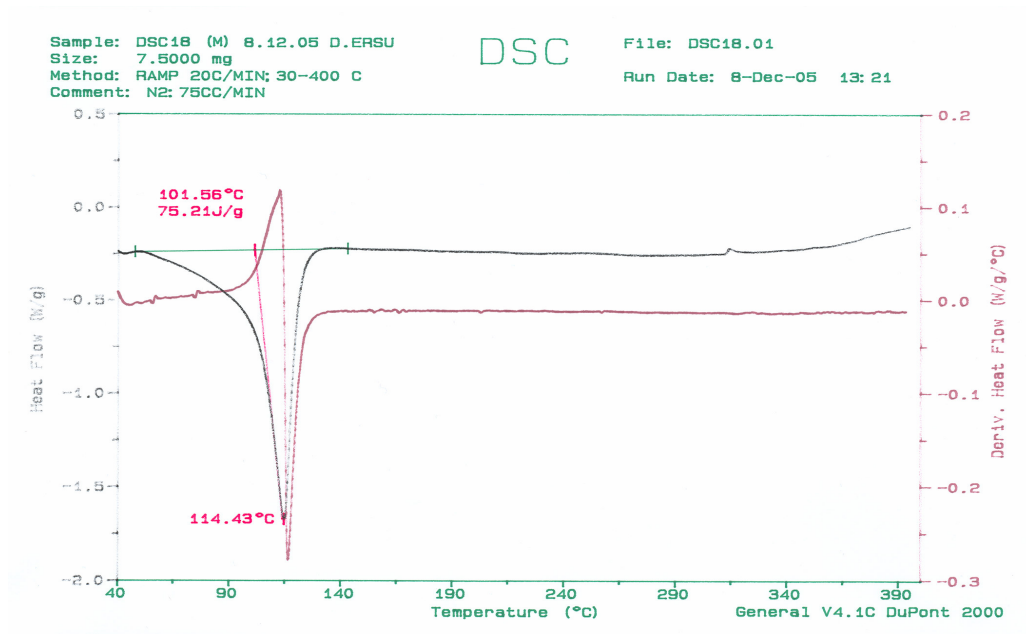
Figure A.22 DSC thermogram of LDPE/Cabosil® M5/Lotader® AX 8900 ternary nanocomposite prepared by FO1 mixing order and including 2 wt.% silica.
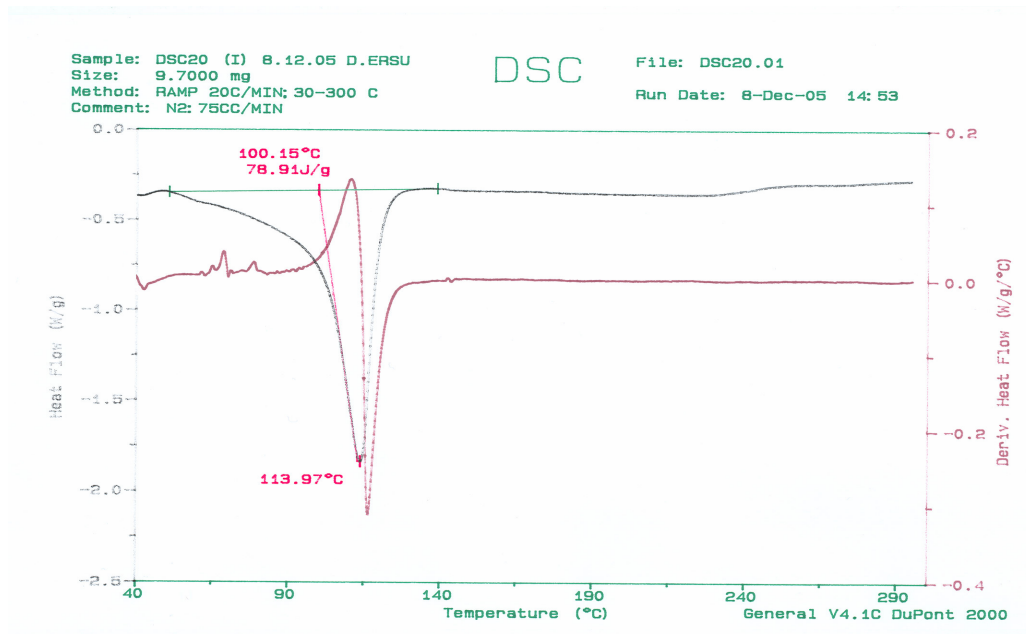
Figure A.23 DSC thermogram of LDPE/Cabosil® M5/Lotader® AX 8900 ternary nanocomposite prepared by FO2 mixing order and including 2 wt.% silica.
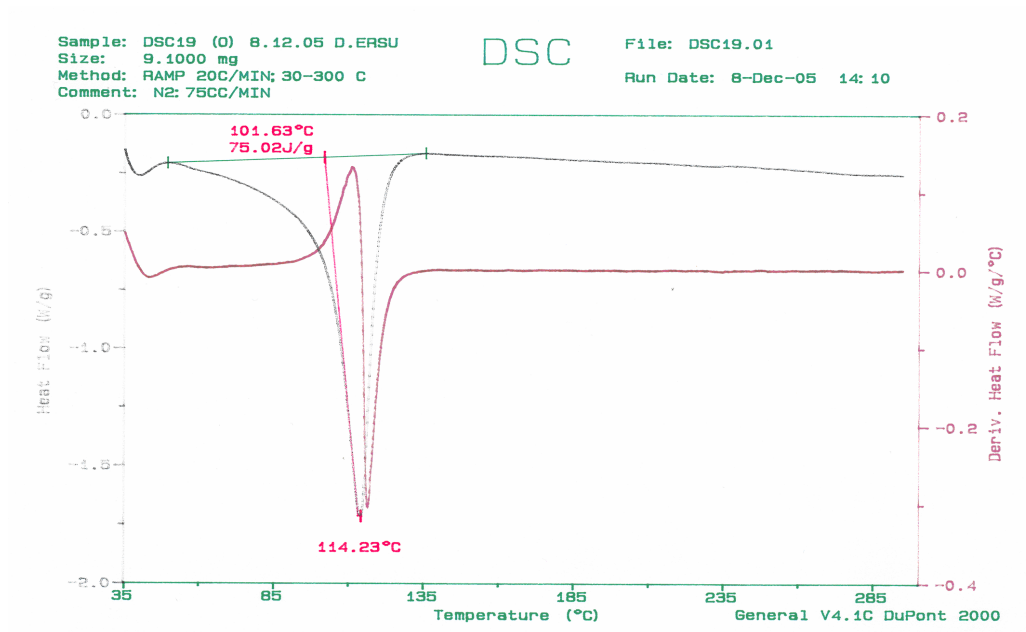
Figure A.24 DSC thermogram of LDPE/Cabosil® M5/Lotader® AX 8900 ternary nanocomposite prepared by FO1 mixing order and including 5 wt.% silica.
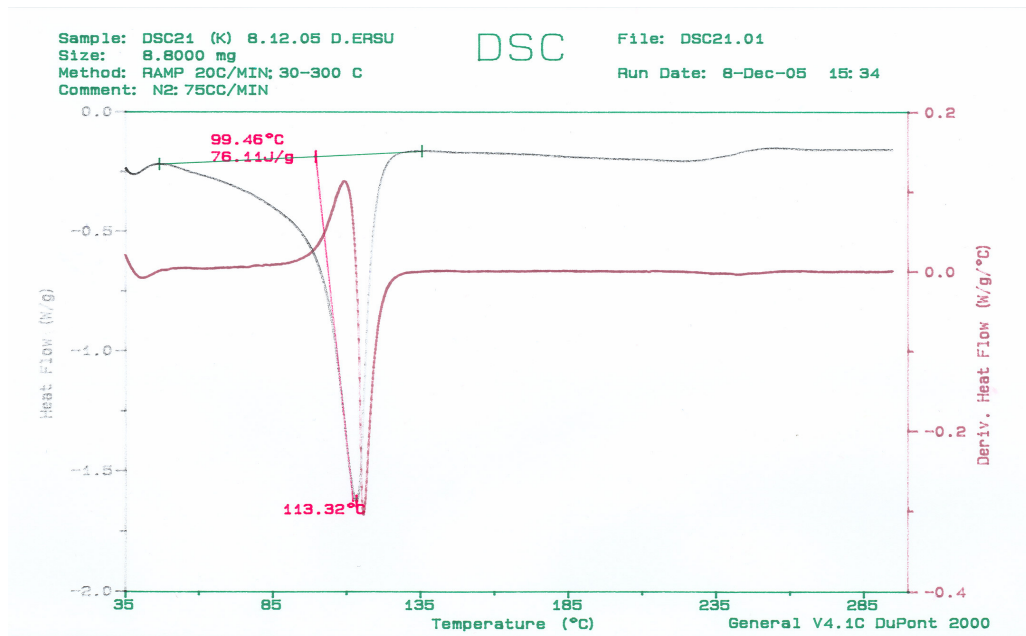
Figure A.25 DSC thermogram of LDPE/Cabosil® M5/Lotader® AX 8900 ternary nanocomposite prepared by FO2 mixing order and including 5 wt.% silica.

Appendix B

Mechanical Test Results

Table B.1 Tensile strength data for all samples

Composition	Fumed Silica wt.%	Tensile Strength (MPa)	St. Dev.
LDPE	-	25.6	0.18
LDPE/Compatibilizer			
LDPE/2210	-	23.5	0.18
LDPE/8840	-	24.6	0.35
LDPE/8900	-	24.7	0.02
LDPE/Fumed Silica			
LDPE/M5	2	21.6	0.3
LDPE/M5	5	23.5	0.3
LDPE/2210/M5 Ternary Nanocomposites			
SF:(LDPE+Co+M5)	2	27.1	0.1
SF:(LDPE+Co+M5)	5	32.7	0.02
FO1:(LDPE+Co)+M5	2	31.1	0.2
FO1:(LDPE+Co)+M5	5	31.1	0.4
FO2:(LDPE+M5)+Co	2	32.0	0.2
FO2:(LDPE+M5)+Co	5	30.2	0.1
FO3:(Co+M5)+LDPE	2	32.0	0.02
LDPE/8840/M5 Ternary Nanocomposites			
SF:(LDPE+Co+M5)	2	26.8	0.2
SF:(LDPE+Co+M5)	5	33.1	0.1
FO1:(LDPE+Co)+M5	2	32.9	0.06
FO1:(LDPE+Co)+M5	5	33.8	0.02
FO2:(LDPE+M5)+Co	2	34.7	0.1
FO2:(LDPE+M5)+Co	5	32.9	0.3

Table B.1 Tensile strength data for all samples (Cont'd)

Composition	Fumed Silica wt.%	Tensile Strength (MPa)	St. Dev.
LDPE/8900/M5 Ternary Nanocomposites			
SF:(LDPE+Co+M5)	2	27.1	0.2
SF:(LDPE+Co+M5)	5	29.3	0.2
FO1:(LDPE+Co)+M5	2	32.0	0.7
FO1:(LDPE+Co)+M5	5	32.0	0.1
FO2:(LDPE+M5)+Co	2	31.1	0.4
FO2:(LDPE+M5)+Co	5	32.0	0.2

Table B.2 Tensile modulus data for all samples

Composition	Fumed Silica wt.%	Tensile Modulus (MPa)	St. Dev.
LDPE	-	160	6.6
LDPE/Compatibilizer			
LDPE/2210	-	148	11.0
LDPE/8840	-	151	1.6
LDPE/8900	-	154	0.8
LDPE/Fumed Silica			
LDPE/M5	2	146	0.5
LDPE/M5	5	151	2.2
LDPE/2210/M5 Ternary Nanocomposites			
SF:(LDPE+Co+M5)	2	152	3.9
SF:(LDPE+Co+M5)	5	164	4.8
FO1:(LDPE+Co)+M5	2	197	7.0
FO1:(LDPE+Co)+M5	5	202	8.1
FO2:(LDPE+M5)+Co	2	208	14.5
FO2:(LDPE+M5)+Co	5	176	2.9
FO3:(Co+M5)+LDPE	2	175	1.7
LDPE/8840/M5 Ternary Nanocomposites			
SF:(LDPE+Co+M5)	2	158	2.8
SF:(LDPE+Co+M5)	5	179	5.3
FO1:(LDPE+Co)+M5	2	193	7.9
FO1:(LDPE+Co)+M5	5	192	5.4
FO2:(LDPE+M5)+Co	2	193	3.9
FO2:(LDPE+M5)+Co	5	191	2.4

Table B.2 Tensile modulus data for all samples (Cont'd)

Composition	Fumed Silica wt.%	Tensile Modulus (MPa)	St. Dev.
LDPE/8900/M5 Ternary Nanocomposites			
SF:(LDPE+Co+M5)	2	161	4.2
SF:(LDPE+Co+M5)	5	176	5.5
FO1:(LDPE+Co)+M5	2	186	2.3
FO1:(LDPE+Co)+M5	5	187	3.1
FO2:(LDPE+M5)+Co	2	185	3.7
FO2:(LDPE+M5)+Co	5	180	1.5

Table B.3 Tensile strain at break data for all samples

Composition	Fumed Silica wt.%	Tensile Strain at Break (%)	St. Dev.
LDPE	-	54	2.0
LDPE/Compatibilizer			
LDPE/2210	-	32	0.6
LDPE/8840	-	32	0.7
LDPE/8900	-	29	1.1
LDPE/Fumed Silica			
LDPE/M5	2	50	2.1
LDPE/M5	5	54	2.4
LDPE/2210/M5 Ternary Nanocomposites			
SF:(LDPE+Co+M5)	2	62	5.3
SF:(LDPE+Co+M5)	5	52	1.1
FO1:(LDPE+Co)+M5	2	24	1.2
FO1:(LDPE+Co)+M5	5	32	2.9
FO2:(LDPE+M5)+Co	2	28	2.3
FO2:(LDPE+M5)+Co	5	35	0.2
FO3:(Co+M5)+LDPE	2	35	2.7
LDPE/8840/M5 Ternary Nanocomposites			
SF:(LDPE+Co+M5)	2	57	3.3
SF:(LDPE+Co+M5)	5	46	1.6
FO1:(LDPE+Co)+M5	2	30	3.4
FO1:(LDPE+Co)+M5	5	31	2.7
FO2:(LDPE+M5)+Co	2	34	4.6
FO2:(LDPE+M5)+Co	5	29	4.2

Table B.3 Tensile strain at break data for all samples (Cont'd)

Composition	Fumed Silica wt.%	Tensile Strain at Break (%)	St. Dev.
LDPE/8900/M5 Ternary Nanocomposites			
SF:(LDPE+Co+M5)	2	60	3.2
SF:(LDPE+Co+M5)	5	47	2.4
FO1:(LDPE+Co)+M5	2	31	1.7
FO1:(LDPE+Co)+M5	5	27	4.1
FO2:(LDPE+M5)+Co	2	32	4.6
FO2:(LDPE+M5)+Co	5	31	3.8

Table B.4 Flexural strength data for all samples

Composition	Fumed Silica wt.%	Flexural Strength (MPa)	St. Dev.
LDPE	-	8.0	0.2
LDPE/Compatibilizer			
LDPE/2210	-	7.1	0.0
LDPE/8840	-	7.8	0.0
LDPE/8900	-	7.8	0.3
LDPE/Fumed Silica			
LDPE/M5	2	7.8	0.4
LDPE/M5	5	7.2	0.2
LDPE/2210/M5 Ternary Nanocomposites			
SF:(LDPE+Co+M5)	2	8.5	0.5
SF:(LDPE+Co+M5)	5	9.3	0.0
FO1:(LDPE+Co)+M5	2	9.6	0.4
FO1:(LDPE+Co)+M5	5	10.2	0.2
FO2:(LDPE+M5)+Co	2	10.5	0.3
FO2:(LDPE+M5)+Co	5	9.4	0.0
FO3:(Co+M5)+LDPE	2	8.4	0.6
LDPE/8840/M5 Ternary Nanocomposites			
SF:(LDPE+Co+M5)	2	9.6	0.4
SF:(LDPE+Co+M5)	5	9.7	0.1
FO1:(LDPE+Co)+M5	2	10.3	0.8
FO1:(LDPE+Co)+M5	5	10.3	0.3
FO2:(LDPE+M5)+Co	2	9.9	0.5
FO2:(LDPE+M5)+Co	5	9.3	0.1

Table B.4 Flexural strength data for all samples (Cont'd)

Composition	Fumed Silica wt.%	Flexural Strength (MPa)	St. Dev.
LDPE/8900/M5 Ternary Nanocomposites			
SF:(LDPE+Co+M5)	2	8.5	0.1
SF:(LDPE+Co+M5)	5	8.6	0.2
FO1:(LDPE+Co)+M5	2	9.1	0.6
FO1:(LDPE+Co)+M5	5	9.2	0.6
FO2:(LDPE+M5)+Co	2	9.2	0.0
FO2:(LDPE+M5)+Co	5	9.6	0.1

Table B.5 Flexural modulus data for all samples

Composition	Fumed Silica wt.%	Flexural Modulus (MPa)	St. Dev.
LDPE	-	166	0.2
LDPE/Compatibilizer			
LDPE/2210	-	151	0.2
LDPE/8840	-	156	0.3
LDPE/8900	-	156	0.0
LDPE/Fumed Silica			
LDPE/M5	2	152	0.3
LDPE/M5	5	158	0.3
LDPE/2210/M5 Ternary Nanocomposites			
SF:(LDPE+Co+M5)	2	185	0.1
SF:(LDPE+Co+M5)	5	216	0.0
FO1:(LDPE+Co)+M5	2	229	0.2
FO1:(LDPE+Co)+M5	5	233	0.0
FO2:(LDPE+M5)+Co	2	249	0.2
FO2:(LDPE+M5)+Co	5	187	0.1
FO3:(Co+M5)+LDPE	2	218	0.0
LDPE/8840/M5 Ternary Nanocomposites			
SF:(LDPE+Co+M5)	2	202	0.2
SF:(LDPE+Co+M5)	5	199	0.1
FO1:(LDPE+Co)+M5	2	223	0.1
FO1:(LDPE+Co)+M5	5	243	0.0
FO2:(LDPE+M5)+Co	2	251	0.1
FO2:(LDPE+M5)+Co	5	226	0.3

Table B.5 Flexural modulus data for all samples (Cont'd)

Composition	Fumed Silica wt.%	Flexural Modulus (MPa)	St. Dev.
LDPE/8900/M5 Ternary Nanocomposites			
SF:(LDPE+Co+M5)	2	184	0.2
SF:(LDPE+Co+M5)	5	183	0.2
FO1:(LDPE+Co)+M5	2	189	0.7
FO1:(LDPE+Co)+M5	5	187	0.1
FO2:(LDPE+M5)+Co	2	194	0.4
FO2:(LDPE+M5)+Co	5	171	0.2